

# The Effect of Gravitational Encounters on Binary Planetesimals

*John Gillan*

---

Lund Observatory  
Lund University



2021-EXA183

Degree project of 60 higher education credits (for a degree of Master)  
May 2021

Supervisor: Sebastian Lorek

Lund Observatory  
Box 43  
SE-221 00 Lund  
Sweden

## Abstract

Binary planetesimals in the Kuiper belt can experience close encounters with other bodies. These encounters can disturb the orbital dynamics of the binary in several ways. Energy can be added to the system by the impactor body and lead to the disruption of the binary. Less energetic encounters can alter the orbital elements of the mutual orbit of the binary. The impactor could swap with one of the components of the binary creating a new binary. These interactions are interesting because determining how frequently they occur and what the results of the interactions are, can reveal information about the dynamical evolution of the Kuiper belt, and about planet formation and migration. Contact binaries in the Kuiper belt may be formed by this process.

In this project we investigate encounters involving binaries and similarly sized bodies in the cold classical region of the Kuiper belt. We carry out several experiments; we investigate certain combinations of binary and impactor with small random changes to the initial conditions, and analyse outcome probabilities as a result of these changes; we subject different kinds of binaries to a parameter space of impactors, investigating on a large scale how binaries respond to many different encounter situations; and finally, we follow a single binary in the Kuiper belt as it evolves over the course of many encounters, with the bodies it encounters drawn from a distribution that is representative of the environment there.

We find that the mutual orbital characteristics of a binary are critical to its ability to survive encounters. Wide and eccentric orbits are more susceptible to disruption during encounters. Encounters frequently result in the formation of new binaries composed of one of the original components and the impactor. These new binaries tend to have very high eccentricities. The encounter timescale is an important factor in determining outcomes, with destructive encounters requiring a large encounter timescale. This requires a slow relative encounter velocity, which in turn implies dynamically similar orbits, with low eccentricities and inclinations. Binaries generally evolve over their lifetime to have larger eccentricities as a result of encounters. Around 80% of wide binaries survive  $10^5$  encounters. Collisions that occur as a result of these kinds of encounters typically have speeds similar to the escape speed of the bodies.

## Popular summary

The solar system beyond the orbit of Neptune is currently a region of intense study. It contains many minor bodies much smaller than the planets that we are all familiar with, and these smaller bodies and their orbits have interesting features that can shed light on the formation and evolution of the entire solar system. The greatest concentration of these bodies is in the Kuiper belt, a relatively dense but quite wide region just outside the orbit of Neptune. The bodies in the Kuiper belt are further divided up into several categories depending on their orbital characteristics, such as how circular and how inclined the orbit is.

Many of the objects in the Kuiper belt are what are known as planetesimals, which are intermediate sized bodies larger than around 1 km but not as large as an actual planet. The planetesimals in the Kuiper belt are thought to be pristine leftovers from the formation of the solar system. The low density in this region means they are unlikely to have suffered many destructive collisions with other large bodies, and have not been weathered by impacts from smaller bodies and dust. Because of their small size and great distance from the Earth they are very difficult to study. Most of the images we have of Kuiper belt planetesimals have been taken by the Hubble Space Telescope, and they appear as only points of light. The best images we have of a Kuiper belt planetesimal are of Arrokoth, taken in 2018 by the New Horizons spacecraft, several years after it flew past and imaged Pluto. Arrokoth has an unusual shape, and is thought to be a contact binary, a unique class of object which appears to be two bodies stuck together.

Not all planetesimals in the Kuiper belt orbit the Sun on their own, but many are bound up in mutually orbiting pairs, known as binaries. The exact percentage of bodies bound up in binaries as a function of the total amount of bodies in the Kuiper belt is unknown, but it is thought to be quite high, in the order of 30%. Binaries here are interesting for several reasons. Understanding their formation could reveal information about the environment in which all planetesimals are formed, and help us understand planet formation. If we know how easily they are destroyed, their survival to the present day would tell us about the dynamical environment of the Kuiper belt. It could also tell us at what distance from the Sun they originally formed and how they got to their current location, which could then tell us about the migration of the planets, and the large scale evolution of the entire solar system.

In this project we examined how the orbits of binaries in the Kuiper belt change during the course of their lifetime, as a result of close encounters with other similarly sized Kuiper belt bodies. To achieve this we used numerical simulations, which simulate the gravitational effects of objects on each other. We were interested in how resilient different kinds of binaries are to disruption, as this could help explain the current prevalence of binaries. We were also interested in whether encounters such as these are a possible formation pathway to creating contact binaries such as Arrokoth. We were also interested in how a binary's orbit changes under the influence of non-destructive encounters, and how this affects how the binary evolves over its lifetime.

We found that the way a binary reacts to a close encounter is heavily dependant on the characteristics of the mutual orbit of the binary components around each other, in particular how wide or tight the binary is, but also on how circular the orbit is, and other similar parameters. Tighter binaries are able to survive longer. We also saw that binaries where both components are the same size can stay bound together more easily than if one of the components is much smaller than the other. We concluded that these types of encounters do not seem to be efficient formation pathways for contact binaries.

# Contents

<b>1</b>	<b>Introduction</b>	<b>1</b>
1.1	Orbital Elements	2
1.2	The Hill Sphere	3
1.3	The Kuiper belt	5
1.3.1	Kuiper belt populations	6
1.3.2	Origin of the Kuiper belt	7
1.4	Binary planetesimals	8
1.5	Contact binaries	10
1.6	Aim of the project	12
<b>2</b>	<b>Methods</b>	<b>14</b>
2.1	Simulation setup	15
2.1.1	Placement of components	15
2.1.2	Timing encounters with eccentric and inclined orbits	19
2.2	Computing orbital elements	22
2.3	Effects of impactor on binary	23
2.4	Collisions	24
<b>3</b>	<b>Results</b>	<b>27</b>
3.1	Example encounters	27
3.2	Chaotic encounters	33
3.3	Parameter study	39
3.3.1	Binary survival in parameter space	40
3.3.2	Binary changes in parameter space	45
3.4	Single binary	46
3.4.1	Frequency of encounters	46
3.4.2	Binary evolution over lifetime	48
3.5	Collision analysis	53
<b>4</b>	<b>Discussion</b>	<b>55</b>
4.1	Binary survival	55
4.2	Binary mass ratios	56
4.3	Formation of contact binaries	56
4.4	Binary lifetime	58
4.5	Encounter timescale	59
4.6	Limitations of this approach	59
<b>5</b>	<b>Conclusion</b>	<b>61</b>

# Chapter 1

## Introduction

The origin and dynamics of smaller bodies in the outer solar system can teach us a lot about the solar system and planet formation as a whole. Binary planetesimals are especially interesting as their presence and orbital configuration places restrictions on the dynamical evolution of the solar system on a large scale.

A simple definition of astronomical binaries is that they are pairs of bodies that are gravitationally bound to each other. Within our own solar system examples of binaries are found in the minor bodies, and current estimates suggest they are especially prevalent in the Kuiper belt (Noll et al. 2020). Their presence in this region is interesting for many reasons. Pairs of bodies bound together by their mutual gravitational attraction have the potential for their mutual orbits to be altered by encounters, which could come in the form of encounters with very massive bodies such as planets, or less massive bodies such as other similarly sized planetesimals. Changes in the orbits of binaries can affect their ability to stay bound, and may disrupt the binary, or unbind the two components, or they could become more tightly bound.

Planetesimals are objects, found mostly in the Kuiper belt, which are larger than about 1 km but smaller than the planets. They can be defined as objects large enough that their orbits are dominated by mutual gravitational attraction, as opposed to aerodynamic coupling to the gas disc (Armitage 2010).

The present day configurations of binary planetesimals in the Kuiper belt are important for understanding the dynamical processes that guided the evolution of the outer solar system. The prevalence of binaries in the Kuiper belt places restraints on the dynamical evolution of the outer solar system (Parker & Kavelaars 2010), and the wideness or tightness of those binaries can also tell us about the history of that region (Nesvorný & Vokrouhlický 2019).

This project is an examination of changes in binary orbital characteristics as a result of encounters with other similarly sized planetesimals. We will examine binary survivability, that is, the probability of the binary staying bound as a result of single encounters, and over the course of its lifetime. We will investigate how encounters produce changes to the eccentricity and semi-major axis of the binary orbit. We will track the effect of multiple encounters on a particular binary and how the different possible characteristics of the bodies that they encounter produce different outcomes.

To carry out these experiments and examine the results of interactions between multiple astronomical bodies we will require numerical simulations. Analytical descriptions of systems with more than two bodies are not possible in general, although they can be achieved in restricted cases, introduced in Chapter 2. In our work we are investigating 4-body systems; the Sun, the two components of the binary, and the body that the binary encounters. The Sun is an important component of this investigation, which will be explained in section 1.2. Numerical integrations

of the equations of motion of multiple bodies in a system allow the simulation of gravitational encounters between the bodies.

The rest of the introduction will lay the background for this project and explain the scientific questions we are trying to answer, and is structured as follows: To understand the structure of binary orbits and how they can be configured, section 1.1 will first introduce the basics of Keplerian orbits and section 1.2 introduces the Hill sphere. Then section 1.3 introduces the Kuiper belt, the environment in which all of our interactions take place, focusing on the cold classical region of the Kuiper belt, and how it differs from the other populations. Section 1.4 then discusses binaries in the Kuiper belt, the focus of the project; how common they are and their physical characteristics. Section 1.5 discusses contact binaries in the Kuiper belt, a particularly interesting class of object, and how they might be formed. And then finally in section 1.6 the aim of the project will be explained in more detail.

## 1.1 Orbital Elements

Before analysing the changes in a binary orbit as a result of gravitational encounters it is necessary to first understand how the shape and orientation of an orbit is described. A Keplerian orbit of one body around another can be characterised by the six orbital elements: semi-major axis, eccentricity, inclination, longitude of ascending node, argument of periapsis, and true anomaly. Figure 1.1 shows a 2D orbit from above. The two bodies are in orbit around each other, and the central body is much more massive than the outer body. The semi-major axis  $a$ , determines the size of the ellipse. It is one half the length of the major axis, or half the distance between the periapsis and the apoapsis. The eccentricity determines the shape of the

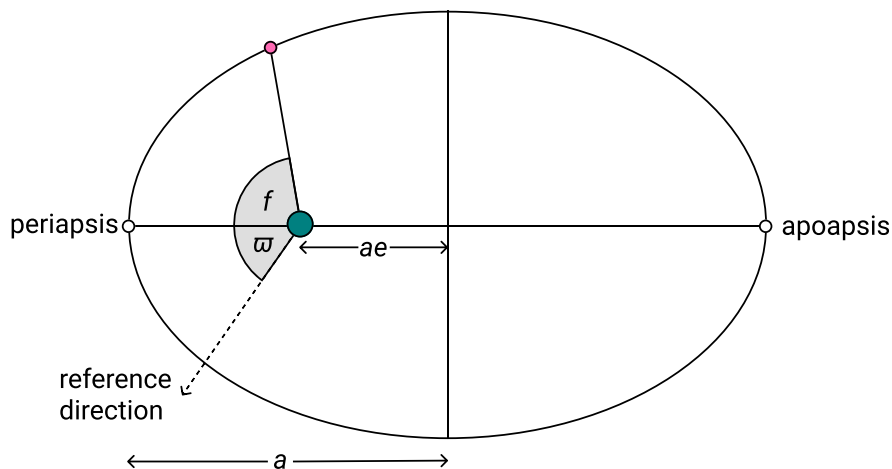


Figure 1.1: An ellipse with semi-major axis  $a$ , eccentricity  $e$ , longitude of periapsis  $\omega$ , and true anomaly  $f$ .

ellipse, by measuring its deviation from circular, and can range from 0 to 1. An eccentricity of  $e = 0$  means that the orbit is perfectly circular, while an eccentricity of 1 means that the orbit is a parabola and that the orbiting object is unbound. An eccentricity greater than  $e = 1$  means that the orbit is unbound and that it takes the shape of a hyperbola. While  $a$  and  $e$  determine the shape of the orbit, to determine its orientation requires a reference direction to measure against. In a 2D orbit the longitude of periapsis  $\omega$ , is the angle between the periapsis of the orbit and a chosen reference direction. Then to find the position of an orbiting body

at a particular time requires the true anomaly  $f$ , which is the angle between the longitude of periapsis and the current position of the orbiting body. When discussing the placement of the components in a simulation, the reference direction will be the direction of the Sun.

Figure [L.2](#) shows a similar orbit but in three dimensions. With an added dimension we require both a reference direction and a reference plane. The inclination,  $i$ , is the angle between the plane of the orbit and the reference plane. In general in the solar system the reference plane is the plane of the ecliptic, which is the plane of the Earth’s orbit around the Sun. In our case

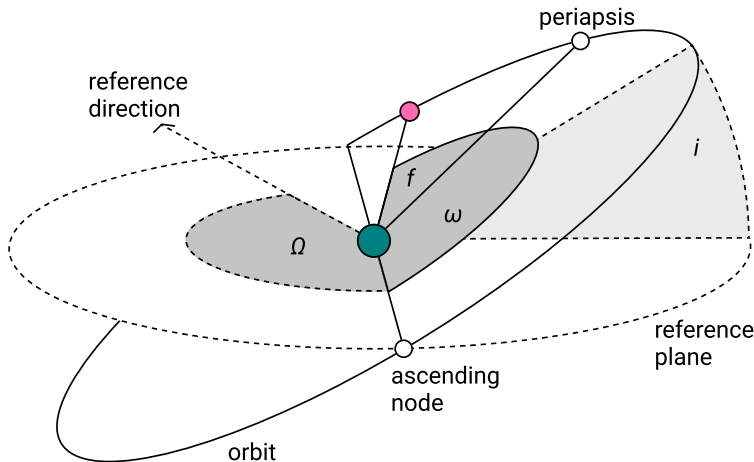


Figure 1.2: An ellipse with an inclination  $i$  with respect to a reference plane  $i$ , longitude of ascending node  $\Omega$ , argument of periapsis  $\omega$ , and true anomaly  $f$ .

we will take the reference plane to be the plane of the orbit of the binary around the Sun.  $\Omega$  gives the location of the ascending node, which is the point at which the orbit rises above the reference plane. The argument of periapsis,  $\omega$ , measures the angle between the ascending node and the periapsis, and finally the true anomaly,  $f$ , again determines the current location of the orbiting body along the ellipse by measuring the angle between the periapsis and the current position of the body.

Taken altogether these orbital elements can completely describe the orbit of two bodies around each other, and will be referred to extensively in the rest of this work.

## 1.2 The Hill Sphere

An important concept when investigating the dynamics of bodies in the outer solar system is the Hill sphere. Simply put, the Hill sphere of a body is the region in which its gravity dominates. The extent of this region is governed by several factors, and is measured in terms of its radius, known as the Hill radius. The Hill sphere of an object is not an intrinsic property of that object, but is dependant on the interaction between its gravitational field and that of a close-by more massive object. The Hill radius of an object in a circular orbit is found by

$$r_H = a \left( \frac{m}{3M} \right)^{1/3}, \quad (1.1)$$

where  $a$  is the semi-major axis of the orbit,  $m$  is the mass of the body whose Hill radius we are measuring, and  $M$  is the mass of the more massive body. Figure [L.3](#) shows the gravitational

potential in the restricted 3-body problem. The restricted 3-body problem is a simplification of the standard 3-body problem in which one of the bodies has zero mass, and will be explained in more detail in Chapter 2. For now though, what we need to recognise in the figure is that the lines represent zero velocity curves, and are paths that the third massless body would theoretically follow in the gravitational field produced by the two more massive bodies, and that the Hill sphere of the smaller massive body is the region between the  $L_1$  and  $L_2$  points. The third, massless body would need to be within this region to facilitate a stable orbit around the smaller massive body. The more massive body will have its own Hill sphere around it but we are only interested in the Hill sphere of the less massive body, because this is relevant in the case of binaries. In the solar system, the Sun is the more massive body and all objects in the solar system are by definition within its Hill sphere.

A typical planetesimal in the Kuiper belt with a radius in the order of 100 km will have a Hill radius of around  $5 \times 10^5$  km. Their great distance from the Sun results in a Hill radius that is large even though they are not particularly massive. In the case of a binary in the Kuiper belt, to remain stable one of the bodies needs to be well within the other's Hill radius. Orbits close to the full extent of the Hill radius will eventually become unstable due to perturbations from the Sun. The Hill radius will be used throughout the rest of the thesis as a useful unit of

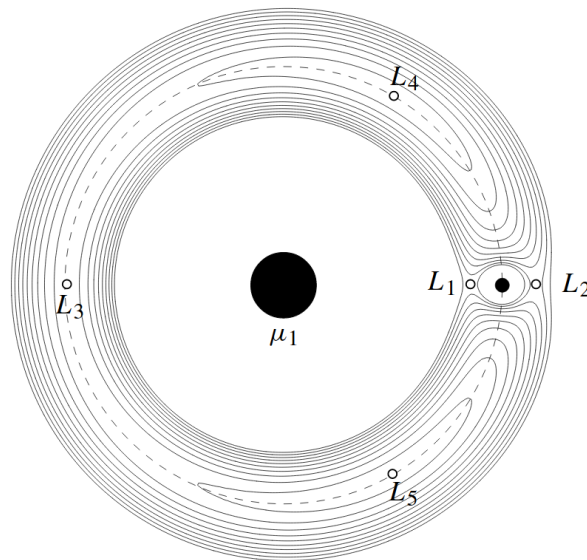


Figure 1.3: Gravitational potential in restricted 3-body problem.  $\mu_1$  is the mass of the more massive body times  $G$ . The Lagrange points are the points where the gravitational potential balances between the two more massive bodies. The Hill sphere of the smaller body lies between  $L_1$  and  $L_2$ . Image credit: [Murray & Dermott \(2008\)](#).

measurement, as a body's position in the Hill radius of another body is a determining factor in how the dynamics of the system proceed, more so than simple measurements in metres.

Figure 1.3 also shows other interesting features of possible orbits in a restricted 3-body system. The points labelled  $L_1$  to  $L_5$  are the Lagrange points, and are points where the gravitational pulls of the two massive bodies cancel each other out. Only  $L_4$  and  $L_5$  are stable enough for a body to orbit those locations. A zero mass third body placed exactly at any one of these five points should stay in the same position relative to the other two without the interference of any other perturbing force. As mentioned above, the lines represent possible paths for the

massless third body. This can lead to unusually shaped orbits, for example tadpole orbits, in which the third body orbits around the  $L_4$  or the  $L_5$  point in the shape of a tadpole. Then there are horseshoe orbits, which occur when both tadpole orbits around both  $L_4$  and  $L_5$  join up, causing a third body to appear to orbit in a horseshoe shape in the rotating frame of reference of the system. Both of these kinds of orbits occur in the solar system, for example the Jupiter Trojans (Jewitt et al. 2000).

We will now temporarily step away from gravitational dynamics to examine in more detail the environment in which the planetesimals under investigation are located.

### 1.3 The Kuiper belt

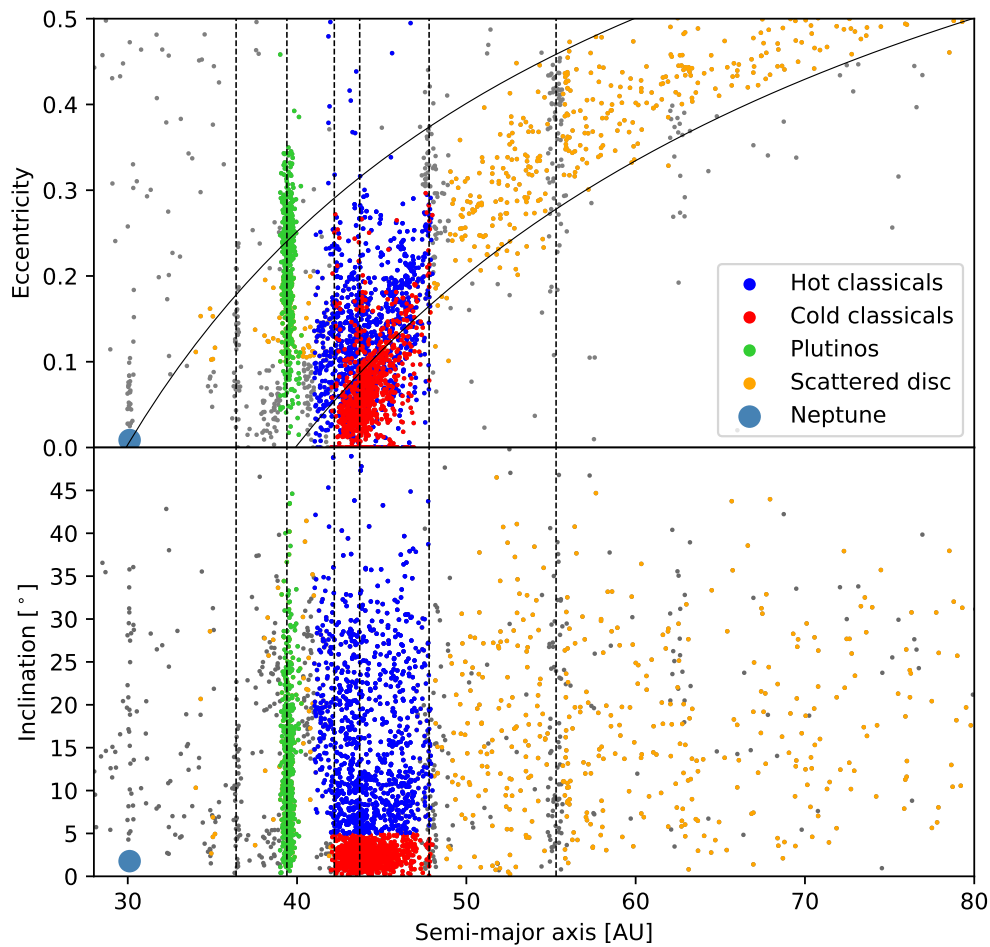


Figure 1.4: Semi-major axis, eccentricity, and inclination of objects in the Kuiper belt. The hot classicals, the cold classicals, the scattered disc objects, and the largest resonant population, the plutinos, are highlighted. Also shown is Neptune. The vertical dashed lines indicate several of the major resonances. The region between the curved lines in the top figure indicate points at which a body will have a perihelion between 30 and 40 AU. Created with data taken from <https://www.minorplanetcenter.net>.

### 1.3.1 Kuiper belt populations

We are investigating planetesimals in the Kuiper belt so it is important to become familiar with this region of the solar system, its current configuration, and its origin and evolution, as these are closely tied to the prevalence and characteristics of the binary systems located there. The Kuiper belt is a complicated and interesting region of the solar system. Figure 1.4 shows the eccentricity and inclination of many of the known Kuiper belt objects as a function of their semi-major axis. The Kuiper belt consists of objects beyond the orbit of Neptune, with semi-major axes between around 30 and 50 AU. These are not strict boundaries, and there is no precise definition of where it ends. The first Kuiper belt object discovered other than Pluto and Charon was 1992 QB<sub>1</sub> (Jewitt & Luu 1993). The distance to the Kuiper belt and the difficulty of observing objects there have made the cataloging of the bodies of the region difficult. Surveys in more recent years have discovered several thousand more objects (Elliot et al. 2005). The Kuiper belt is by convention divided up into several different sub-groups and populations, classified by their dynamical features (Gladman et al. 2008). The main groups are the resonant populations, the classical belt, and then further out, the scattered disc and the detached objects. Neptune is a dominant force in creating and maintaining the structure of the Kuiper belt.

The resonant populations contain objects in a resonant orbit with Neptune and form the most striking features of the Kuiper belt in the figure, where they can be clearly seen as vertical strips. A particularly dense resonant group are the plutinos, shown in green, of which Pluto is the largest member. Bodies in a resonant orbit with Neptune have orbital periods that are whole number ratios of the orbital period of Neptune. For example, the plutinos complete two orbits every time Neptune completes three, and as such are in a 3:2 resonance with Neptune (Jewitt & Luu 2000). There are many other resonant groups in the Kuiper belt that have different period ratios with Neptune (Malhotra et al. 2000, Millis et al. 2002).

The scattered disk contains objects with very high eccentricity, as high as 0.8, and inclinations as high as 40°, and whose perihelion bring them close to Neptune. The curved lines in the figure are the boundaries of orbits that have perihelia that are between 30 and 40 AU. Most of the scattered objects are thought to have been scattered by close approaches to Neptune (Gladman et al. 2002). There is another population of detached objects, which have extremely large semi-

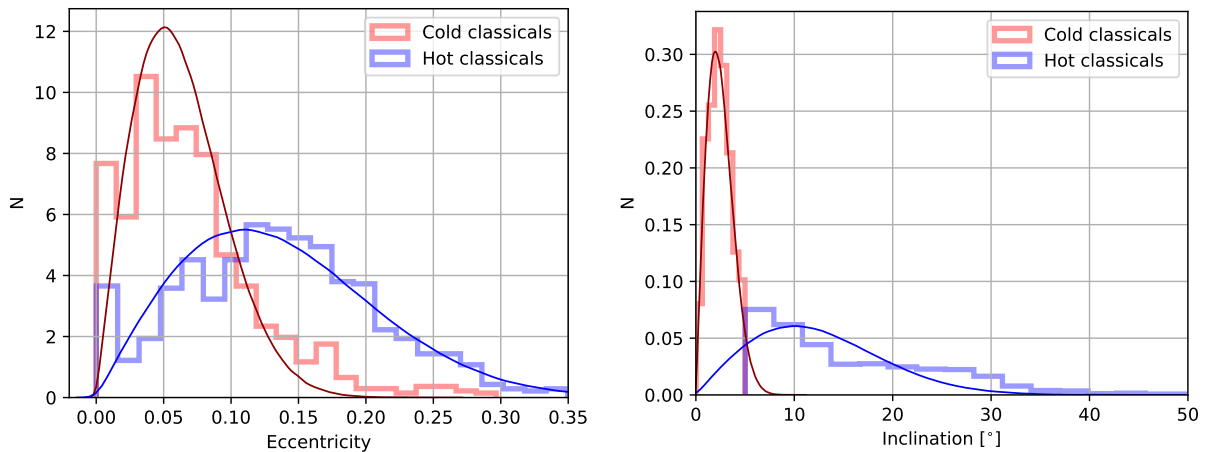


Figure 1.5: Distribution of eccentricities and inclinations in the classical Kuiper belt. The histograms roughly follow Rayleigh distributions which are overlaid. Created with data taken from <https://www.minorplanetcenter.net>.

major axes and eccentricities, that do not experience any close encounters with Neptune or any of the other giant planets (Emel'yanenko et al. 2003).

The region that is the focus of this project is the classical belt, and in particular the dynamically cold region of the classical belt. Figure 1.5 shows how the eccentricities and inclinations of the classical Kuiper belt objects are distributed. The classical belt extends from around 42 AU to 47 AU and is characterised by bodies that are not in a resonance with Neptune. They have orbits that do not bring them close to Neptune and so have relatively stable, long-lived orbits. As seen in figure 1.5 they are characterised by a bimodal inclination distribution (Brown 2001, Gulbis et al. 2010). This roughly divides it into the hot classicals and the cold classicals, with the classification based on inclination (Noll, Grundy, Stephens, Levison & Kern 2008). The division is at about  $5^\circ$  as seen in figure 1.4, and while this is not an exact cutoff, there are other physical differences between the two groups that validate this choice. We can see in figure 1.5 that there is a sudden concentration of objects once we go below around  $5^\circ$ , but there has likely been significant mixing between the two groups (Volk & Malhotra 2011). The total mass of the classical Kuiper belt is around  $0.01 M_\oplus$  (Bernstein et al. 2004).

As well as the cold classicals having low inclinations, and tending to have lower eccentricities than the hot classicals, they also have a redder colour than the hot classicals (Tegler & Romanishin 2000, Doressoundiram et al. 2001). They also tend to have a higher albedo (Brucker et al. 2009, Stansberry et al. 2008). The higher albedo means they appear brighter for a given size, and are therefore easier to detect. The difference in albedo between the two populations does not yet have an agreed upon explanation, but it is likely related to the different conditions under which they were formed (Fraser et al. 2014).

### 1.3.2 Origin of the Kuiper belt

The origin of the Kuiper belt, and the presence of the different dynamical populations there, has been a subject of interest and investigation since its discovery. The dispersion of bodies into these groups was explored in simulations (Malhotra 1993, 1995), and it was eventually shown that much of the structure could be explained by the outward migration of Neptune into a primordial disc of planetesimals, much denser than is present today in the Kuiper belt (Morbidelli et al. 2003, Gomes 2003, Levison & Morbidelli 2003), including the occupation of the resonances (Hahn & Malhotra 2005). The most influential theory explaining the outward migration of Neptune and the current structure of the Kuiper belt is known as the Nice model (Tsiganis et al. 2005, Morbidelli et al. 2005, Gomes et al. 2005). This model proposes that after the dissipation of the gas disc in the early solar system the giant planets were on orbits much closer to the Sun than their current locations. They were surrounded by a much denser disc of planetesimals than the current Kuiper belt. Gravitational interactions between the interior of the disc of planetesimals and the outer giant planets pulled the planetesimals closer to the Sun, and as angular momentum was exchanged this led to the giant planets being pushed out further away from the Sun. This effect was small as each planetesimal was much less massive than the planets, but over time the individual contributions of the planetesimals added up to a significant migration of the giant planets outwards. Planetesimals reaching in to the orbit of Jupiter found themselves thrown outwards again as a result of its larger mass and gravitational pull, leading to Jupiter migrating inwards while the outer planets migrated outwards.

This proceeded until a critical point when the orbits of Jupiter and Saturn crossed a 2:1 orbital resonance, causing an instability, and throwing Uranus and Neptune out into the disc of planetesimals in a relatively short time period. 99% of the original disc of planetesimals was scattered out of the solar system, and the remaining bodies were pushed out to the current

location of the Kuiper belt. The dynamically hot populations of the Kuiper belt, including the detached, scattered, resonant objects, and the hot classicals, are thought to have originated in this dense primordial disc closer to the Sun, and migrated to their current location. In this model the cold classicals are thought to have formed in situ. [Batygin et al. \(2011\)](#) showed that the cold classicals could have survived this injection of the inner, more dynamically hot populations intact.

How this theory of Kuiper belt formation and evolution relates to the prevalence of binaries in the different populations, as well as how it is related to this work, will be explained in section [1.6](#).

## 1.4 Binary planetesimals

We now narrow our focus to binaries in the Kuiper belt, which are the topic of this thesis. We can learn a lot about the early dynamical evolution of the Kuiper belt and the solar system as a whole by examining the structure of its different dynamical populations. Binaries are of importance as they may provide a record of dynamical encounters. The first Kuiper belt binary (other than the Pluto/Charon system) to be discovered was 1998 WW<sub>31</sub> ([Veillet et al. 2002](#)), and as of now there are around 100 known Kuiper belt binaries spread around the different dynamical populations ([Noll et al. 2020](#)). Most binaries have been discovered by the Hubble Space Telescope ([Noll, Grundy, Chiang, Margot & Kern 2008](#)). As mentioned earlier, the cold classical region of the Kuiper belt is the region we are most interested in here as it contains a higher fraction of binaries than the other Kuiper belt populations, with a binary fraction of around 30% ([Grundy et al. 2011](#)). It is possible that a much higher percentage of planetesimals in this region may have formed as binaries and were subsequently disrupted ([Fraser et al. 2017](#)). The binary fraction is relatively constant as a function of the radius of the largest component of the binary ([Nesvorny et al. 2011](#)). The cold classical belt is also home to more wide binaries than the other regions ([Parker & Kavelaars 2010](#)).

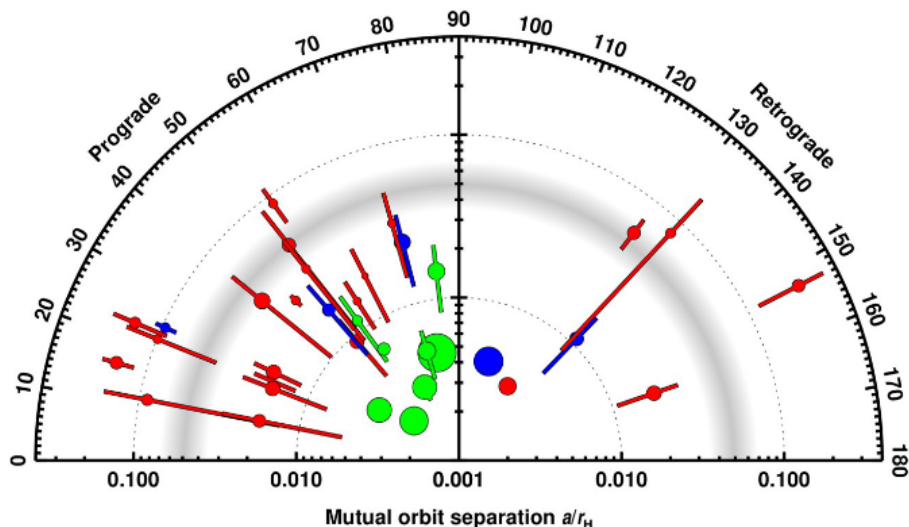


Figure 1.6: Orbital parameters of mutual orbits of known binaries. Cold classicals are shown in red, with hot classicals in blue. Also shown are centaurs, (a group of bodies closer to the Sun than the Kuiper belt) in green. Image credit: [Grundy et al. \(2019\)](#)

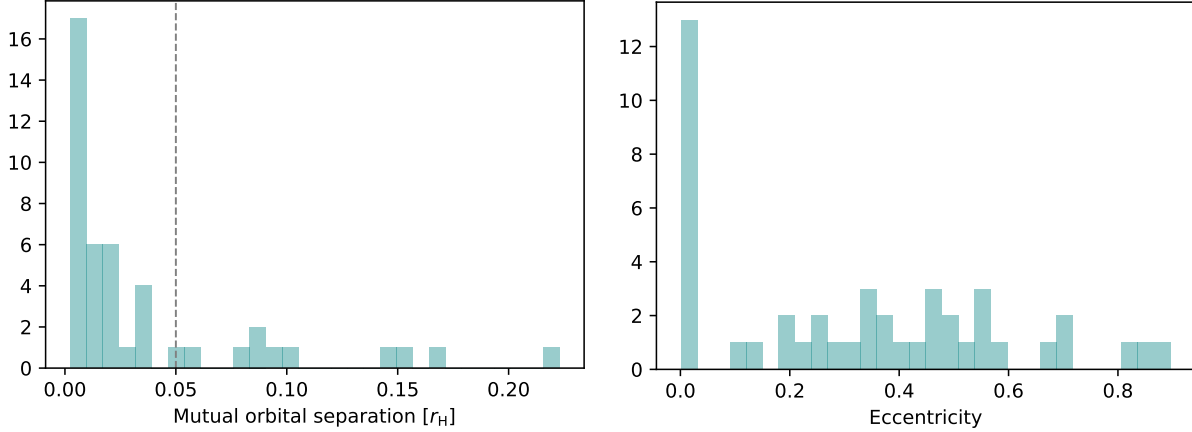


Figure 1.7: Mutual orbital separation (left panel) and eccentricity (right panel) of 45 known binary orbits. Created with data taken from [Noll et al. \(2020\)](#). The vertical dashed line indicates a rough boundary between wide and tight binaries.

A useful convention for describing the orbital separation of binaries is to measure it in terms of the Hill radius of the more massive component. As the smaller component of a binary must remain well within the Hill sphere of the more massive one to maintain a stable orbit, this system can be used to compare the orbital separation of binaries of different masses. This allows them to be divided into categories depending on their orbital separation.

Figure [1.6](#) shows the orbital characteristics of known Kuiper belt binaries. The dots indicate the semi-major axis as a fraction of the Hill radius. The outer end of the line represents the apoapsis while the inner end represents the periapsis so the length of the line gives an indication of the eccentricity of the binary. The angle of the line represents the inclination of the binary mutual orbit with respect to the ecliptic, showing that there are more binaries with prograde inclinations than retrograde. The grey shaded area at around  $0.05 a/r_H$  can be thought of as a rough division between tight and wide binaries.

Figure [1.7](#) shows the distribution of mutual orbital separation and eccentricity for binaries with known orbits. Binaries can exist with a wide range of orbital separations, but extremely wide binaries are rare ([Grundy et al. 2019](#)). The boundary between wide and tight binaries is also shown.

The wide binaries may be subject to the Kozai-Lidov effect ([Kozai 1962](#), [Lidov 1962](#)), where perturbations from the Sun will cause oscillations between their eccentricity and inclination, however, this mechanism requires a minimum inclination of  $39.2^\circ$  to be effective. There is a concentration of binaries with low mutual orbital separations, and also many binaries have very low eccentricities. The range is wide, with several having extremely large eccentricities. The eccentricities of wide binaries also indicates that they must have a rigid composition, as otherwise the eccentricity of the binary would have been damped ([Stansberry et al. 2012](#)). Binary formation can occur in a variety of ways, such as dynamical capture during encounters ([Goldreich et al. 2002](#), [Kominami et al. 2011](#)). Equal mass, widely separated binaries in the Kuiper belt are different from binaries seen elsewhere in the solar system and are probably remnants from its formation ([Nesvorný et al. 2010](#)). The matching colours of many binary components also indicate a primordial origin as opposed to any sort of component capture ([Benecchi et al. 2009](#)). It is likely that these binaries formed at the formation of the solar system from gravitational collapse of smaller particles clumped together as a result of the streaming instability ([Nesvorný](#)

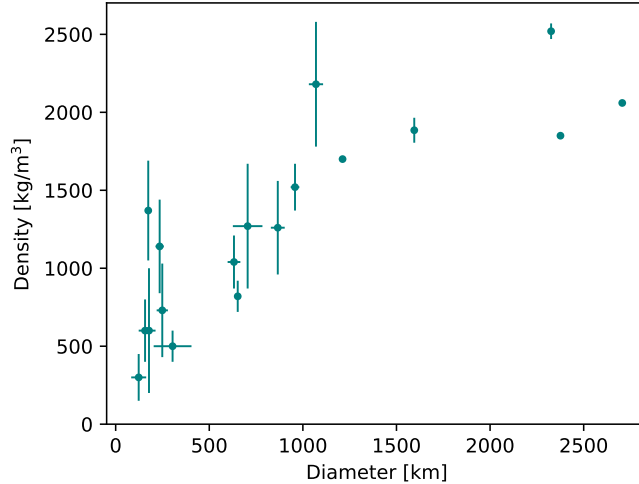


Figure 1.8: Density of several known Kuiper belt objects as a function of size. Created with data taken from [Bierson & Nimmo \(2019\)](#), [Vilenius et al. \(2014\)](#), [Stansberry et al. \(2012\)](#).

[et al. 2010](#)). This occurs in the gas disc when particles experience a drag force from the gas, causing an instability and allowing particles to clump together without the need for self-gravity. The clumps can become large enough for gravity to take over and continue growth ([Youdin & Goodman 2005](#), [Chiang & Youdin 2010](#)). This enables planetesimal formation to bypass the radial drift barrier to growth, which would cause the solid particles to drift into the Sun before colliding and increasing in size ([Johansen et al. 2007](#)). During this process, an excess of angular momentum will cause the particles to collapse into not one, but two separate clumps, which will then continue to grow and lead to the formation of a binary system ([Nesvorný et al. 2010](#)).

The mass of Kuiper belt bodies is difficult to measure accurately. To determine the mass of an astronomical object requires a measure of its gravitational field, which can be found indirectly by precise measurements of the path other objects take in its presence. In the Kuiper belt this is most easily achieved in binaries, where the orbit of the two components of the binary around each other has been used to measure the mass of both bodies ([Bierson & Nimmo 2019](#), [Vilenius et al. 2014](#)). In most of these cases the masses of binary systems have been measured by Hubble Space Telescope observations that resolve the two components of the binary ([Stansberry et al. 2012](#)). The brightness, and therefore size of these objects, has mostly been measured by the Spitzer Space Telescope, which observes in the infrared. [Figure 1.8](#) shows the size and density of Kuiper belt bodies for which there are data. The density uncertainties are quite high as it is very difficult to calculate this accurately. There does seem to be a relationship between size and density, with the larger bodies having greater densities. Because there are so few bodies with known mass in the Kuiper belt there is no exact clear relationship between size and density for these smaller bodies.

## 1.5 Contact binaries

An interesting class of objects in the solar system which may have their origin connected to binary planetesimals are contact binaries. These are small, planetesimal sized bodies that have an unusual appearance, taking the shape of what appears to be two bodies attached together. The formation mechanisms that lead to contact binaries are not yet fully understood, but they

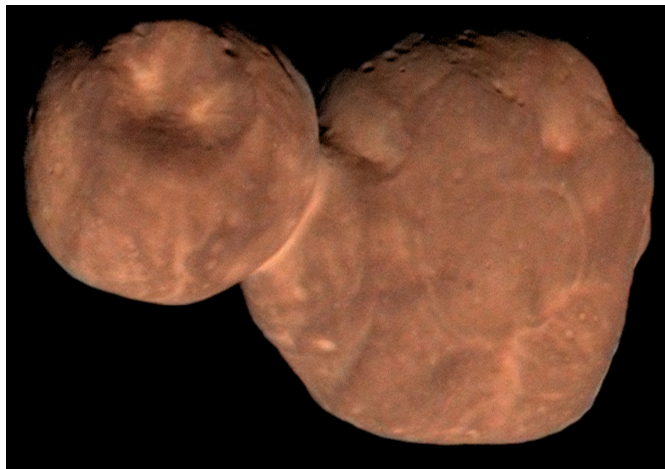


Figure 1.9: The cold classical belt object Arrokoth. The photograph was taken by the New Horizons space probe in 2019. Image credit: NASA/Johns Hopkins University Applied Physics Laboratory/Southwest Research Institute/Roman Tkachenko.

at least appear to consist of two originally separated bodies, which through further dynamical processes are drawn together and collide.

The best example of a contact binary in the Kuiper belt is the cold classical object Arrokoth, shown in figure 1.9, which was photographed by the New Horizons spacecraft in 2019 (Stern et al. 2019). Arrokoth appears to be composed of two planetesimals, one approximately 21 km long and the other approximately 15 km long (McKinnon et al. 2020). The two components are attached by a thinner neck section. It may be a pristine leftover from the formation of the solar system, meaning it has not experienced significant weathering or collisions. There is an impact crater on the smaller lobe that appears to be about 7 km across. While Arrokoth is the only cold classical object that there are high quality images of, other contact binaries have been detected by examining their light curves (Lacerda 2011, Thirouin et al. 2017, Thirouin & Sheppard 2017).

Contact binaries appear to be relatively common, particularly in the cold classical belt. The fraction of contact binaries in the Kuiper belt may be at least 10-20% (Sheppard & Jewitt 2004), and their prevalence requires an explanation. There must be a mechanism that can allow two bodies that formed separately to collide in such a way as to create a contact binary.

There are several proposed theories of contact binary formation. The already mentioned Kozai-Lidov mechanism is a phenomenon that can occur in binary orbits that are perturbed by a third large body, which can be the case in the Kuiper belt with the large body being the Sun. This in combination with gas drag has been proposed as a potential formation pathway for contact binaries (Lyra et al. 2021).

Jutzi & Benz (2016) suggest formation by repeated low velocity collisions on an elongated rotating parent body. Schwartz et al. (2018) suggest formation as a result of catastrophic collisions between much larger bodies. Rickman et al. (2015) suggest collapse to a contact binary via a gentle merger by the primordial accretion of planetesimals. Nesvorný et al. (2018) suggest initial formation as a binary and then merger via small scale impacts and gravitational encounters with planets.

## 1.6 Aim of the project

The aim of this project is to investigate how binary planetesimal systems in the Kuiper belt react to close encounters with other planetesimals.

There are several reasons why binaries are an interesting subject of investigation. The presence of wide binaries in the cold classical Kuiper belt can provide evidence about the conditions in that region of the Kuiper belt, not only now but in the past. How wide a binary is may be a determining factor in predicting its lifetime. Wider binaries will be more weakly gravitationally bound, and so should be easier to disrupt by a passing third body. We will investigate the effect on encounter outcomes that the tightness of a binary has. We are also interested in how the other orbital characteristics of a binary affect the outcome of encounters. Binaries have a range of eccentricities (Grundy et al. 2019), and this may affect binary interactions. The eccentricity of a binary may be altered during an encounter which could increase the chances of more dramatic results in subsequent encounters.

The conditions in the Kuiper belt in the past are also closely linked to the large scale dynamical evolution of the outer solar system. As per the Nice model, while the cold classicals formed close to their current location, the more dynamically hot populations of the Kuiper belt formed closer to the Sun and were pushed out to their present location by the migration of the giant planets, in particular the outward migration of Neptune. This also resulted in the loss of the vast majority of the mass of the original belt of planetesimals. It is to be expected that this push-out of the other Kuiper belt populations would have increased the encounter frequency in the cold classical region, and would have affected the composition and number of binaries there.

Another area of interest with respect to binaries is their relation to contact binaries. The exact chain of events that lead to the creation of a contact binary is not fully understood. In this project we will investigate whether encounters between binaries and impactors can lead to their formation.

It is not possible to analyse interactions such as these analytically, so numerical integrations are required. We will carry out  $N$ -body simulations using an open source  $N$ -body code called REBOUND, which will be explained in more detail in Chapter 2. We will place a binary at a distance from the Sun that would put it in the middle of the classical belt, in a circular orbit around the Sun. This binary will then be approached by a third impactor body. The characteristics of the binary will be varied, such as the mass of the two components, and their orbital separation. These will be set to correspond with likely conditions in the Kuiper belt. The mass and impact parameter of the impactor will be varied.

We will also perform an analysis where we follow one particular binary over the course of its evolution. We will pick specific starting conditions for a binary which are typical for those in the Kuiper belt and then subject it to encounters with other bodies, while using the results of each encounter as the starting conditions for the next simulation. The impact parameter will be drawn randomly and the impactor size will represent the size distribution of objects in the Kuiper belt.

In the rest of the thesis the terms primary and secondary are used to refer to the two components of the binary. In cases where one of the components is more massive than the other, it will be the primary. In cases where both components have the same mass the labels will still be used for simplicity. The term impactor will be used for the third body entering the system.

Simulations of this kind have been carried out in the case of stellar binaries (Weinberg et al. 1987). Our model has the added complication of the Sun at the centre, which requires calculations of Keplerian orbits around the Sun, and the size of the Hill radius. This creates a

much different scenario than that within which only the stars themselves are interacting with each other.

Encounters between satellites on circular orbits around a third much more massive body have been investigated before (Petit & Henon 1986). We build on that work with similar simulations, but with encounters between a binary and another third body, in orbit around a fourth more massive one, as opposed to two small bodies interacting while in orbit around a third more massive one.

We will also check how encounters alter the eccentricity of binaries in the Kuiper belt. As mentioned earlier, a range of eccentricities are present in the binaries located there. If the encounters we investigate serve to change the eccentricity of a binary in a predictable way, that could be compared to the actual eccentricities of observed binaries. Perhaps non-catastrophic encounters have the effect of pumping up the eccentricity of a binary to the point where it is much more susceptible to being disrupted. Higher eccentricities could also then be translated into higher inclinations via the Kozai-Lidov effect.

# Chapter 2

## Methods

$N$ -body calculations find the change in an objects acceleration as a result of the gravitational influence of all other bodies in the simulation. In our case we are dealing with 4-body simulations. Analytical solutions are not possible in systems with more than two bodies, however there have been several simplifications to the 3-body problem. One simplified version of the 3-body problem, where there is a hierarchy of masses in the three bodies, was described by Hill (1878). The Hill approximation simplifies the setup but does not require that the smallest mass is a point mass, only that it is much smaller than the next largest.

$$m_1 \gg m_2 \gg m_3. \quad (2.1)$$

In this restricted 3-body problem there are characteristics of the system that remain constant. The Jacobi integral gives a measure of the energy of the system that will remain constant, and is given by

$$C_J = n^2(x^2 + y^2) + 2 \left( \frac{\mu_1}{r_1} + \frac{\mu_2}{r_2} \right) - \dot{x}^2 - \dot{y}^2 - \dot{z}^2, \quad (2.2)$$

where  $n$  is the period of the orbit of the binary,  $\mu_1$  and  $\mu_2$  are the standard gravitational parameters of the two more massive bodies,  $r_1$  and  $r_2$  are the distances of the smaller body from the two more massive ones, and  $x$ ,  $y$ , and  $z$  represent the position of the smaller body.

This restricted 3-body problem does not fit with our case, but Petit & Henon (1986) presented an approximation that only requires that both  $m_2$  and  $m_3$  are small compared to  $m_1$ ,

$$m_1 \gg m_2, m_1 \gg m_3. \quad (2.3)$$

This approximation can be applicable to our 4-body problem in certain situations. When the impactor lies far outside the combined Hill sphere of both components of the binary, and for a large impactor when the binary is far outside its Hill sphere, then the binary may be treated as a single body, and the system can be reduced to the simplified 3-body problem described by Petit & Henon (1986). When the impactor has a close encounter with the binary this approximation breaks down completely.

We know that much of the structure of the current day Kuiper belt is likely to be the result of planetary migration, particularly the push-out of Neptune into the primordial disc of planetesimals, and that the resonant populations of the Kuiper belt have their orbits closely linked to that of Neptune. In light of this it is worth considering whether it is necessary to include Neptune in any investigation of dynamics in the classical belt. We can look at the Hill radius of Neptune which is

$$r_H = a \left( \frac{m}{3M} \right)^{1/3} = 0.77 \text{ AU}, \quad (2.4)$$

where  $a$  is the semi-major axis of Neptune’s orbit around the Sun, and is  $a = 30$  AU, the mass of Neptune is  $m = 1.02 \times 10^{26}$  kg, and the mass of the Sun is  $M = 2.00 \times 10^{30}$  kg. This is the largest Hill radius of any body in the solar system, but is  $\sim 20$  times smaller than the distance from Neptune to the classical Kuiper belt. This allows us to safely exclude Neptune from individual encounters which take place over a short timescale.

In  $N$ -body simulations the equation that needs to be integrated to move the bodies is

$$\frac{d\mathbf{x}_i}{dt} = - \sum_{i \neq j}^n \frac{Gm_j(\mathbf{r}_j - \mathbf{r}_i)}{|\mathbf{r}_j - \mathbf{r}_i|^3}, \quad (2.5)$$

where the acceleration of body  $i$  is found from the positions,  $\mathbf{r}$ , and masses,  $m$ , of all other bodies. There are many different methods of integrating these equations. In this project we used REBOUND (Rein & Liu 2011) an open source  $N$ -body code designed for collisional dynamics and for straightforward  $N$ -body problems. REBOUND offers several different integrators with different advantages and disadvantages, but in our case we used IAS15 (Rein & Spiegel 2015), which is a fifteenth order integrator that has an adaptive timestep. IAS15 is both faster and more accurate than symplectic integrators and other high-order integrators, and is the fastest that REBOUND offers. The adaptive timestep allows us to capture close encounters, which we expect to occur in our simulations. When two bodies in the simulation approach each other, the calculation of the position and velocity of each component must be carried out more frequently, and an adaptive time-step accounts for this by increasing the frequency of integrations as two bodies approach each other. While a shorter time-step is always going to be more accurate, when the bodies in the simulation are not close to each other it will be a waste of processing power and take much longer for the simulation to be completed. This is why an adaptive time-step allows for a balance between a quicker simulation time and increased accuracy for close encounters.

We will be varying the the size of the bodies in our simulations, and so need a density to calculate their masses. As shown in figure 1.8, the density of Kuiper belt objects shows a tendency to increase with the size of the object. We could quantify this relationship and use this to give each component of the encounter a different density based on its radius, however, the objects we are investigating are around 100 km in radius, and at these smaller sizes in figure 1.8 the uncertainties become large, and there is no clear relationship. Instead of recalculating a different density for each object, we decided to pick a single constant density of  $700 \text{ kg m}^{-3}$  for all the objects in the simulations. This value is approximately the mean of the densities of bodies with diameters less than 500 km in figure 1.8. While this may not be an accurate representation of all similarly sized Kuiper belt planetesimals, it should not change our results in a significant way. Using a different value for the density would result in the same mass ratios between all objects. Although we did not investigate this thoroughly, there may be a tiny difference in collision frequency as bodies of a given mass will have different radii, allowing, for example, previous near misses to become glancing collisions.

## 2.1 Simulation setup

### 2.1.1 Placement of components

We know that we want to solve a 4-body problem, but now we need to correctly place all four components and initialize their velocities. We have the Sun, the primary, the secondary, and the impactor. REBOUND allows particles to be added to simulations using orbital elements, where

each is added in sequence, and with respect to the previously added particle. Figure 2.1 shows the result we are trying to achieve from a top down 2D perspective. We start by placing the

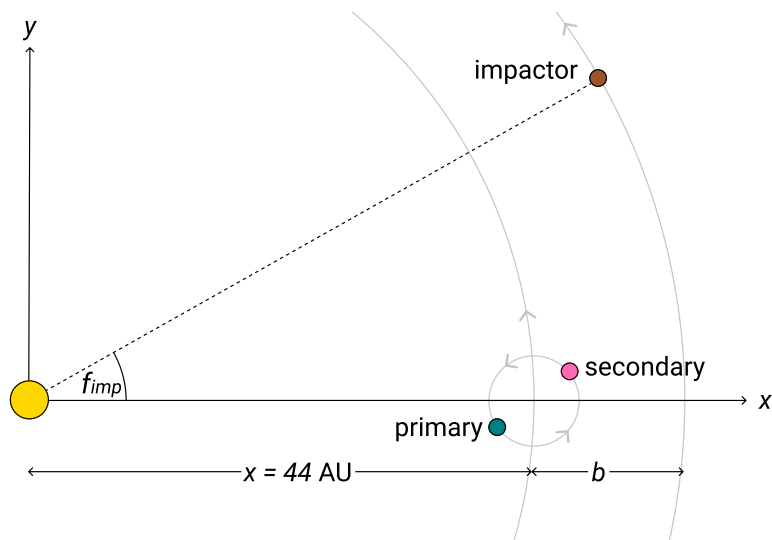


Figure 2.1: Position of bodies before encounter.

Sun at the origin, then the primary is added with respect to the Sun with a semi-major axis of  $a = 44$  AU, and eccentricity  $e = 0$ . This will place it at  $(x = 44 \text{ AU}, y = 0)$ . The secondary is added with respect to the primary with mutual orbital separation  $a_{\text{bin}}$ , eccentricity  $e_{\text{bin}}$ , true anomaly  $f_{\text{bin}}$ , argument of periapsis  $\omega_{\text{bin}}$ , obliquity  $i_{\text{bin}}$ , and longitude of ascending node  $\Omega_{\text{bin}}$ . We refer to the inclination of the secondary with respect to the primary as the obliquity to distinguish it from the inclination of orbits around the Sun.

The centre of mass of the binary will maintain a circular orbit around the Sun. If the masses of the primary and the secondary are  $m_{\text{prim}}$  and  $m_{\text{sec}}$  respectively, this will place them either side of the centre of mass of the binary with their distance from the centre depending on their relative masses.

$$x_{\text{prim}} = -\frac{m_{\text{sec}}}{m_{\text{prim}} + m_{\text{sec}}} \times a_{\text{bin}} \quad (2.6)$$

$$x_{\text{sec}} = \frac{m_{\text{prim}}}{m_{\text{prim}} + m_{\text{sec}}} \times a_{\text{bin}} \quad (2.7)$$

The average orbital speed of the primary and secondary around each other will be

$$v_{\text{orb}} = \sqrt{\frac{G(m_{\text{prim}} + m_{\text{sec}})}{a_{\text{bin}}^3}}, \quad (2.8)$$

and for the individual bodies this will be

$$v_{\text{orb,prim}} = -\frac{m_{\text{sec}}}{m_{\text{prim}} + m_{\text{sec}}} \times v_{\text{orb}}, \quad (2.9)$$

$$v_{\text{orb,sec}} = \frac{m_{\text{prim}}}{m_{\text{prim}} + m_{\text{sec}}} \times v_{\text{orb}}. \quad (2.10)$$

The Keplerian velocity of the centre of mass of the binary is

$$v_{\text{K}} = \sqrt{\frac{GM_{\odot}}{a}}. \quad (2.11)$$

The initial velocities of the primary and the secondary will be  $v_K$  plus their own individual mutual orbital velocities. This will result in a stable binary orbiting the Sun, with each component orbiting each other. For a non-zero binary eccentricity the initial velocities will be different. The initial velocity of each body if they are started at the apoapsis with eccentricity  $e_{\text{bin}}$  will be

$$v_{\text{orb}} = \sqrt{G(m_{\text{prim}} + m_{\text{sec}}) \left( \frac{2}{r_a} - \frac{1}{a_{\text{bin}}} \right)}, \quad (2.12)$$

where the apoapsis of the mutual orbit is

$$r_a = a_{\text{bin}}(1 + e_{\text{bin}}). \quad (2.13)$$

The next step is to add the impactor. We want to add it in a location that will result in a close encounter with the binary. We first move to the centre of mass of the system, which is now the Sun, as the impactor will be placed in orbit around the Sun. For the simple case where the impactor is on a circular orbit, all that is required to create an encounter is an impact parameter  $b$ , and a true anomaly for the impactor  $f_{\text{imp}}$ , as illustrated in figure 2.1. An inclination can be added to the impactor's orbit around the Sun, or to the mutual orbit of the binary components around each other. Figure 2.2 shows this setup in 3D with the added inclinations. As shown in the image, the plane of reference is always the plane of the orbit of the centre of mass of the binary around the Sun, and the inclination of the impactor and the obliquity of the binary are always measured with respect to this plane. We now need an encounter timescale that is long

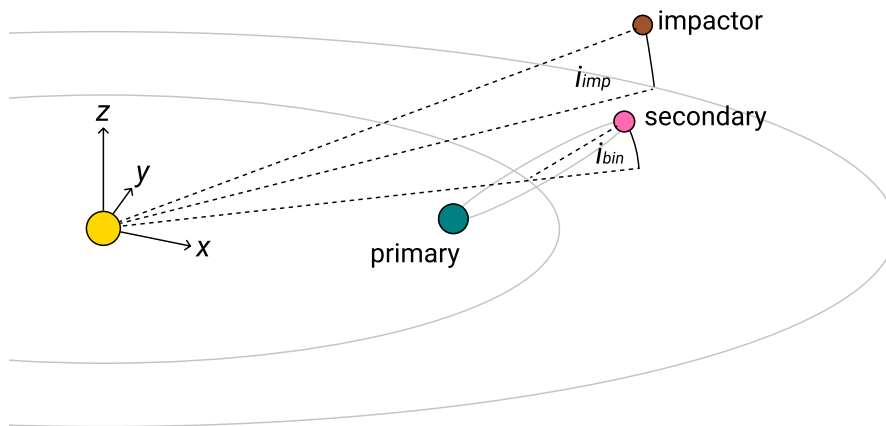


Figure 2.2: Example of binary before encounter with impactor.

enough to allow us to capture the entire encounter. The orbital period of the binary around the Sun is

$$P_{\text{orb}} = \frac{2\pi}{\Omega_K} = 292 \text{ yr}, \quad (2.14)$$

where

$$\Omega_K = \sqrt{\frac{GM}{a^3}}. \quad (2.15)$$

The impact parameter of the impactor will affect the time required for the encounter to occur. The difference in orbital velocity between the binary and the impactor is found with the Keplerian shear.

$$v_{\text{shear}} = -1.5\Omega_K b, \quad (2.16)$$

where  $b$  is the impact parameter of the impactor. The relative velocity is proportional to the impact parameter, so smaller impact parameters require longer simulation times. For example, if the initial impact parameter of the impactor is halved, then its relative approach velocity will also fall by half, and the simulation time will need to be doubled to record the entire encounter. This is a useful consideration as these simulations can be computationally expensive, and we want to focus on the encounters. More massive impactors will also have to be initialized further from the binary as their larger mass will mean that their gravitational sphere of influence will be greater. Without a larger initial  $y$  component with respect to the binary there could be the nonphysical effect of the impactor appearing to suddenly materialize and suddenly change the gravitational potential around the binary.

Figure 2.3 shows the basic setup of a typical simulation in the frame of reference of the orbiting binary. The units of the plot are in terms of the Hill radius of the primary. The two components of the binary are in a mutual orbit around each other, and the centre of mass of the binary is on a circular orbit around the Sun at 44 AU. The obliquity of the binary is  $i_{\text{bin}} = 0$ . The impactor is on a higher orbit, further away from the Sun than the binary, with an impact parameter  $b = 3 r_H$ , and with  $e = 0$  and  $i = 0$ . The frame of reference of the plot begins centred on the initial location of the centre of mass of the binary and then follows that reference point as it orbits the Sun. The Sun is always on the left of the plot. The circles around each body represent the extent of their Hill Sphere. The initial mutual orbital separation of the binary in this case is  $0.4 r_H$ .

In this example the impact parameter is positive, and so the impactor appears to approach on the right in the rotational frame of reference of the binary, as the higher orbit means a slower orbital velocity is required to maintain a circular orbit. A negative impact parameter would mean a lower orbit which would result in a faster orbital velocity, making the impactor appear to approach from the bottom left in this frame of reference.

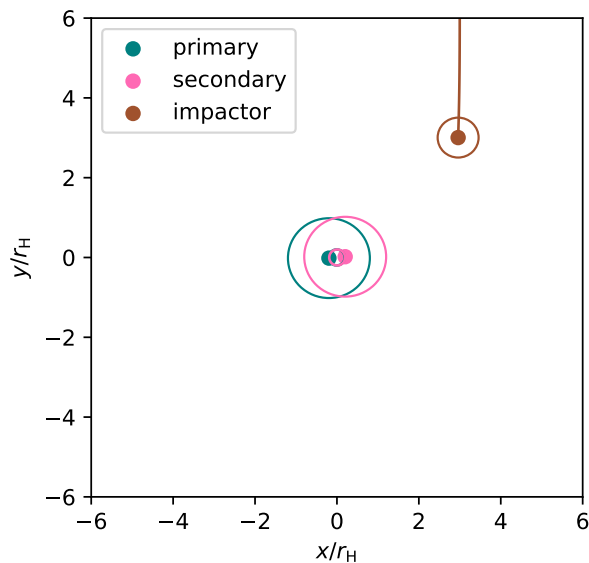


Figure 2.3: Example of binary before encounter with impactor. The impactor approaches from the top right of the figure. The circles around each body indicate the extent of their Hill sphere.

### 2.1.2 Timing encounters with eccentric and inclined orbits

When  $e = 0$  and  $i = 0$  for both the binary and the impactor then encounters will always eventually occur as long as the impact parameter is small enough. If the orbit of the impactor has an inclination with respect to the binary, then further calculations are required to engineer a close encounter, or the impactor and the binary will pass by each other at a great distance. The encounter needs to occur when the impactor passes through the plane of the orbit of the binary. If the closest approach of the impactor to the binary occurs at a different time, then the impactor will pass by the binary much too far away to have any effect. For a low inclination of  $1^\circ$  at 44 AU the impactor will be at its furthest from the plane of the ecliptic at 44 AU  $\times \sin 1^\circ = 0.8$  AU, or about 300 times the Hill radius of the primary. We therefore need to make sure the encounters occur at the closest approach of the two orbits. Figure 2.4 shows that in two circular orbits with non-zero inclination with respect to each other, the only two points where close encounters can occur are the nodes of the orbit. In the case of a positive impact

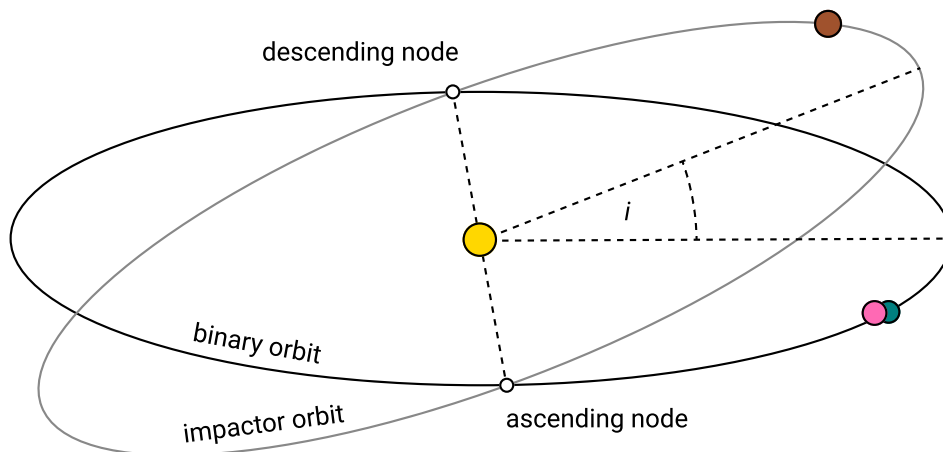


Figure 2.4: Two orbits with  $e = 0$  and non-zero inclination with respect to each other will only have two possible locations for close encounters to occur.

parameter, the impactor will be on a slightly higher orbit and the time it takes to reach the descending node will be different to the time it takes the centre of mass of the binary to arrive at the same point. The mean motion of the binary around the Sun will be

$$n_{\text{bin}} = \sqrt{\frac{GM_{\odot}}{a^3}}. \quad (2.17)$$

For the simple case where the impactor is also on a circular orbit with impact parameter  $b$ , its mean motion will be

$$n_{\text{imp}} = \sqrt{\frac{GM_{\odot}}{(a+b)^3}}. \quad (2.18)$$

If we decide that we wish the encounter to occur at  $\pi$  rad from the starting position of the binary, that means we need the descending node to be located at  $\pi$ . The time after beginning the simulation that the encounter will occur is the time it takes the binary to reach  $\pi$ ,

$$t_{\text{enc}} = \frac{\pi}{n_{\text{bin}}}. \quad (2.19)$$

The angle that the impactor will cover in this time is  $\theta = t_{\text{enc}} \times n_{\text{imp}}$ , so the impactor will need to be placed at an initial position of  $f_{\text{imp}} = \pi - \theta$ . In this way both the binary and the impactor will arrive at the descending node at the same time. The higher the inclination of the impactor the greater the relative encounter velocity will be at this point. Things become more complicated when the impactor has a non-circular orbit. In all of our experiments the eccentricity of the centre of mass of the binary is zero, but we can vary the eccentricity of the impactor. Figure 2.5 shows the intersection points of two orbits around the same focus with zero inclination and two different eccentricities. In this setup there are only two possible intersection points. To engineer

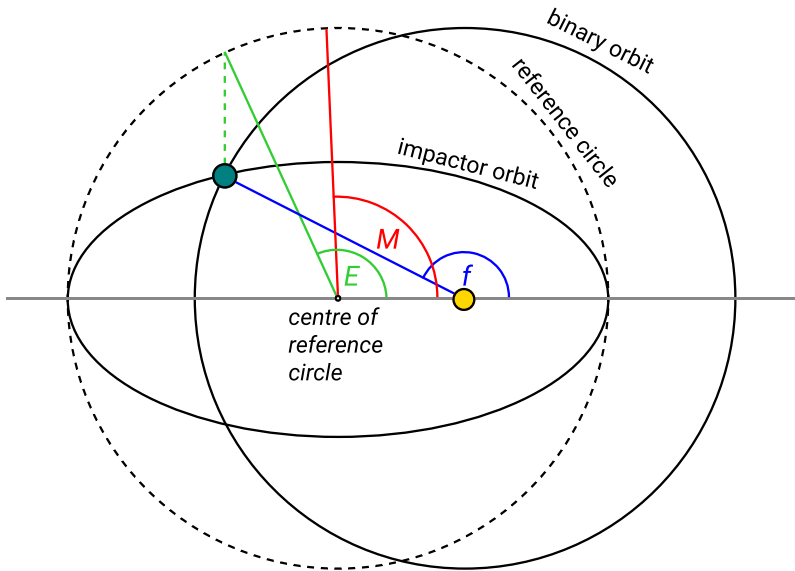


Figure 2.5: Overlapping orbits with  $e = 0$  and  $e = 0.5$ . The true anomaly  $f$ , the eccentric anomaly  $E$ , and the mean anomaly  $M$ , of the impactor at the intersection of the two orbits are shown.

a close encounter the true anomaly of the impactor will have to be the same as the true anomaly of the binary at the crossover point, and this will also have to be the descending node of the impactor's orbit around the Sun. The true anomaly at this point can be found from the radial equation for an eccentric orbit. The intersection will be at the point where the radial distance of the impactor from the Sun is equal to its own semi-major axis. The radial equation is

$$r = \frac{a(1 - e^2)}{1 + e \cos f}, \quad (2.20)$$

where  $f$  is the true anomaly,  $a$  is the semi-major axis of the binary centre of mass, and  $r$  is the instantaneous distance between the Sun and the impactor. Rearranging for  $f$ ,

$$f = \cos^{-1} \left( \frac{r(1 - e^2)}{ea} - \frac{1}{e} \right). \quad (2.21)$$

As the encounter will occur at  $r = a$  then this equation simplifies to  $f = \cos^{-1}(-e)$ . We need to ensure that the impactor arrives at this point at the same time as the binary, so we need the time it takes for the binary to reach this point, then use this time to find the correct starting position for the impactor. This time is  $t_{\text{enc}} = f/n_{\text{imp}}$ , but to track the progress of the impactor back

through time the true anomaly is not sufficient. As the angular speed of an eccentric orbit is not constant, the true anomaly needs to be converted to the mean anomaly, which does change at a constant rate. The three anomalies used to locate a body's path on an elliptical orbit are shown in figure 2.5. To convert the true anomaly to the mean anomaly, first the eccentric anomaly needs to be found,

$$\tan E = \frac{\sqrt{1 - e^2} \sin f}{e + \cos f}. \quad (2.22)$$

And then the mean anomaly can be found with Kepler's equation,

$$M = E - e \sin E. \quad (2.23)$$

The mean anomaly of the impactor when the binary begins at  $x = 44$  AU and  $y = 0$  is then

$$M_0 = n_{\text{imp}} \times t_{\text{enc}} + M, \quad (2.24)$$

where  $n$  is the mean angular motion of the impactor. This new  $M_0$  needs to be transformed back through the eccentric anomaly to the true anomaly to give the required starting position of the impactor that will lead to a close encounter. The transformation from  $M_0$  back to the initial  $E_0$  using Kepler's equation has no closed form solutions, and needs to be solved numerically. With  $E_0$  the initial true anomaly is then

$$f_0 = \tan^{-1} \left( \frac{\sqrt{1 - e^2} \sin E_0}{\cos E_0 - e} \right) \quad (2.25)$$

With this value of  $f_0$  we will always have an encounter at  $\pi$  rad no matter what combination of  $e$  and  $i$  the binary has. This is illustrated in figure 2.6 where an impactor with large eccentricity

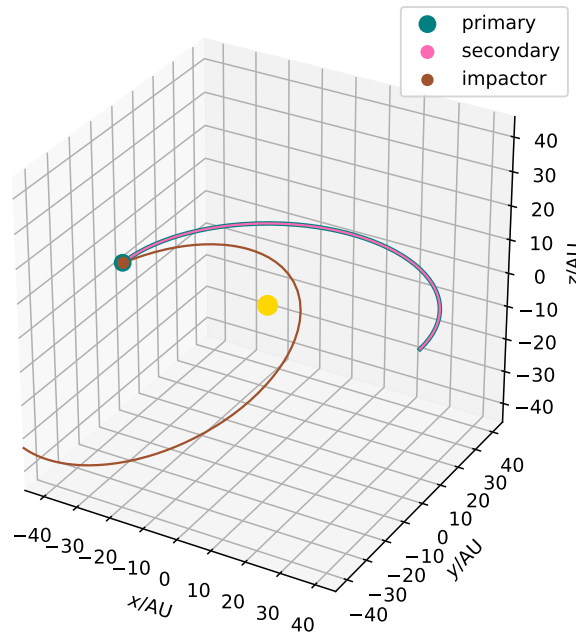


Figure 2.6: Close encounter at  $\pi$  rad between a binary on a circular orbit and an impactor with  $i = 80^\circ$  and  $e = 0.8$ .

and inclination has a close encounter with the binary. Encounters between the binary and impactors with non-zero eccentricity or inclination will have greater encounter velocities and shorter encounter timescales.

## 2.2 Computing orbital elements

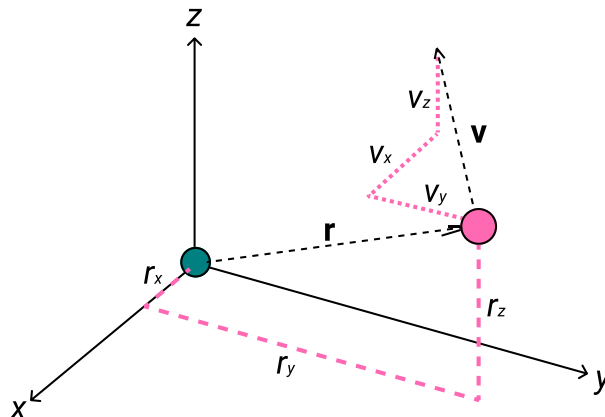


Figure 2.7:  $\mathbf{r}$  and  $\mathbf{v}$ , the position and velocity vectors of secondary relative to primary.

During an encounter we record the position and velocity of each particle at every time-step, and then these vector quantities can be used to calculate the semi-major axis, eccentricity, and inclination. We need to transform these vectors into the required orbital elements. We define the position vector of the secondary relative to the primary as  $\mathbf{r}$ , and the velocity vector of the secondary as  $\mathbf{v}$ , as in figure 2.7.

First we need to calculate the specific relative angular momentum of the binary directly from the position and velocity vectors,

$$\mathbf{h} = \mathbf{r} \times \mathbf{v}. \quad (2.26)$$

We can then use this to calculate the eccentricity vector,

$$\mathbf{e} = \frac{\mathbf{v} \times \mathbf{h}}{\mu} - \frac{\mathbf{r}}{|\mathbf{r}|}, \quad (2.27)$$

where  $\mu$  is the standard gravitational parameter,  $\mu = G(m_{\text{prim}} + m_{\text{sec}})$ . The eccentricity is then the magnitude of this:  $e = |\mathbf{e}|$ . To calculate the semi-major axis we need the specific orbital energy of the binary. For a two body system with gravitational parameter  $\mu$  this is found with

$$E = \frac{v^2}{2} - \frac{\mu}{r}, \quad (2.28)$$

where  $r$  is distance between the two bodies, or the magnitude of the position vector, and  $v$  is the magnitude of the velocity vector. The specific orbital energy is also given by  $E = -\mu/2a$ , so we can rearrange this and use it to find the semi-major axis,

$$a = -\frac{\mu}{2E}. \quad (2.29)$$

To find the inclination we require the specific angular momentum again. The specific angular momentum of an orbit is perpendicular to the plane of the orbit. As the  $z$  component of this is relative to the reference plane we want to measure against to find the inclination, we can use the magnitude of the specific angular momentum and its component in the  $z$  direction.

The inclination is then found with

$$i = \arccos \frac{h_z}{|\mathbf{h}|}. \quad (2.30)$$

Armed with the positions and velocities of all the bodies in the system, and with the orbital elements of each pair of particles with respect to each other, we can better understand how encounters proceed and how they affect these parameters.

### 2.3 Effects of impactor on binary

We can engineer encounters and calculate the orbital properties as a result of these encounters, but now we look at what are the effects that an encounter can have on a binary. An encounter between a binary and an impactor will affect the orbital parameters and energy of the binary. The gravitational force holding the two components together is

$$F = G \frac{m_{\text{prim}} m_{\text{sec}}}{a_{\text{bin}}^2}. \quad (2.31)$$

The angular momentum of the system is

$$\mathbf{h} = \mathbf{r} \times \mathbf{v}, \quad (2.32)$$

where  $\mathbf{r}$  and  $\mathbf{v}$  are the position and velocity vectors of each component with respect to the centre of mass of the binary system. The total energy of the system is the sum of the kinetic energy of both bodies and the gravitational potential energy,

$$E = \frac{1}{2} m_{\text{prim}} v_{\text{prim}}^2 + \frac{1}{2} m_{\text{sec}} v_{\text{sec}}^2 - G \frac{m_{\text{prim}} m_{\text{sec}}}{a_{\text{bin}}}. \quad (2.33)$$

For a binary to remain bound this total energy must be negative. As energy is conserved the only way for the total energy of the system to change is for the addition of a third body. Any encounter between this binary system and a third body has the potential to alter the binding energy. In a typical encounter the impactor approaches from infinity, or from a distance where its gravitational pull diminishes to insignificance. As the impactor approaches the binary, its gravitational effect on the binary will increase.

[Heggie \(1975\)](#) describes binary encounters in the context of stars. While the type of binary encounters that we are investigating have the added complication of the Sun at the centre, these encounters with stars are helpful in forming a system of classifying encounters between planetesimals. They describe an encounter between a binary and a third body, in which the third body begins at infinity with velocity  $v_0$ , approaches and flies past the binary, and then continues on to infinity with new velocity  $v_1$ . The velocity of the third body changes during the encounter, and the total binding energy of the binary is also changed. If the initial total binding energy of the binary is  $E_0$ , and the final binding energy is  $E_1$ , and the masses of all three bodies are the same, conservation of energy in the rest frame of the centre of mass of the three bodies means

$$\frac{1}{3} m v_1^2 = \frac{1}{3} m v_0^2 + (E_1 - E_0). \quad (2.34)$$

If the change in binding energy,  $E_1 - E_0$ , is greater than zero, or is less than zero but greater than  $-\frac{1}{3} m v_0^2$ , then the impactor will escape the encounter. If in this second case we also have  $-E_0 < (E_1 - E_0)$ , then the binary will survive the encounter. If  $-\frac{1}{3} m v_0^2 < (E_1 - E_0) < -E_0$

the binary is destroyed. To create a new binary requires that both the binary is destroyed and that the impactor does not escape to infinity, or that  $-\frac{1}{3}mv_0^2 > (E_1 - E_0)$ , although even with these criteria satisfied a new binary is not guaranteed.

We can also have the passing impactor remove enough energy and angular momentum from the system that the two components of the binary collide. As the angular momentum of the binary is decreased the two components will slow down and their mutual orbital separation will decrease, which in extreme circumstances could lead to the two components colliding. Collisions between any two of the three bodies during the course of the encounter are possible, and collisions will be described in more detail in the next section. As well as quantities such as energy and angular momentum changing as a result of encounters, the eccentricity and other orbital elements of the binary can be affected. Illustrations of the different possibilities will be shown in section [3.1](#), with examples of encounters and their outcomes.

A critical component influencing the results of an encounter will be the encounter timescale. For an impactor to have a significant effect on the binary will require an encounter time low enough for the processes described here to take place. If the encounter speed is too high, then the encounter timescale will be too low, and the impactor will pass by the binary without affecting it. For circular orbits with different semi-major axes the encounter speed can be found with the Keplerian shear,

$$v_{\text{shear}} = -1.5\Omega_K b, \quad (2.35)$$

where  $\Omega_K$  is

$$\Omega_K = \sqrt{\frac{GM}{a^3}}, \quad (2.36)$$

where  $a$  is the semi-major axis of the binary orbit around the Sun.  $v_{\text{shear}}$  is proportional to the impact parameter so the encounter velocity goes up linearly with  $b$ . This only holds for the simple case of two circular orbits in the same plane. In our simulations the eccentricity of the binary around the Sun is always zero, but the eccentricity of the impactor, and the inclination of the impactor's orbit with respect to the orbit of the binary around the Sun, can take non-zero values. The velocity of an impactor with a non-zero eccentricity and inclination relative to a binary with a circular orbit can be estimated as [\(Lissauer & Stewart 1993\)](#)

$$v = (e^2 + i^2)^{1/2} v_K, \quad (2.37)$$

where  $v_K$  is the Keplerian velocity of the binary. This shows that the encounter velocity becomes large quickly as eccentricity or inclination increase.  $v_K$  at 44 AU is  $4490 \text{ m s}^{-1}$  so an eccentricity of 0.1 would mean an encounter velocity of  $449 \text{ m s}^{-1}$ .

## 2.4 Collisions

When observing close encounters such as these, we want to track and record any collisions that occur. We first have to decide on how to handle such collisions. The possibilities available in REBOUND are that the bodies can bounce off each other, or that they can merge, creating a new body and conserving mass and momentum. Neither of these is an exact physical analogue to how collisions actually occur. The consequences of collisions are not the focus of the project, and while we are interested in the physics of collisions, we are not as concerned with what happens after a collision, and can classify the encounter as complete at that point. Therefore we just want to record the position and velocity vectors of both bodies at the moment of any collision so that we can quantify it. During a collision between two bodies it is helpful to consider one of

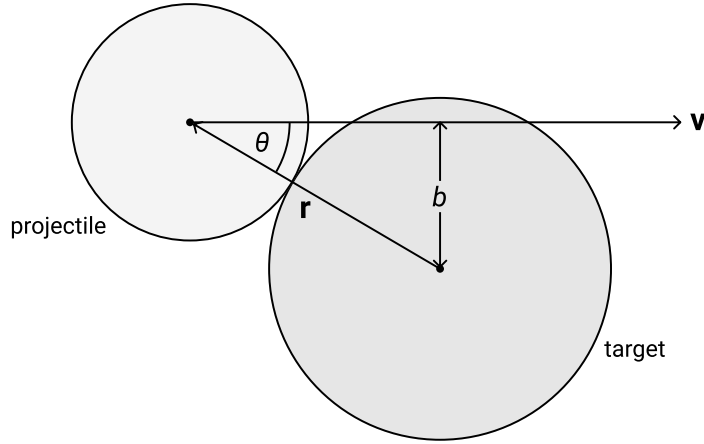


Figure 2.8: Schematic of the collision of two bodies in the frame of reference of the target body. The reference frame is chosen so that the target is at rest and so that the velocity vector  $\mathbf{v}$  of the projectile is horizontal going from left to right.

the bodies as stationary, and the other body as moving in this reference frame. Figure 2.8 shows the geometry of such an impact. [Leinhardt & Stewart \(2012\)](#) provide a conceptual framework for thinking about collisions between planetesimals. Here the body at rest is referred to as the target, and the body impacting it is referred to as the projectile. The position vector of the target to the projectile is

$$\mathbf{r} = \mathbf{r}_{\text{proj}} - \mathbf{r}_{\text{targ}}, \quad (2.38)$$

and the velocity vector is

$$\mathbf{v} = \mathbf{v}_{\text{proj}} - \mathbf{v}_{\text{targ}}. \quad (2.39)$$

[Leinhardt & Stewart \(2012\)](#) give the centre of mass specific impact energy as

$$Q_r = \frac{0.5\mu v^2}{m_{\text{tot}}}, \quad (2.40)$$

where  $m_{\text{tot}} = m_{\text{proj}} + m_{\text{targ}}$ , and  $v$  is the collision speed. The destructive power of a collision depends not only on the speed of the collision, but also on  $\theta$ , the angle that the velocity vector makes with the position vector. The component of the collision speed along the position vector can be found with  $\mathbf{v} \cdot \hat{\mathbf{r}}$ , where  $\hat{\mathbf{r}}$  is the position unit vector.

So we can calculate the impact energy of a collision but we need to determine how different energies will affect the bodies. The gravitational binding energy of a body is found with

$$U = \frac{3GM^2}{5R}. \quad (2.41)$$

We are interested in the kinds of collisions that would cause a body to be destroyed, and also those that could create a contact binary. For a destructive collision a possible cutoff between a body surviving and one which does not survive is if the collisional energy is larger than the gravitational binding energy of either body, then that body will be destroyed. This will only apply in the case of a rubble pile, held together just by its own gravity. This will not be exact as the composition of the body will have an affect on the outcome of the collision ([Benz &](#)

Asphaug 1999). Also there will be a gradual change where collisions less energetic than the binding energy of a body can still be very destructive. Stewart & Leinhardt (2009) describe how when a collision occurs at an energy greater than a critical energy, then fragmentation can occur, but in this work we avoid these complications as we are more interested in the dynamics of the bodies in question, and generating fragments to follow would draw away from the main focus.

For collisions that could result in a contact binary we need a collision energy below which a contact binary could be formed. In the case of Arrokoth, McKinnon et al. (2020) found that to reproduce a body such as Arrakoth by collisions between Kuiper belt objects would require very low approach velocities, in the order of a few metres per second. This corresponds with the escape velocity of Arrakoth, which while not known exactly, as the mass is not exactly known, is also around a few metres per seconds. The comet 67P Churyumov/Gerasimenko (Jorda et al. 2016) is another possible contact binary that we have lots of information about as it has also been visited by spacecraft. Although not currently located in the Kuiper belt, it likely formed there (Nesvorný et al. 2018), and may provide evidence of the environment for binaries there. 67P has several differences when compared to Arrakoth. It is much more weathered as a result of having been subjected to the more volatile environment of the inner solar system. It has had much closer approaches to the Sun and so has suffered outgassing. It is also much smaller than Arrakoth, at a width in the order of several kilometres. Modelling of collisions (Jutzi & Benz 2016) suggest its creation as a result of collision speeds in the order of the escape speed.

There is indirect evidence of collisions between Kuiper belt bodies from looking at the surface of Arrokoth. While much smoother and less weathered than 67P, Arrokoth does have what appears to be an impact crater on the surface of its smaller lobe, indicating a subcatastrophic impact in its past. We know that objects in the inner solar system, such as asteroids, experience much more frequent impacts from smaller bodies as they are more weathered (Binzel et al. 2004). They are more collisionally evolved and are not representative of the primordial planetesimal population that is present in the Kuiper belt.

# Chapter 3

## Results

Before presenting the results of the several different experiments that were performed during the course of the project, we will describe example encounters. As previously mentioned, encounters can be classified depending on their outcome. Different possible outcomes will be shown, and then will be examined in more detail, including changes to the physics involved. Then we will move on to examining many encounters with slightly varied initial conditions. This will display both the chaotic nature of certain interactions, as well as how different outcomes are more likely to occur than others. This is followed by an examination of encounters between certain fixed binaries and a broad range of impactors. The final experiment follows single binaries as they evolve as a result of many encounters.

### 3.1 Example encounters

In this section we first examine individual encounters. Figure 3.1 shows potential outcomes that can occur during an encounter. These simple examples are all restricted to the same plane, with  $i_{\text{bin}} = 0$  and  $i_{\text{imp}} = 0$ , and with all orbits having  $e = 0$ . The radius of both the primary and the secondary in all of these examples is 100 km. As mentioned earlier, we chose a constant density for all bodies of  $700 \text{ kg m}^{-3}$ . The units of measurement in the figures are in Hill radii of the primary. In these examples the Hill radius of the secondary is the same size but this will not always be the case. The circles in the plots around each body indicate the extent of their respective Hill spheres.

A flyby as seen in figure 3.1a describes an encounter where the impactor does not enter the Hill radius of the binary, and neither of the two components of the binary enter the Hill radius of the impactor. In this case the impactor is less massive than the two components of the binary, and its low mass allows the binary to survive relatively undisturbed. When this occurs the results are more predictable than in other types of encounters. As long as the impactor stays far from the centre of mass of the binary, the binary itself can be considered as a single body, and the encounter a kind of 2-body problem. This will not be entirely accurate as there will be an exchange of energy and angular momentum between the passing impactor and the binary.

When the impact parameter of the binary is low, as in figure 3.1b, the relative approach velocity will be small, as the difference in velocity between two circular Keplerian orbits with two different semi-major axes is  $v_{\text{shear}} = -1.5\Omega_K b$ , which is directly proportional to the impact parameter  $b$ . This low approach velocity means that the impactor is pulled into a lower orbit by the gravitational attraction of the binary before the binary catches up to it. Then when it achieves this new lower orbit, it is now closer to the Sun and it has a greater orbital speed and

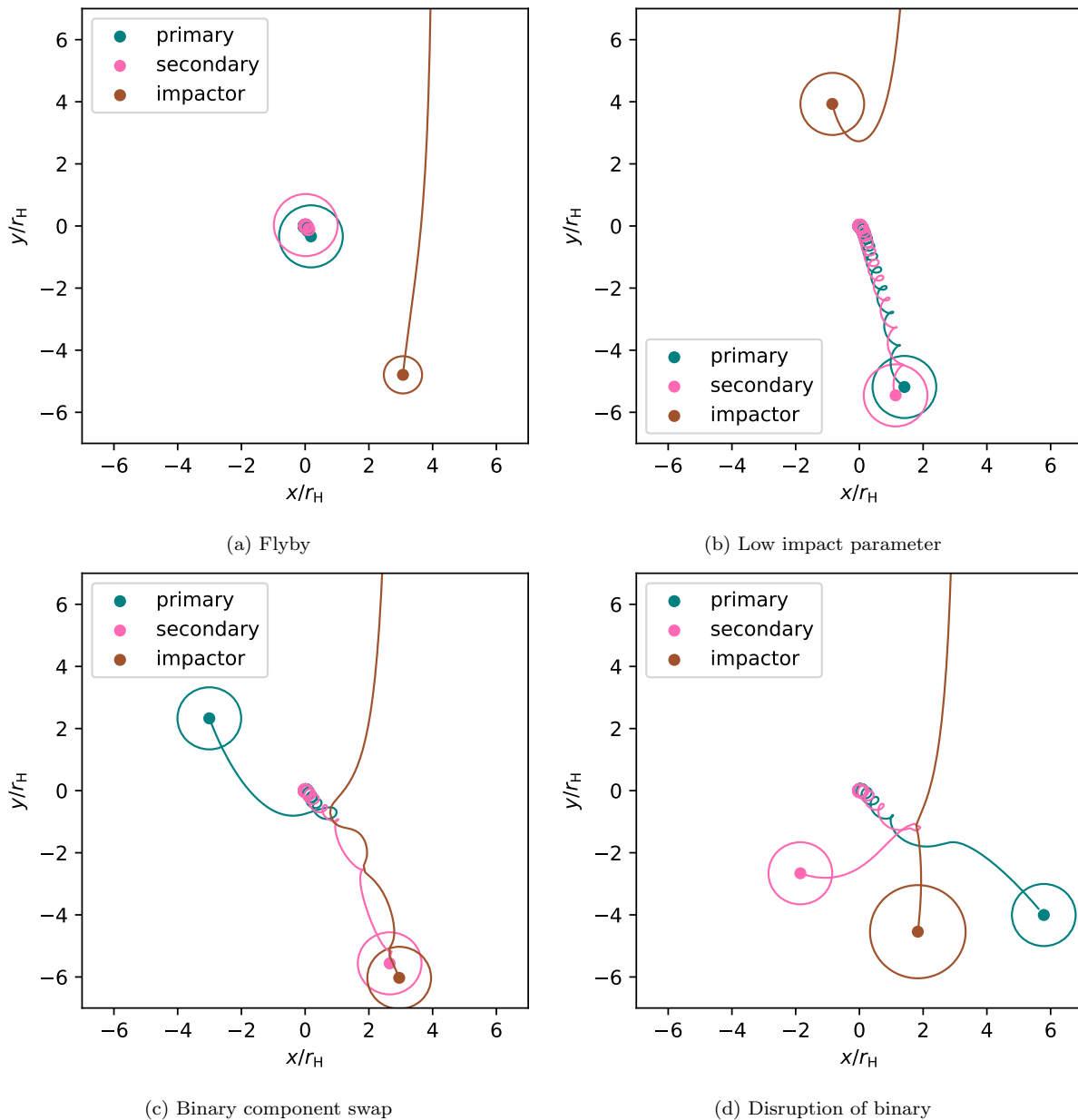


Figure 3.1: Results of four individual simulations with varied initial conditions showing the range of possible outcomes. The circles around each body represent their Hill spheres. In figure 3.1a the impactor passes by the binary and has its orbit deflected. In figure 3.1b the impactor approaches with a low impact parameter  $b = 1.5 r_H$ . This results in a slow relative velocity, and the impactor is drawn into a lower orbit, increasing its velocity relative to the binary and causing the distance between them to increase. In Figure 3.1c the impact parameter results in an encounter that causes the swapping of components in the binary. In Figure 3.1d the impactor is more massive, with radius 150 km, leading to the disruption of the binary.

recedes in the frame of reference of the binary. This is an example of a horseshoe orbit described in section [1.2](#).

When the encounter causes the Hill sphere of the impactor to overlap with the Hill sphere of either component of the binary, then the results become more unpredictable and extremely sensitive to the initial conditions of the encounter. Figure [3.1c](#) shows an interaction between the binary and an impactor with radius 100 km and an impact parameter of  $b = 2.5 r_H$ . The impactor disrupts the binary, pulling the secondary away from the primary, but in the process it captures the secondary and creates a new binary. The primary is then released to follow its own new orbit around the Sun.

Figure [3.1d](#) shows a similar situation except with a more massive impactor. The impactor in this case has radius 150 km and its mass is therefore  $1.5^3 = 3.375$  times greater. The greater mass can be seen as the larger circle around the impactor illustrates its larger Hill sphere. The result is that the impactor disrupts the binary entirely and no new binary is formed. All three components are now orbiting the Sun on their own separate paths.

We now look at a selection of encounters in more detail. Figure [3.2](#) visualises a flyby where the binary survives and the impactor escapes to infinity. The impactor is the same size as both components of the binary, with a radius of 100 km, and the impact parameter is  $b = 3.4 r_H$ . Figure [3.2a](#) provides a top-down view as shown in the previous examples. The impactor approaches and gets drawn into a lower orbit by the binary, and in turn pulls the binary into a higher orbit. The sharp turn in the path of the impactor indicates the point of closest approach. At this point the gravitational pull between the binary and the impactor is not strong enough to cause an overlap of the Hill spheres of the components, the impactor speeds up as a result of the lower orbit and conservation of angular momentum, then this greater velocity pushes it back out to a higher orbit and away from the binary. The change in binding energy of the binary,  $E_1 - E_0$ , will be greater than  $-\frac{1}{3}mv_0^2$ , where  $v_0$  is the initial velocity of the impactor. As the impactor begins with an impact parameter of  $b = 3.4 r_H$ , then the relative approach velocity of the impactor is

$$v_0 = -1.5\Omega_K b = -2 \text{ m s}^{-1}, \quad (3.1)$$

which then means that

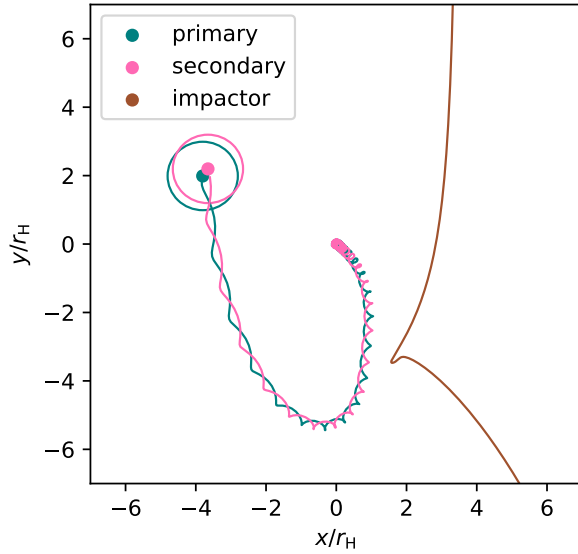
$$-\frac{1}{3}mv_0^2 = -4 \times 10^{18} \text{ J}. \quad (3.2)$$

Per unit mass of the impactor this is  $-1.1 \text{ J kg}^{-1}$ . The change in the binding energy of the binary is  $E_1 - E_0$  which is equal to around  $0.003 \text{ J kg}^{-1}$ . As this is greater than  $-\frac{1}{3}mv_0^2$ , the binding energy of the binary is sufficient to keep the two components bound to each other.

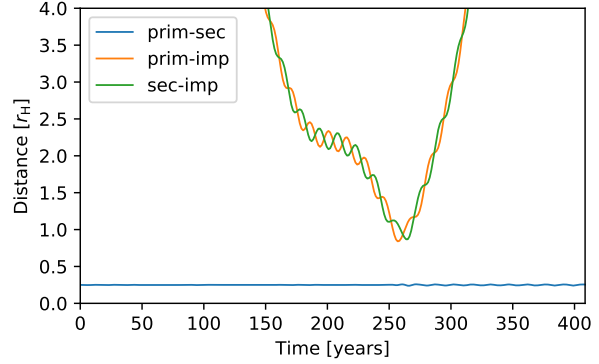
Figure [3.2b](#) shows the distance between each pair of bodies over the course of the encounter. The encounter covers a period of 400 years, or around 1.5 times the orbital period of the binary around the Sun. The distance between the binary and the impactor reaches a minimum at around 270 years. The blue line indicating the distance between the primary and the secondary stays constant up until that point, which shows that the initial eccentricity of the binary is very low. After the closest point of the encounter the value gains a small but noticeable oscillation.

The orbital energy of each pair of components is shown in figure [3.2c](#). A steady negative total energy is required for a stable binary and this is the case for the binary throughout the encounter. While the binary stays bound, we see in figure [3.2d](#) that the eccentricity is not constant. Around the time of the closest approach of the impactor the eccentricity is pumped up to a higher value. This higher eccentricity is also noticeable in figure [3.2b](#) as the regularly changing distance between the primary and secondary.

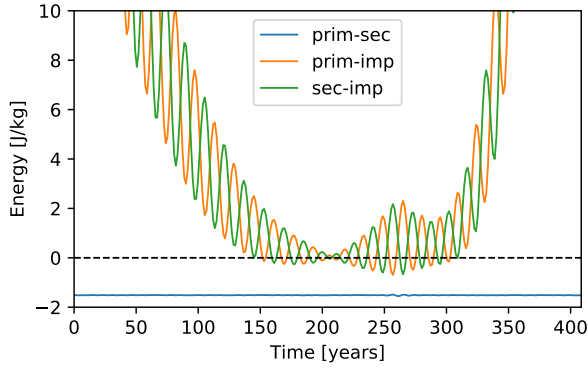
Figure [3.3](#) shows the result of the encounter is an exchange of components leading to a new binary composed of the primary and the impactor. We see in figure [3.3b](#) that the closest point



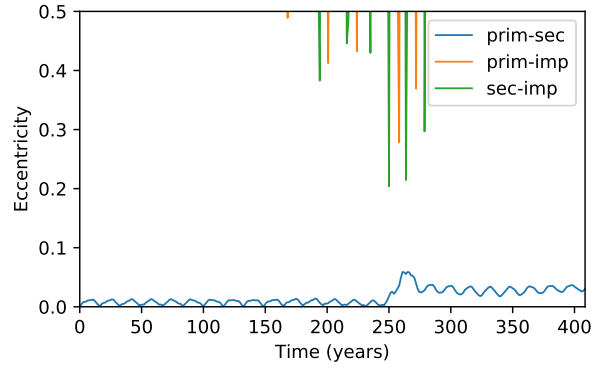
(a) Result of the encounter



(b) Distance between components

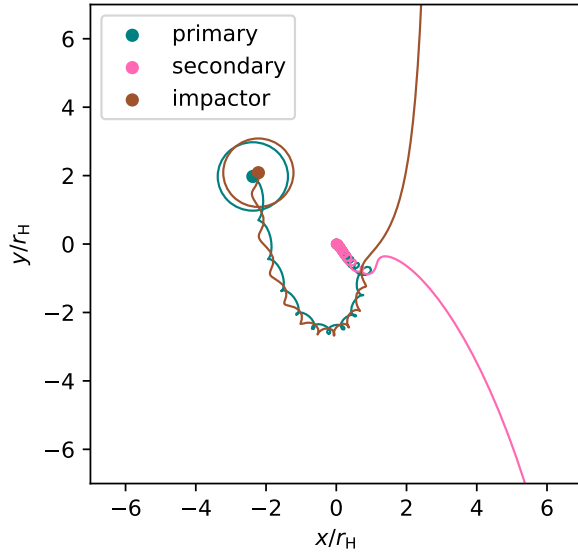


(c) Energy of pairs of components

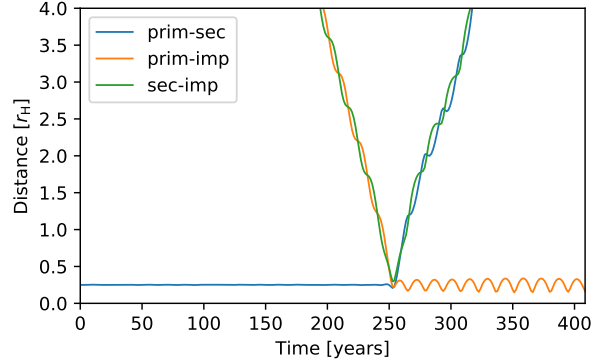


(d) Eccentricity of pairs of components

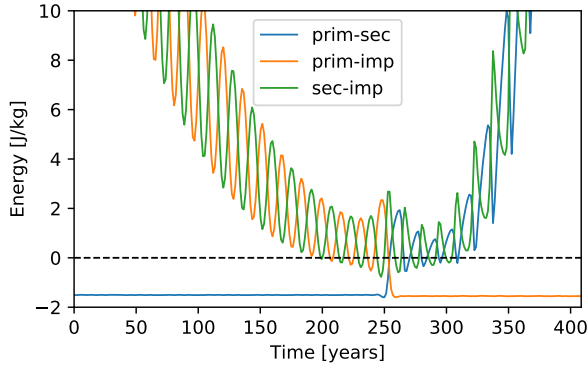
Figure 3.2: Encounter between an equal mass binary where both components have radius  $100 \text{ km}$  and an impactor of the same size with impact parameter  $b = 3.4 r_H$ . Figure 3.2a shows the path of the bodies. The impactor approaches the binary but escapes its pull. 3.2b shows how the distance between each pair of bodies changes over the course of the encounter. 3.2c shows the changes in energy. 3.2d shows how the eccentricity of the binary changes during the encounter.



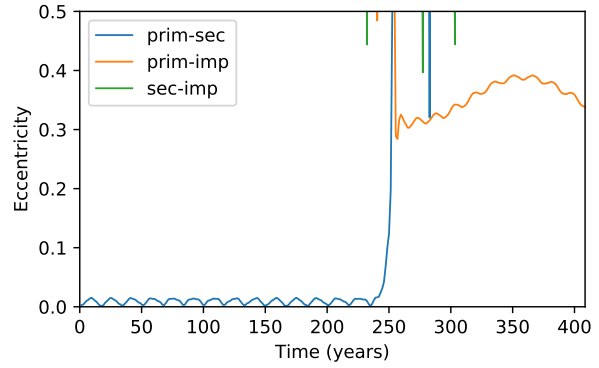
(a) Result of the encounter



(b) Distance between components



(c) Energy of pairs of components



(d) Eccentricity of pairs of components

Figure 3.3: Encounter between binary and impactor with  $b = 2.6 r_H$ . Figure 3.3a shows the paths of the bodies. The impactor is swapped with the primary and a new binary is formed composed of the secondary and impactor. 3.3b shows how the distance between each pair of bodies changes over the course of the encounter. 3.3c shows the changes in energy. 3.3d shows how the eccentricity of the binary changes during the encounter, and the eccentricity of the new binary.

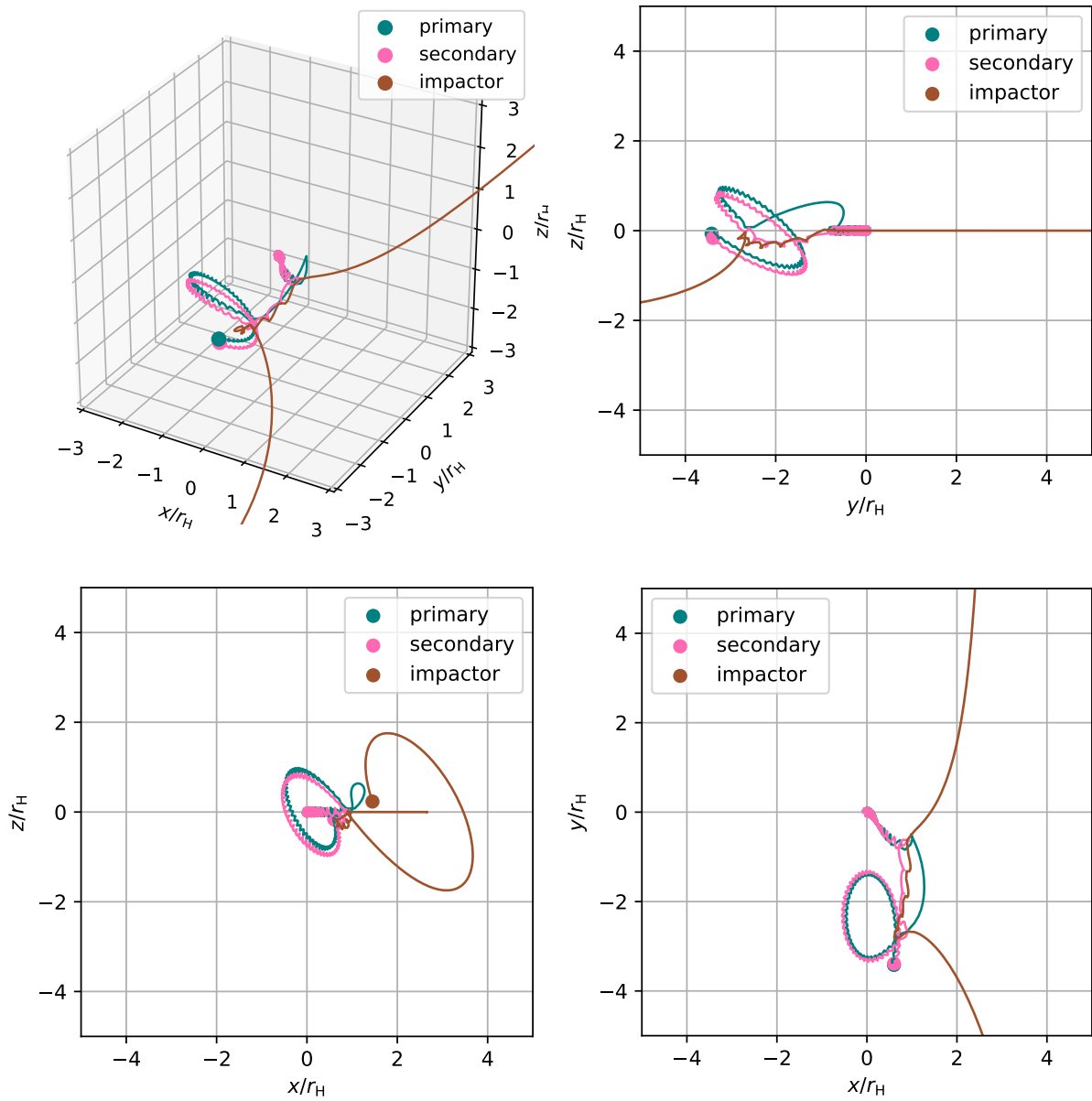


Figure 3.4: Encounter in three dimensions in which the binary has an obliquity of  $i = 80^\circ$  and impactor has  $i = 0.5^\circ$ . Each panel shows the encounter from a different perspective.

of approach between the impactor and the binary occurs at around 250 years, and after this point the distance between the primary and the impactor stays low but oscillates, indicating that the new binary has a higher eccentricity. In figure 3.3c the total gravitational binding energy of the binary is constant below zero up until the point of the close encounter. There is a spike in the energy of each pair of components as the three interact closely, and then the new binary composed of the primary and the impactor now has a steady negative total energy. Meanwhile the total energy of the other two pairs of components displays sharper spikes upwards and downwards in time with the mutual orbital period of the new binary, which we can also see in figure 3.3b is around 15 years.

Figure 3.3d shows explicitly what has already been learned from the other plots about the eccentricity of the new binary. The eccentricity of the original binary is small, and after the interaction and component swap the eccentricity of the new binary is higher, over 0.3.

Both of these examples have been restricted to the 2D plane, but now in figure 3.4 we have a more complicated situation in three dimensions, with an interaction in which the binary survives the encounter. Here the binary had an initial obliquity of  $80^\circ$  and the impactor had low but non-zero initial inclination. The original binary is intact after the encounter is complete and the impactor escapes. This only occurs after an intermediate period where the binary is disrupted, and the secondary and impactor are briefly bound together. The primary is ejected upwards above the plane when this happens, but is pulled back by the new binary for a further interaction which results in another component swap and the recombination of the original binary. This interaction demonstrates the chaotic nature of these kinds of interactions and the impossibility of analytical investigations, which is discussed more in the next section.

## 3.2 Chaotic encounters

The previous section showed a distinction between encounters that are flybys and those where there is a close encounter. Flyby encounters can be predictable, as we can think of the interaction as a kind of two-body interaction with the binary constituting a single body. Without the overlap of the Hill sphere of the impactor with either of the components of the binary, the impactor cannot strip a component away from the binary. This simplification breaks down when the Hill spheres of the impactor and binary become very close and overlap. At this point the outcome becomes highly dependant on initial conditions. The same encounter can have different outcomes depending on the arbitrary selections we make at the beginning of the simulation. The time it takes the impactor to reach the binary is a function of its starting location. We place it at a distance where the gravitational pull of the binary is negligible, but the exact location it begins at will determine the phase of the binary when it catches up to the impactor. So the true anomaly of the secondary with respect to the primary will be different depending on where the impactor begins, possibly resulting in a different class of interaction.

The sensitive dependence of the results of the encounter on the initial conditions are illustrated in figure 3.5. Each panel in the figure shows the effect of changes in the initial true anomaly of the mutual orbit of the binary components around each other. The same binary is present in each simulation, with both components having the same mass, and radius of 100 km. The impactor is also the same size as the binary components in each simulation. The encounters all take place in the same plane, with  $e = 0$  and  $i = 0$  for all orbits. The only initial condition that is different between the plots is  $f_{\text{bin}}$ , the starting true anomaly of the secondary around the primary. The components of the binary are therefore initialized in a different location around the orbit. The impactor will arrive at the binary at the same time in each simulation, but with

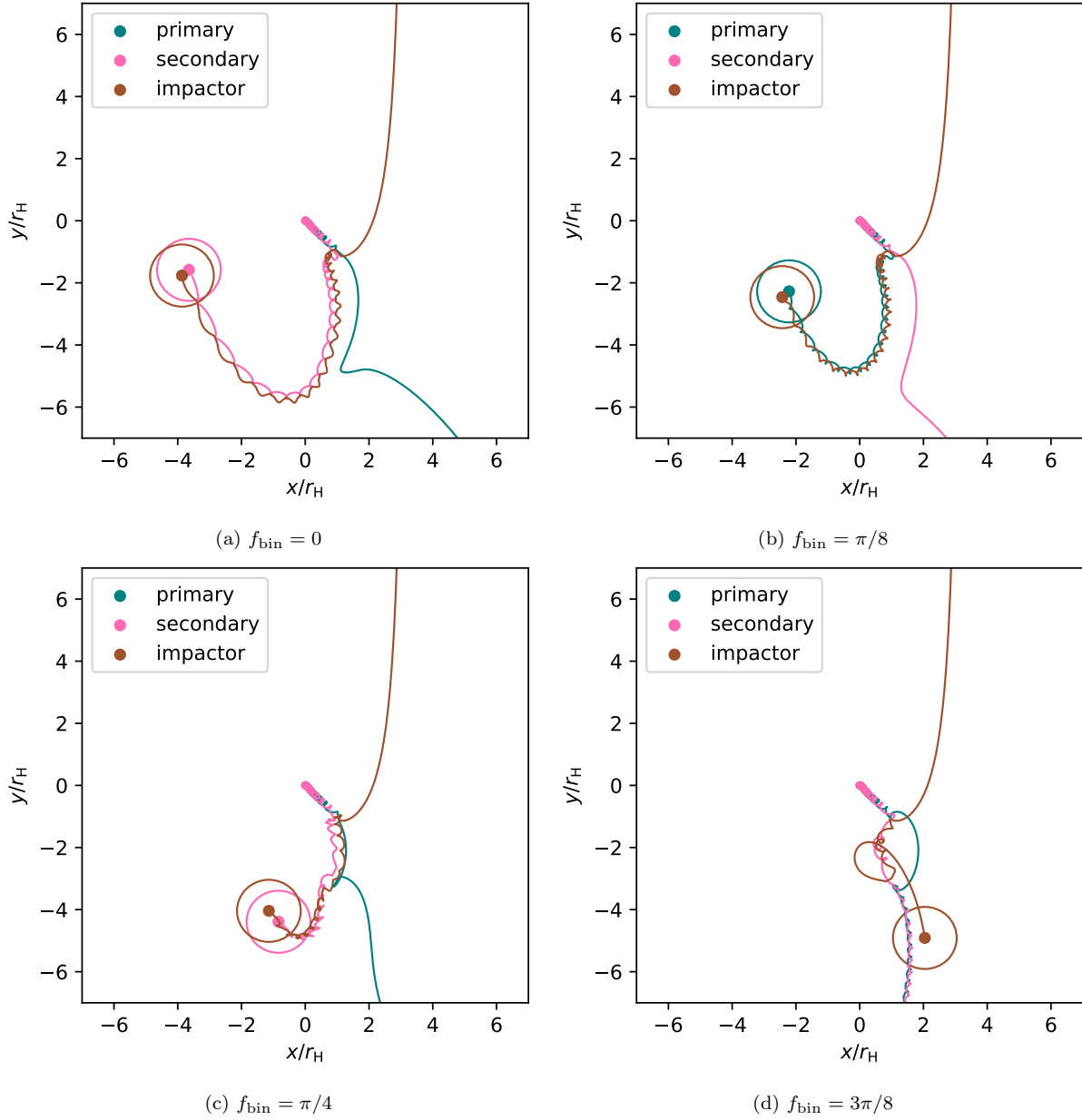


Figure 3.5: The same three components in the same orbital configuration can cause different results with slightly different initial conditions. In each of these plots the only different initial condition was the true anomaly,  $f_{\text{bin}}$ , of the binary components' mutual orbit around each other. The binary is disrupted in all cases, but new binaries are formed, or the original recombines. Notice how the impactor follows the exact same path up until the point at which the Hill spheres overlap.

the binary in a different phase in each case. As can be seen in these plots, this change in  $f_{\text{bin}}$  can lead to completely different outcomes for the encounter, illustrating the sensitivity of the results to the starting positions of the binary components.

Slight variations in the shape of the orbit are illustrated in figure 3.6. Here the eccentricity of the binary is  $e_{\text{bin}} = 0.3$  in both cases but the argument of periapsis is varied. When  $\omega_{\text{bin}} = 0$  the encounter results in a component swap for the binary, with a new binary being formed composed of the impactor and the secondary. When  $\omega_{\text{bin}} = \pi/4$ , this time the encounter results in the disruption of the binary. The same chaotic dependence of the results of the encounter on slight variations of the initial conditions can be shown not only for  $f_{\text{bin}}$  and  $\omega_{\text{bin}}$ , but also for the longitude of ascending node  $\Omega_{\text{bin}}$  with a set value of  $i_{\text{bin}}$ . So the binary can have the

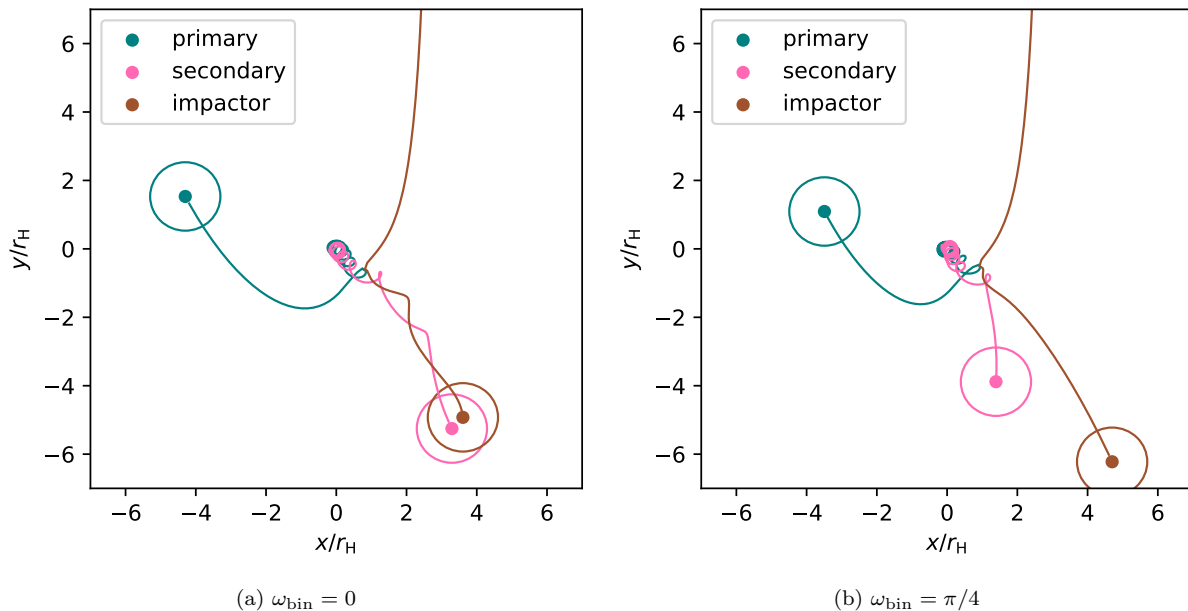


Figure 3.6: Encounters between a 100 km impactor and a binary with 100 km components. The eccentricity of the binary orbit was  $e_{\text{bin}} = 0.3$  in both cases, but the argument of periapsis was different in each case.

same shape orbit, but its orientation and starting point will change the results of the encounter. These changes that occur with the different initial conditions change the results as a function of the starting location of the impactor. The impactor is initialized at a location that is far enough away to ensure the initial gravitational force is negligible, as well as to engineer an encounter if the impactor has non-zero  $e_{\text{imp}}$  and  $i_{\text{imp}}$ .

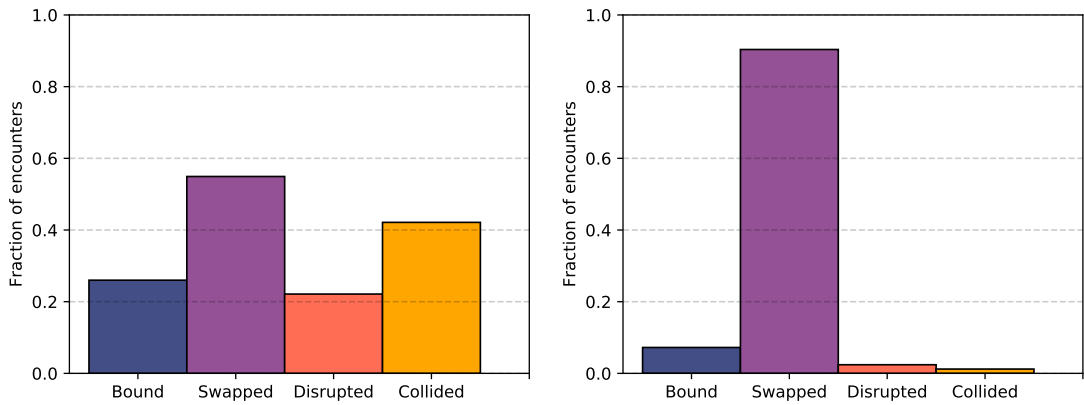
This is an arbitrary choice as the location of the encounter is selected to be  $\pi$ , and the effect of changing this slightly means that the binary will be in a different orbital state by the time the impactor arrives. This arbitrary randomness can be captured by varying the starting conditions of the binary instead. The orbital element that has the most variation as a result of this choice of starting position is  $f_{\text{bin}}$ , as  $\omega_{\text{bin}}$  and  $\Omega_{\text{bin}}$  complete one revolution as the binary orbits the Sun, but the binary components' mutual orbit around each other is much faster, and  $f_{\text{bin}}$  completes many revolutions and returns to zero many times as the binary itself completes a single orbit around the Sun.

To investigate this chaotic quality of the encounters, we focus in this section on individual combinations of impactor size and impact parameter, and their effect on a binary with constant mass, mass ratio, mutual orbital separation, and eccentricity, but with varying initial true anomaly and argument of periapsis. While the examples shown in figures 3.5 and 3.6 at first

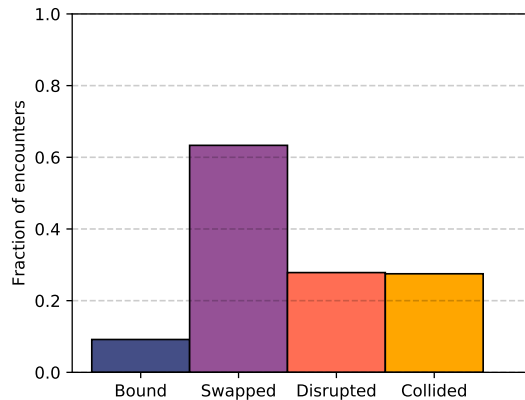
glance appear to indicate that the results are random, perhaps different binary mass ratios and orbit sizes will skew the probability that a particular outcome will occur.

Figure 3.7 shows the distribution of outcomes for different sets of encounters that are restricted to the 2D plane. We simulate the encounter 500 times with all the same initial conditions except for  $f_{\text{bin}}$ , which was selected from a uniform distribution between 0 and  $2\pi$  for circular orbits. For non-circular orbits we first select the mean anomaly,  $M_{\text{bin}}$ , from a uniform distribution, and then transform it to  $f_{\text{bin}}$ . This ensures our distribution does not over represent the sections of the orbit where the components spend relatively less time. The *Bound* column indicates the fraction of binaries that survived the encounter. The *Swapped* column shows the fraction of encounters where the result was a new binary. The *Disrupted* column shows the fraction of encounters where the initial binary was disrupted, and the *Collided* column shows the fraction of encounters where any collisions occurred. This collision could have occurred between any two components of the encounter. Every encounter fits into one of the first three columns, and the collisions can have occurred in any one of the other situations.

The results in figure 3.7 show a preference for new binary creation in all scenarios, although with substantial differences depending on the state of the binary and impactor. In figure 3.7a around 50% of encounters result in component swaps.



(a) Equal mass binary.  $m_{\text{imp}}/m_{\text{prim}} = 1$ ,  $r_{\text{imp}} = 100$  km,  $b = 3 r_{\text{H}}$ . (b) Equal mass binary.  $m_{\text{imp}}/m_{\text{prim}} = 4$ ,  $r_{\text{imp}} = 160$  km,  $b = 3.2 r_{\text{H}}$ .



(c) 10:1 mass ratio binary.  $m_{\text{imp}}/m_{\text{prim}} = 1$ ,  $r_{\text{imp}} = 100$  km,  $b = 2.7 r_{\text{H}}$ .

Figure 3.7: Distribution of encounter outcomes. In all cases:  $r_{\text{prim}} = 100$  km,  $a_{\text{bin}} = 0.2 r_{\text{H}}$ ,  $e_{\text{bin}} = 0$ ,  $i_{\text{bin}} = 0$ ,  $e_{\text{imp}} = 0$ ,  $i_{\text{imp}} = 0$ . In each case  $f_{\text{bin}}$  was randomly selected from a uniform distribution between 0 and  $2\pi$ .

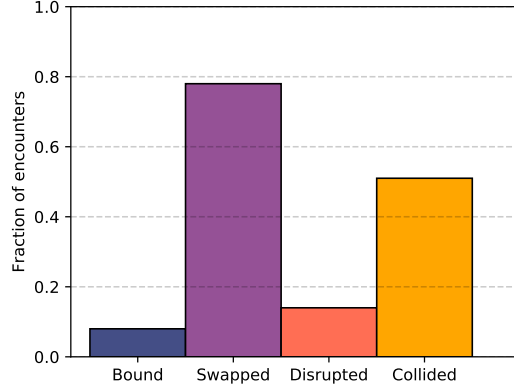


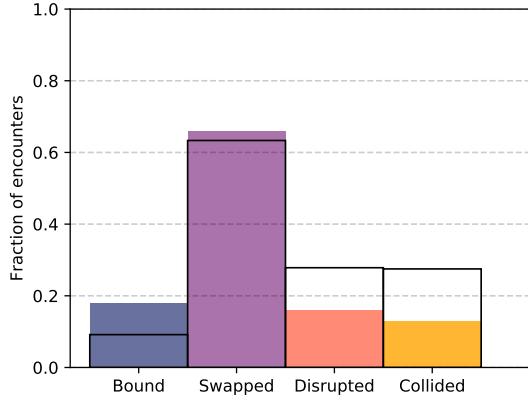
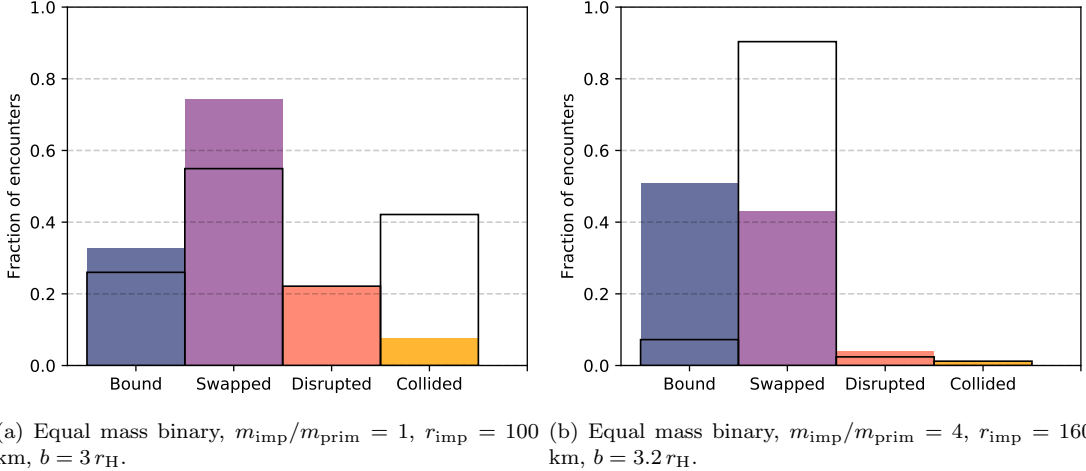
Figure 3.8: Distribution of encounter outcomes. Equal mass binary,  $m_{\text{imp}}/m_{\text{prim}} = 1$ ,  $a_{\text{bin}} = 0.2 r_{\text{H}}$ ,  $e_{\text{bin}} = 0.5$ ,  $i_{\text{bin}} = 0$ ,  $e_{\text{imp}} = 0$ ,  $i_{\text{imp}} = 0$ . The mean anomaly,  $M_{\text{bin}}$ , and  $\omega_{\text{bin}}$  were randomly selected from a uniform distribution between 0 and  $2\pi$ .

Also, collisions occur in around 40% of cases. It is important to remember that collisions can occur with the encounter continuing, and finishing up in one of the other categories. As a result of this, although the total between the first three columns will always add up to 1, the total over the four columns can add up to more than 1 when collisions are included. This large frequency of collisions may be a consequence of the restriction to the 2D plane.

In figure 3.7b, the larger impactor leads to around 90% of encounters ending with a new binary created. This is a consequence of the much greater gravitational pull of the more massive impactor, allowing it to strip one or other of the binary components away and then capture them. Less than 5% of encounters in this case result in collisions, possibly because the impactor disrupts the binary from a greater distance, and lowering the possibility of further close encounters.

The 10:1 mass ratio binary encounters shown in figure 3.7c result in component swaps in around 60% of cases. This may be explained by the impactor more easily stripping away and capturing the less massive secondary. The gravitational pull between the two components in this case is not as strong as when the components are of equal mass.

In figure 3.8 we see an equal mass binary with a high eccentricity of  $e_{\text{bin}} = 0.5$ . In this case we also randomise the argument of periapsis. Compared to the circular version with  $e = 0$  in figure 3.7a, the binary now survives in less than 10% of cases, and there are even more collisions, with these occurring in over 50% of encounters. But what happens to the binaries that do not survive is different now as well. Binary component swaps occur now in almost 80% of cases, but total disruptions happen less often, showing that binaries with high eccentricity are more susceptible to having their components pulled away from each other by the impactor, but are less able to escape the encounter and are more likely to be captured by the impactor. We now examine zero eccentricity binaries with the added factor of binary obliquity in figure 3.9. Here, the binary is not only given a random initial true anomaly, but also a random obliquity and longitude of ascending node. This produces a binary orbit with a constant size and shape, but with random orientation with respect to the plane of the ecliptic. Figure 3.9 also shows the results from figure 3.7 overlaid for comparison. In the configuration with an equal mass impactor in figure 3.9a, there is a greater preference for component swaps, which occur in almost 80% of the encounters, and there are far fewer collisions. This is similar to figures 3.7c and 3.8. Possibly the added dimension gives the three bodies extra freedom to avoid collisions. We also



(c) 10:1 mass ratio binary.  $m_{\text{imp}}/m_{\text{prim}} = 1$ ,  $r_{\text{imp}} = 100$  km,  $b = 2.7 r_H$ .

Figure 3.9: Distribution of encounter outcomes.  $a_{\text{bin}} = 0.2 r_H$ ,  $e_{\text{bin}} = 0$ ,  $e_{\text{imp}} = 0$ ,  $i_{\text{imp}} = 0$ . In each case  $f_{\text{bin}}$ ,  $i_{\text{bin}}$ , and  $\Omega_{\text{bin}}$  were randomly selected from uniform distributions between 0 and  $2\pi$ . The solid outlines indicate the 2D versions of the experiment that are also seen in figure 3.7

see fewer total disruptions, now happening in less than 5% of cases. Almost all binaries now either survive, or a new binary is created. The three bodies seem to have a more difficult time escaping from each other.

In the encounters with the more massive impactor in figure 3.9b, there is a drastic reduction in the amount of binary component swaps. Now the binary survives intact in around 50% of cases. Encounters with binaries with very high obliquity probably mean that the impactor has a more difficult time adding energy to the system and disrupting the binary. Again there is a reduction in collisions with the addition of the extra dimension. We will test the dependency of the encounter outcome on the parameters of the impactor in the next section.

The large mass ratio binary in figure 3.9c now survives in almost 20% of encounters, and disruption have less frequently in around 15% of encounters. The number of collisions is halved, and they now occur in just over 10% of encounters. The reduction in the amount of collisions is more effective for the equal mass binaries, suggesting that the smaller secondary can more easily be drawn into collisions with the impactor.

### 3.3 Parameter study

There are many individual parameters that will influence the outcome of an encounter. With regards to the binary, changes in the mass of the components, as well as the orbital configuration,  $a_{\text{bin}}$ ,  $e_{\text{bin}}$ ,  $\omega_{\text{bin}}$ ,  $f_{\text{bin}}$ ,  $i_{\text{bin}}$ , and  $\Omega_{\text{bin}}$ , all have the potential to change the outcome of the encounter. As for the impactor, changes in its mass and in the impact parameter  $b$ , can change the outcome of the encounter, as can the eccentricity and inclination of the impactor’s orbit around the Sun. Non-zero  $e_{\text{imp}}$  and  $i_{\text{imp}}$  will increase the encounter speed and decrease the encounter timescale.

There are an infinite amount of different combinations of parameters that could possibly be examined, the mutual orbital separation of the binary could be any value between a few times their combined radius and the Hill radius of the primary. The masses of all three bodies could

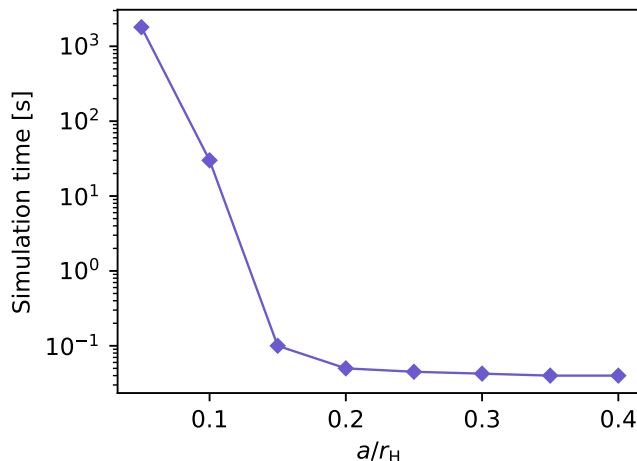


Figure 3.10: Computation time as a function of  $a_{\text{bin}}$  for simulations of binaries for  $P_{\text{orb}} = 291$  years.

be any value from a range of our choosing. As examining every combination of all these different possibilities would be time consuming we divided the expected most important factors into bins.

The first of these is the mutual orbital separation of the binary. Here we had to decide how to balance the excessive computation time required for the tighter binaries with their increasing frequency in the Kuiper belt. Figure 3.10 shows the computation time required for four different values of  $a$  in Hill radii. Computation times increase rapidly as the binary separation decreases.

We chose to divide the binaries into groups with mutual orbital separations of:  $a_{\text{bin}} = 0.4 r_H$ ,  $a_{\text{bin}} = 0.2 r_H$ ,  $a_{\text{bin}} = 0.1 r_H$ , and  $a_{\text{bin}} = 0.05 r_H$ . Binaries with semi-major axes of around 5% of their Hill radius are considered roughly on the border of wide and tight in the context of the Kuiper belt (Grundy et al. 2019), so here we have excluded the tightest binaries. Nesvorný & Vokrouhlický (2019) showed that tight binaries in the cold classical belt have a high survival probability during the push-out of the dynamically hot populations by Neptune, leading us to assume that if they survive encounters with Neptune they will be unlikely to be affected by encounters with similarly sized dynamically cold planetesimals.

Figure 3.10 shows how sensitive the simulation time is to this particular parameter. Smaller mutual orbital separations mean more frequent integrations. More than anything else, this determines the computation time required to simulate an encounter. In the calculations used to create the figure, only a binary was simulated, so these times do not take into account an increased frequency of integrations required for close encounters with an impactor. They are therefore a rough minimum simulation time per encounter.

For the mass of the bodies we have already selected a constant density of  $700 \text{ kg m}^{-3}$ . The observed Kuiper belt binaries have components with radii in the order of 100 km (Noll et al. 2020). This is unlikely to be representative of the binary population as a whole as these larger binaries are much easier to detect. We have selected a constant primary radius of 100 km, concentrating our study on the larger binary planetesimals.

After selecting a primary component we need to select a mass ratio for the binary and use this to calculate the size of our secondary. The mass of a 100 km primary component with density  $700 \text{ kg m}^{-3}$  will be  $m_{\text{prim}} = 2.9 \times 10^{18} \text{ kg}$ . Equal mass binaries are common among the larger planetesimal sized objects in the cold classical belt, and therefore it will be interesting to investigate encounters involving them. We will also investigate binaries that have larger mass ratios. For this a mass ratio of 10:1 was chosen.

This gives us several possible combinations of  $a_{\text{bin}}$ ,  $m_{\text{prim}}$ , and binary mass ratio. For each combination we will subject it to many encounters with a range of impactors and impact parameters.

### 3.3.1 Binary survival in parameter space

Now that we have combinations of binary parameters to investigate, we need a way to compare them. To do this we need to engineer encounters between our binaries and a range of impactors. For the 2D version of this experiment the impactor properties that we can vary are the radius of the impactor itself, and the impact parameter when it is initialized. Figure 3.11 shows the results of interactions between four different sets of binaries that have components of equal mass but all have different mutual orbital separations.

Our range of impactor radii was chosen from 50 to 300 km. 300 km is arbitrary but this choice is reasonable as bodies larger than this quickly become rare in the Kuiper belt (Bierson & Nimmo 2019). It follows that encounters with such bodies will also be rare. Below around 50 km the impactor will very rarely disrupt the binary. The range of impact parameters was chosen to include most of the interesting interactions within this range of impactor sizes. In the figure the coloured squares represent two bound components in a binary with the colours corresponding to the pair of bodies that are bound together. The dark blue squares are unchanged binaries with a bound primary and secondary, while purple squares represent a new binary composed of the original primary component of the binary and the impactor, and orange represents the corresponding result with the secondary. An empty square represents disruption of the binary without any new binary being formed, leaving all three components of the simulation now on their own separate orbits around the Sun. The crosses represent collisions between two bodies corresponding to the colours. It is immediately noticeable in each case that there is a region where the combination of impactor and impact parameter result in disruption of the binary. Within this region every possible outcome can be found. There is complete disruption, new binaries with both possible new combinations, and collisions between each pair of bodies, and also less rare, the original binary can become bound again. Outside of this region the binary survives intact, but other changes to it can occur. Beyond an impact parameter of around  $6 r_{\text{H}}$  it takes a very large impactor to have an effect on the binary, as the Hill radius of the impactor scales linearly with its physical radius.

We can very clearly see the region where the results become unpredictable. In the top left of each of the plots in figure 3.11 the binary remains intact for a wide range of combinations of impact parameters and impactor size. The top left of the plots represent small impact parameters and large impactors. What is happening here is that with a low impact parameter the impactor is orbiting with a low relative velocity compared to the binary, but its large mass pulls the

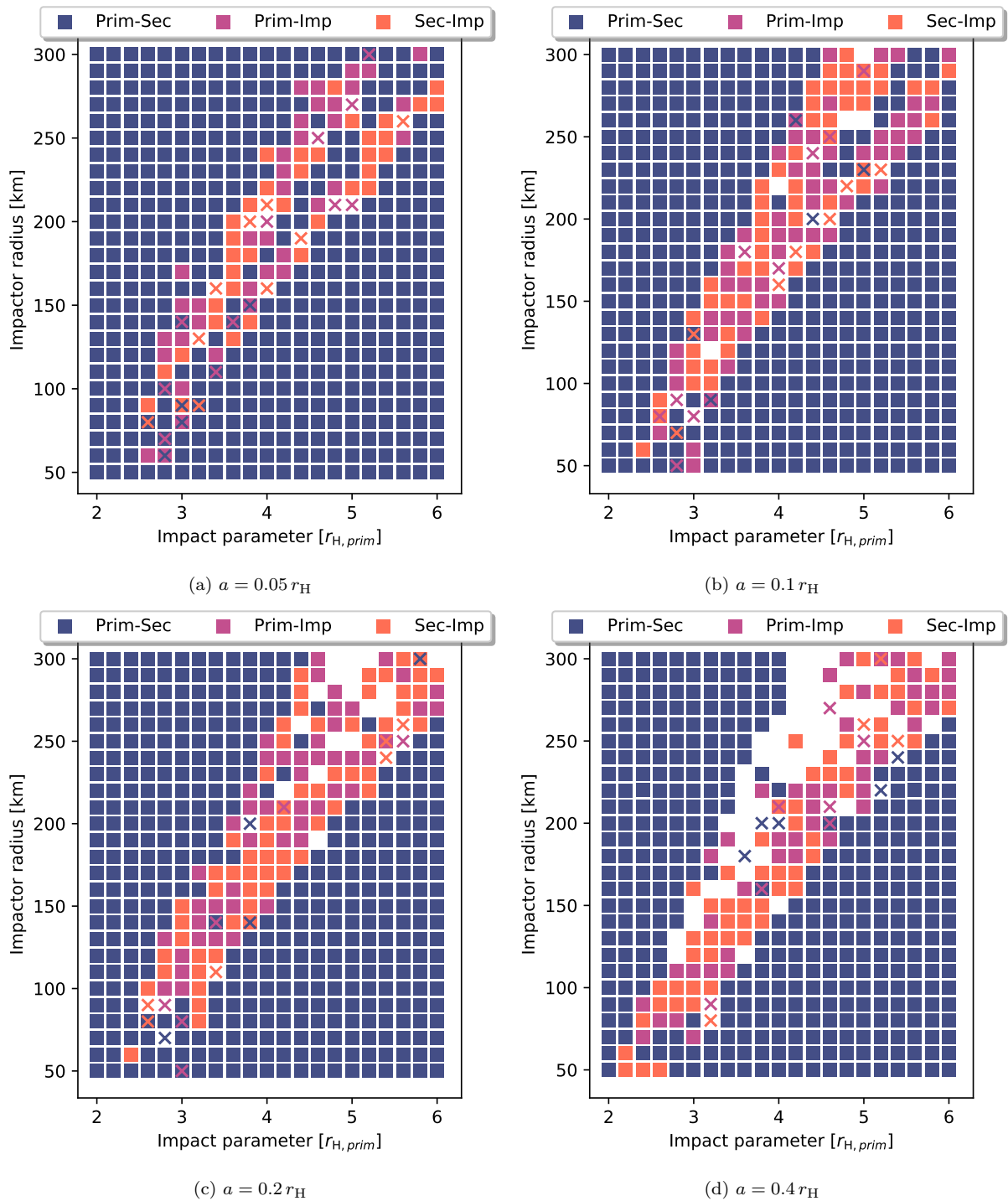


Figure 3.11: Each figure here shows the results of encounters with equal mass binaries of different width. Each point represents the outcome of an encounter. The squares represent two bound components, with the colour indicating which pair of components are bound. The crosses indicate two components colliding, while empty squares indicate total disruption of the binary.

binary up into a higher orbit, slowing it down and causing it to recede away from the impactor in a horseshoe orbit. In the bottom right the region of stability is the result of the combination of high impact parameter and low impactor mass. The low mass impactors here are passing by the binary too fast to draw them together and cause a close encounter. We can see that binary width has a large effect on the outcomes of encounters. As the binary width increases, the region of chaotic results widens, and as the region widens we also see a greater proportion of total disruptions compared to component swaps. The original binary survives more often if it is tighter.

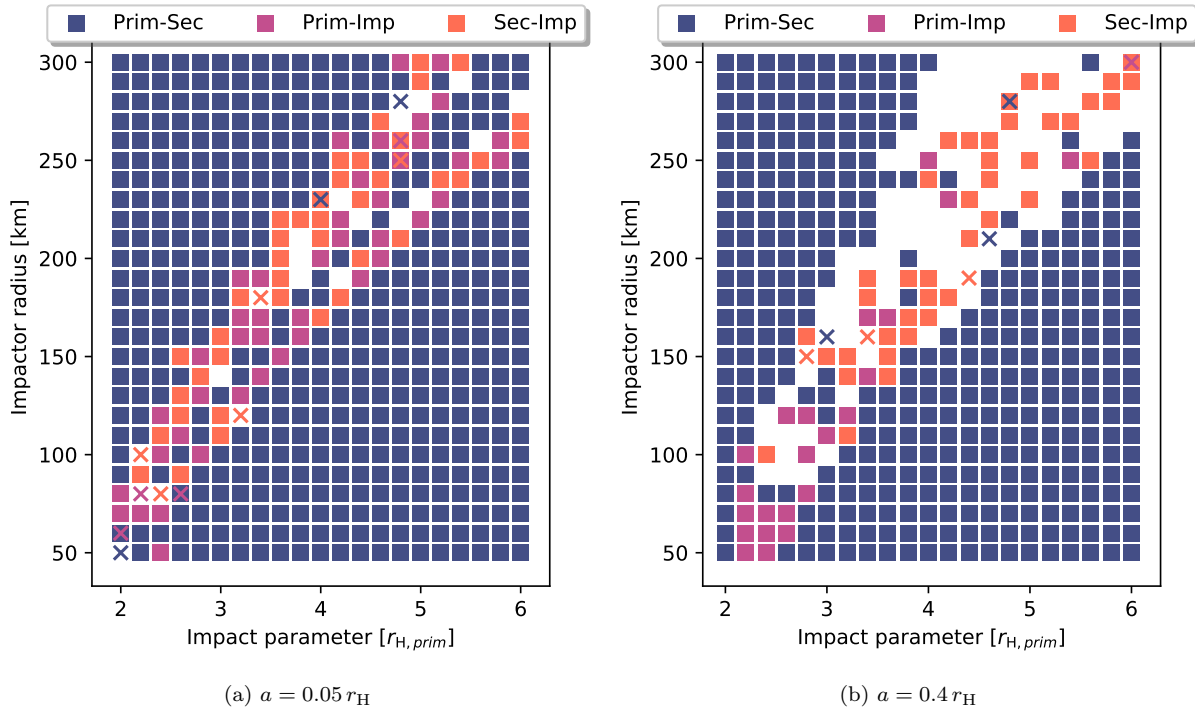


Figure 3.12: 10:1 mass ratio binaries. The squares represent two bound components, crosses represent collisions, while empty squares indicate total disruption of the binary.

Figure 3.12 shows binaries with a large mass ratio. In this case there is a widening of the chaotic region. There are also more total disruptions, and new binaries composed of the primary and the impactor are rare. Figure 3.13 shows the effect that a non-zero initial binary eccentricity has. For the wider binaries this tends to result in even more disruptions. Here we also see a further widening of the chaotic region, and an increase in the amount of total disruptions.

Within the region covering the close encounters, there will be a spread of chaotic outcomes that depend sensitively on the arrival time of the impactor, as shown in the previous section. Therefore we can't draw specific conclusions about any one particular interaction from this plot, but can look at the overall trends. We can also simulate the entire parameter space multiple times, and simulate different impactor arrival times by initializing the binary with  $e_{\text{bin}} = 0$ , and  $f_{\text{bin}}$  randomly chosen from a uniform distribution as in the previous section.

This sensitivity is illustrated further in figure 3.14. Here we have two suites of simulations with the same setup but with a randomised initial  $f_{\text{bin}}$  for the binary mutual orbit. In each case we can see the region of close encounters stay roughly the same. There do seem to be patterns of a sort when we compare the two plots. Disruptions are common in both, but there also does seem to be a concentration of disruptions on the left side of the region of close encounters. So

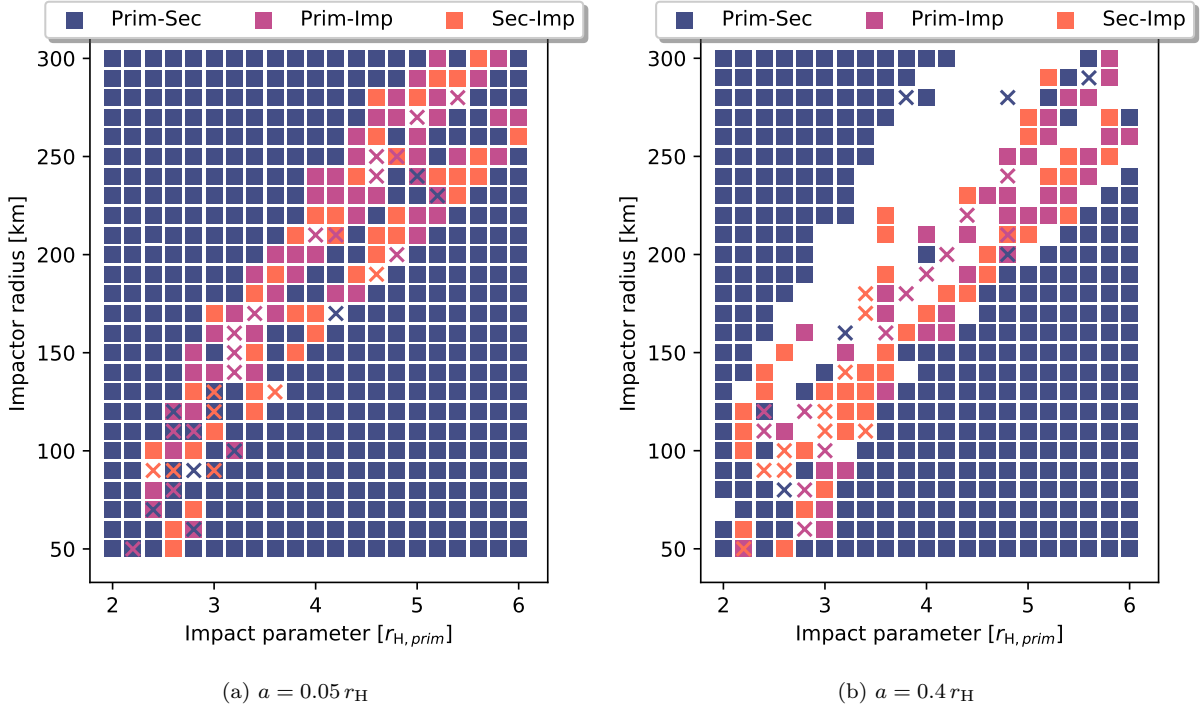


Figure 3.13: Binaries with high eccentricity,  $e_{\text{bin}} = 0.5$ . The squares represent two bound components, crosses represent collisions, while empty squares indicate total disruption of the binary.

within the range of possible close encounters this means that for a given impact parameter, disruptions are more likely the more massive the impactor is.

For a given impactor mass there is a tendency for more disruptions at lower impact parameters. So slower more massive impactors will more easily disrupt the binary, while faster less massive ones will tend to not only disrupt the binary but capture one of the escaping components and form a new binary.

We attempted to quantify this randomness by repeating each experiment multiple times. We repeated each parameter space experiments five times with randomized  $f_{\text{bin}}$  for each configuration. Figure 3.15 compares encounter outcomes for different sets of binaries. In general around 80% of original binaries survive in each case, but there is a steady trend where the tighter binaries survive more often. This rate of decline is similar for both the equal mass binaries and the binaries with a 10:1 mass ratio.

Between the other possible outcomes, encounters with the binaries with the larger mass ratio are more likely to result in disruptions, and this effect increases with binary width. Almost 20% of the encounters between the widest 10:1 mass ratio binaries result in disruptions. Disruptions also increase with binary width for the equal mass binaries, but not to the same extent. Disruptive encounters with the equal mass ratio binaries are more likely to result in a new binary being formed. This happens in around 20% of cases across all binary widths except for the tightest  $a = 0.05 r_H$  binaries, where this figure is lower. For the tighter binaries across both mass ratios, total disruptions are rare, at around 5% of outcomes. Even disruptive encounters with these tighter binaries easily allow two of the bodies to become gravitationally bound again. Collisions do not seem to display any trend in likeliness across different combinations of mass ratio and mutual orbital separation. They occur in around 5% of encounters across all of these parameters.

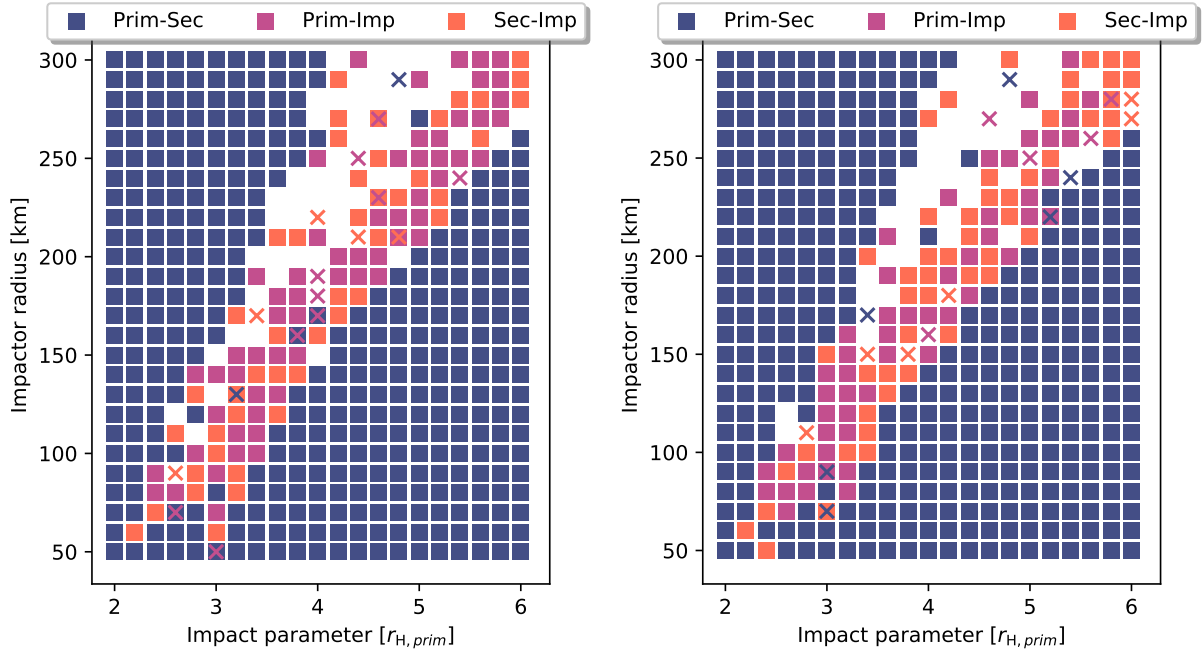


Figure 3.14: Final configuration of equal mass,  $a = 0.4 r_H$ ,  $e_{\text{bin}} = 0$  binaries after encounters with different impactors. Each run was randomised by a randomly selected initial  $f_{\text{bin}}$  for the binary mutual orbit. The squares represent two bound components, crosses represent collisions, while empty squares indicate total disruption of the binary.

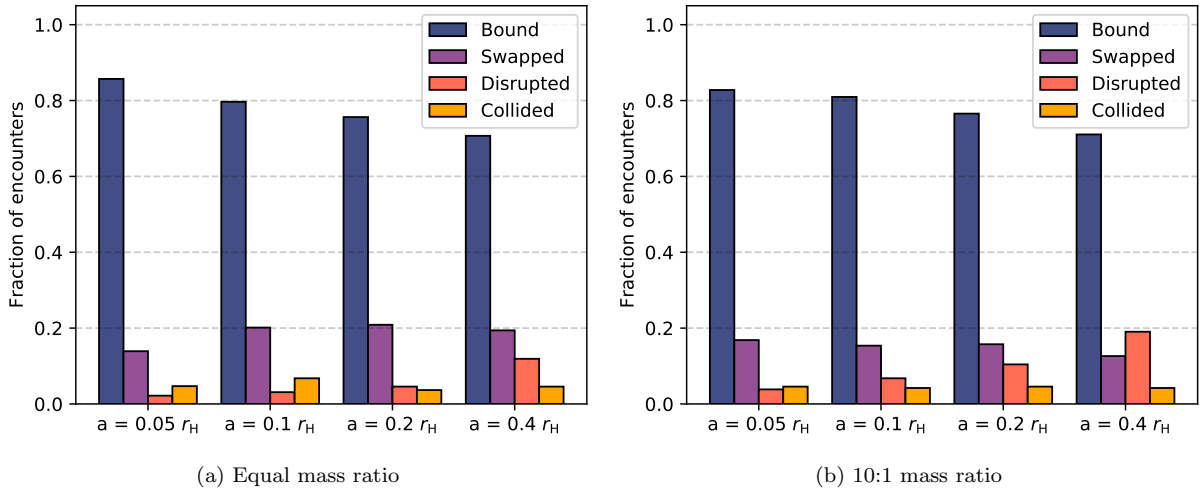


Figure 3.15: Distribution of results for encounters on an equal mass binary, and a binary with a 10:1 mass ratio. The results are separated by initial semi-major axis.

### 3.3.2 Binary changes in parameter space

In the region of the parameter space where binaries tend to survive they may be affected in other ways. While the binary may stay bound after the encounter there could be changes to the mutual orbital separation and eccentricity. The removal of energy by the passing impactor will remove angular momentum and cause the mutual orbital separation to decrease.

Figure 3.16a shows the final eccentricity of binaries after encounters with the same impactors as in the previous section. Outside of the corridor of chaotic results there are changes to the eccentricity of the binary. The new eccentricity is highly dependant on the proximity and mass of the impactor. There does seem to be a limit to the size of the impact parameter  $b$ , where

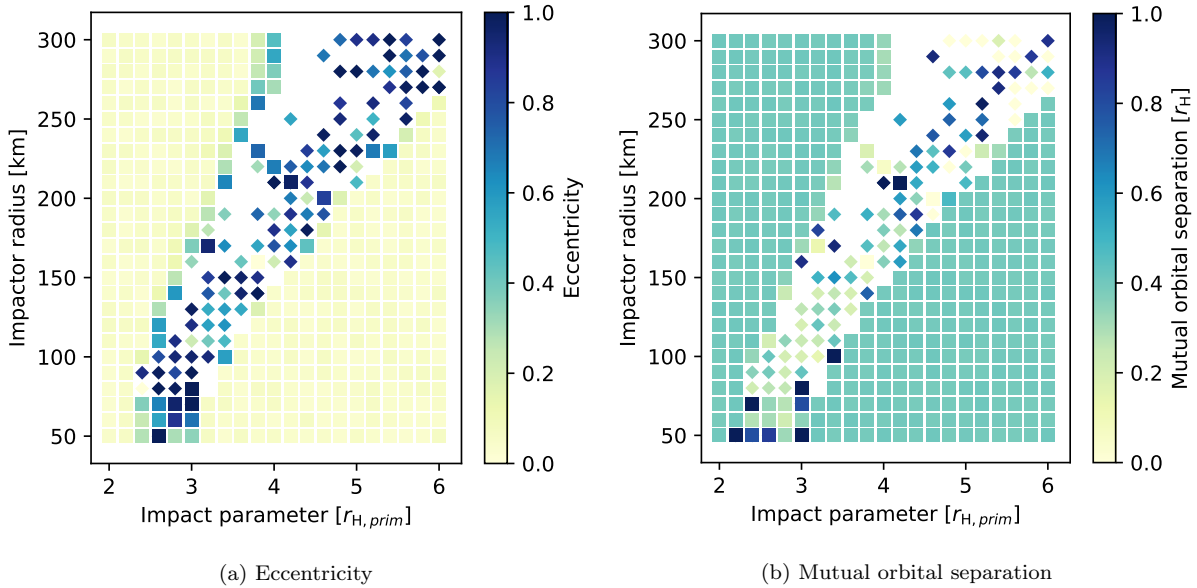


Figure 3.16: Ultra wide binaries with  $a = 0.4 r_H$ . New binaries are indicated by diamonds, while the original binary is represented by a square.

beyond it there is very little effect on the eccentricity. Possible small repeated increases to the eccentricity could eventually result in disruption of the binary, or collision between the primary and the secondary. Along the left side of the region of close encounters, the eccentricity is more likely to be pumped up. We can also see in the figure the eccentricities of all the newly created binaries composed of either the impactor and the primary or the impactor and the secondary. These new binaries tend to have extremely large eccentricities.

Figure 3.16b shows the final mutual orbital separation of the binaries after the same set of interactions. Away from the region of close encounters, this stays steady at  $0.4 r_H$  but within this region the new binaries tend to have mutual orbital separations that are relatively tight in the lower half of this region. For the higher mass impactors and higher impact parameters the newly created binaries tend to have mutual orbital separations greater than the original binary. These new wider binaries can have stable orbits, as our unit of measurement is the Hill radius of the original primary component. These new binaries towards the top of the figure will have the impactor as the new primary, allowing orbital separations of around  $0.8 r_H$  without further disruption.

Figure 3.17 shows what happens to a slightly tighter binary with  $a = 0.2 r_H$ . In this case more new binaries are formed, but they almost universally have high eccentricities. We also see the same pattern as in figure 3.16b with the mutual orbital separation of the new binaries being

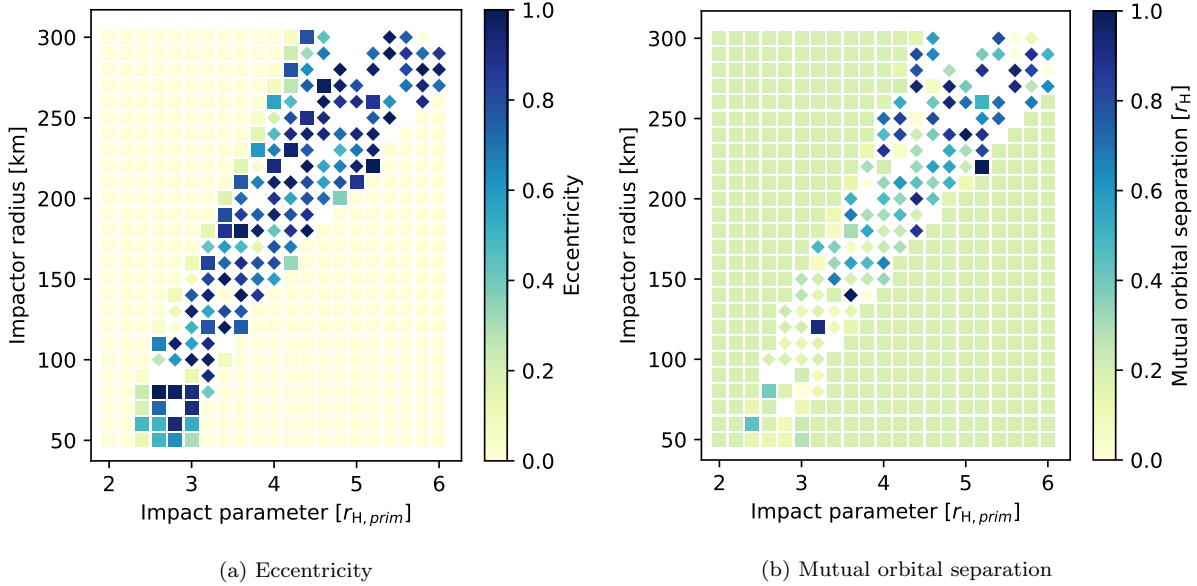


Figure 3.17: Wide binaries with  $a = 0.2 r_H$ . New binaries are indicated by diamonds, while the original binary is represented by a square.

tighter than the original binary for the less massive impactors, and wider than the original for the more massive impactors.

What we see in general is that new binaries are frequently formed during disruptive encounters, with the majority of such encounters for almost every original binary width resulting in a new binary, and with these new binaries being highly excited.

### 3.4 Single binary

Now that we have examined the ways in which different kinds of binaries react to encounters with different impactors, we move on to how a single binary experiences encounters throughout its lifetime. We will initialize a binary, and then subject it to the kinds of encounters it is likely to experience. The size of impactors it will meet will be chosen from a distribution, and the encounter velocities will be a function of the eccentricity and inclination of the impactor, taking into account the possible eccentricities and inclinations that are present in the Kuiper belt.

#### 3.4.1 Frequency of encounters

Before we subject the binary to encounters, we need an estimate of how many encounters a binary is likely to endure during the course of its lifetime. Encounters between binaries and third bodies depend on the number density of objects in the region. Also important is the mass function of cold classicals. Although more massive bodies will have a much larger encounter cross section due to gravitational focusing, they are rare in the Kuiper belt, resulting in encounters with large bodies occurring less frequently than encounters with smaller objects. The cold classical belt is defined as extending from about 42 AU to about 47 AU. The objects there are defined as having an inclination of less than  $5^\circ$ . The volume of the cold classical region can be estimated as a roughly torus shaped segment of a sphere as in figure 3.18. The height of this region can be found using the inclination of the cold classical belt,  $i = 5^\circ$ , and the distance from the Sun

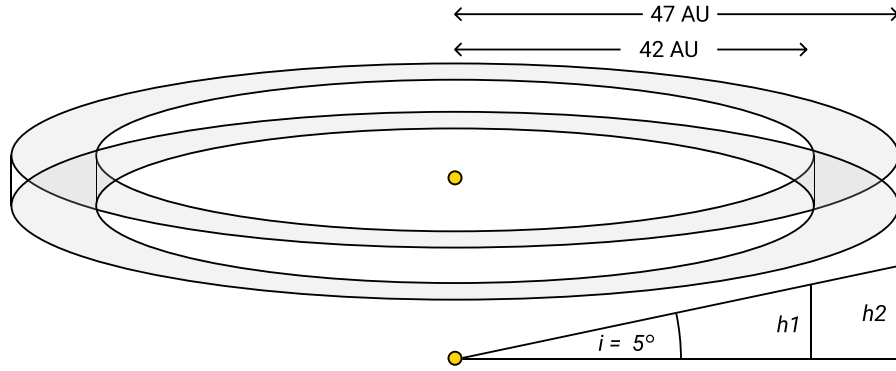


Figure 3.18: Volume of the cold classical region of the Kuiper belt. The cold classical region is roughly torus shaped, with an inner edge at 42 AU and an outer edge at 47 AU. The height can be approximated from  $i = 5^\circ$ , the boundary between the hot and cold populations.

that we want to measure at. With the classical belt spanning the region between 42 AU and 47 AU, a simplifying midpoint value of 44 AU can be used. The height of this region is

$$h = a \sin i = 3.8 \text{ AU}, \quad (3.3)$$

where  $a = 44 \text{ AU}$  and  $i = 5^\circ$ . Therefore the volume of the region is

$$V = 2\pi h(x_1^2 - x_0^2) \approx 10^4 \text{ AU}^3. \quad (3.4)$$

where  $x_1 = 47 \text{ AU}$  and  $x_0 = 42 \text{ AU}$ , and we multiply  $h$  by 2 to account for the height above and below the ecliptic. The cold classical binaries we are investigating are not only subject to encounters with other cold objects, but with other dynamical populations as well. Although the cold classicals are dynamically cold and restricted to within  $5^\circ$ , hot classicals with larger inclinations will have to pass through the ecliptic and through the cold objects, and the higher inclinations will lead to much shorter encounter timescales and a far smaller probability of a significant interaction, so the encounters here will be restricted to those with other cold classicals. We now need a total amount of bodies that have a reasonable chance of encountering our binary over the course of its lifetime. To calculate the total number of objects in the classical Kuiper belt we need the total mass of the region. Estimates of the total mass of the Kuiper belt put it at  $1.97 \pm 0.030 \times 10^{-2} M_\oplus$  (Pitjeva & Pitjev 2018), with the mass of just the cold classical region at  $3 \times 10^{-4} M_\oplus$  (Fraser et al. 2014). Assuming that the cold classicals are representative of the original population of planetesimals, the streaming instability probably played a large role in their formation, and can be used to determine their mass distribution. The initial mass function of bodies formed by the streaming instability is estimated to be (Schäfer et al. 2017, Simon et al. 2017)

$$\frac{dN}{dM} \propto M^{-1.6}. \quad (3.5)$$

Integrating this over the total range of masses expected in this region, from 10 kg to a maximum of  $10^{21} \text{ kg}$  which is about the mass of a 1000 km body, and using the total mass of the region

to find the constant of proportionality  $k$ ,

$$\begin{aligned} M_{\text{tot}} &= k \int_{M_{\text{min}}}^{M_{\text{max}}} M \times M^{-1.6} dM \\ &= k \frac{1}{0.4} \times 3 \times 10^{18} \text{ kg}^{0.4}. \end{aligned} \quad (3.6)$$

So with  $M_{\text{tot}} = 3 \times 10^{-4} M_{\oplus} = 1.8 \times 10^{21} \text{ kg}$ , that gives us  $k = 3 \times 10^{12} \text{ kg}^{0.6}$ , and we can then calculate  $N$ . We are only interested in objects with a minimum size of around 1 km, as small objects will not significantly affect the binary,

$$N = k \int_{M_{\text{min}}}^{M_{\text{max}}} M^{-1.6} dM \approx 3 \times 10^5. \quad (3.7)$$

To calculate the encounter rate for a particular binary we need an encounter cross section. We did not explicitly calculate the effect that gravitational focusing would have on enlarging the encounter cross section, however we saw from the earlier parameter space experiments that for objects smaller than around 300 km, the maximum distance at which the path of the binary will be focused into an encounter with the impactor is around  $6 r_{\text{H}}$ . We can therefore take the encounter cross section to be a circle around the binary with a radius of  $6 r_{\text{H}}$  of the primary. For a 100 km body with our standard density of  $700 \text{ kg m}^{-3}$  and distance from the Sun of 44 AU, this radius will be

$$r = 6 \times 44 \text{ AU} \left( \frac{m_{\text{prim}}}{3M_{\odot}} \right)^{1/3} = 3 \times 10^9 \text{ m}. \quad (3.8)$$

Then the cross section is  $\sigma = \pi r^2 = 3 \times 10^{19} \text{ m}^2$ . The encounter rate is then

$$C = n\sigma dv, \quad (3.9)$$

where  $n$  is the number density,  $n = N/V = 10^{-32} \text{ m}^{-3}$ ,  $\sigma$  the encounter cross section, and  $dv$  the typical encounter velocity. The typical encounter velocity between objects on circular Keplerian orbits can be estimated from the Keplerian shear at this distance, using a value of  $r = 4 r_{\text{H}}$  as the typical radial difference in position,

$$v_{\text{shear}} = -1.5\Omega_{\text{K}}r = 2.1 \text{ m s}^{-1}. \quad (3.10)$$

So equation [3.9](#) becomes

$$C \approx 10^{-12} \text{ s}^{-1}. \quad (3.11)$$

We are left with an average encounter frequency of  $10^{-12} \text{ s}^{-1}$ , or  $3 \times 10^{-5} \text{ yr}^{-1}$ . This is a very simplified calculation, which does not take into account things like how much of the mass is tied up in binaries, and the rate at which the hot classicals and other scattered and detached objects enter this region. Therefore the true rate could be higher or lower. It also ignores the likely much more cataclysmic period of push-out by Neptune, which would possibly have created a higher encounter rate.

### 3.4.2 Binary evolution over lifetime

With a typical encounter frequency as described in the previous section, we can now follow a binary as it evolves as a result of multiple encounters with other bodies. Multiplying the encounter frequency by the age of the solar system should give an estimation of the total amount

of encounters the typical binary can expect to have during its lifetime. This is assuming a constant encounter rate, which is reasonable if considering the period after push-out by Neptune, and the settling of the Kuiper belt into its current configuration. The number of encounters is then  $N_{\text{enc}} = C \times T = 1.3 \times 10^5$ . We reduced this to  $10^5$  total encounters for the sake of simplicity and computation time, and with the knowledge that simplifying assumptions were made at every step of the calculation that led to this number.

To attempt a realistic representation of the collisional environment that a binary in the cold classical belt will experience, encounters were engineered with impactors of random mass and random impact parameter. The mass of the impactor was randomly drawn from a distribution which corresponds to the size distribution of objects in the Kuiper belt. We use the streaming instability power law to determine the size distribution of planetesimals in the classical belt (Schäfer et al. 2017, Simon et al. 2017). The impact parameter before each encounter is drawn

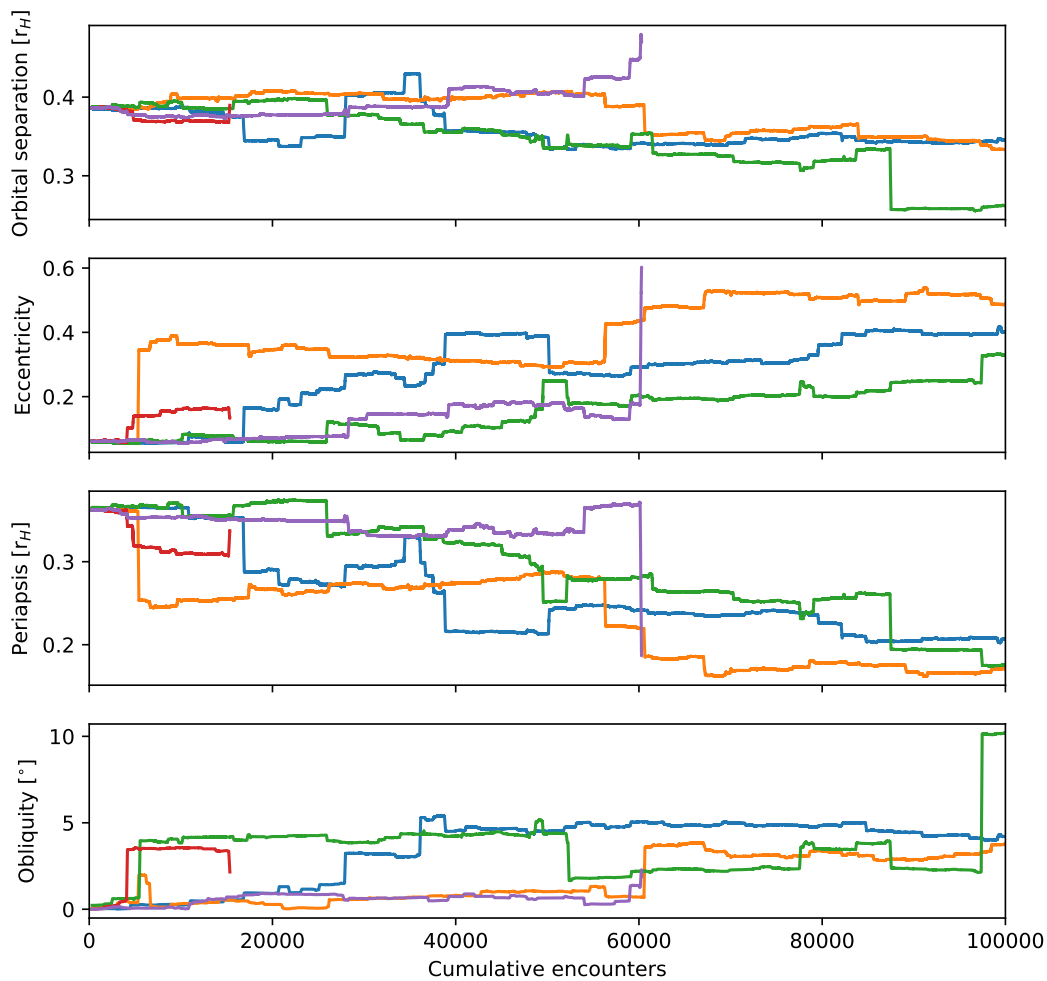


Figure 3.19: Evolution of orbital elements of 5 different binaries over the course of  $10^5$  random encounters. Each coloured line represents a different binary. The original binaries all begin with the same eccentricity and semi-major axis, in this case  $a_{\text{bin}} = 0.4 r_{\text{H}}$  and  $e_{\text{bin}} = 0$ .

from a uniform distribution of  $-6 r_{\text{H}}$  to  $6 r_{\text{H}}$  as this is the width of the encounter cross section  $\sigma$  used in the previous section to calculate the encounter frequency. The eccentricity of the impactor is chosen from a Rayleigh distribution with  $\sigma = 0.05$ , and the inclination is chosen

from a Rayleigh distribution with  $\sigma = 2^\circ$ , which correspond to the observed distributions in the cold classical belt (Brown 2001, Noll, Grundy, Stephens, Levison & Kern 2008, Gulbis et al. 2010). After every encounter the binary is reset to the origin of the coordinate system and the six orbital elements of the binary at the end of the simulation are used to recreate the binary in the next simulation. If a collision occurs one of several additional steps are taken. A collision between the two components of the binary will end the experiment, and the collision energy investigated. If the collision occurs between either the primary and the impactor, or between the secondary and the impactor, the chain of simulations will continue as long as the collision was not catastrophically energetic. If this is not the case the two colliding components will merge with conservation of energy and momentum and at the beginning of the next simulation the new binary will contain the new updated masses.

Figure 3.19 shows the evolution of semi-major axis and eccentricity of five binaries over  $10^5$  encounters. In each case the original binary was composed of two equal mass components with radius 100 km. The original semi-major axis was  $a_{\text{bin}} = 0.4 r_{\text{H}}$  and the original eccentricity was  $e_{\text{bin}} = 0$ .

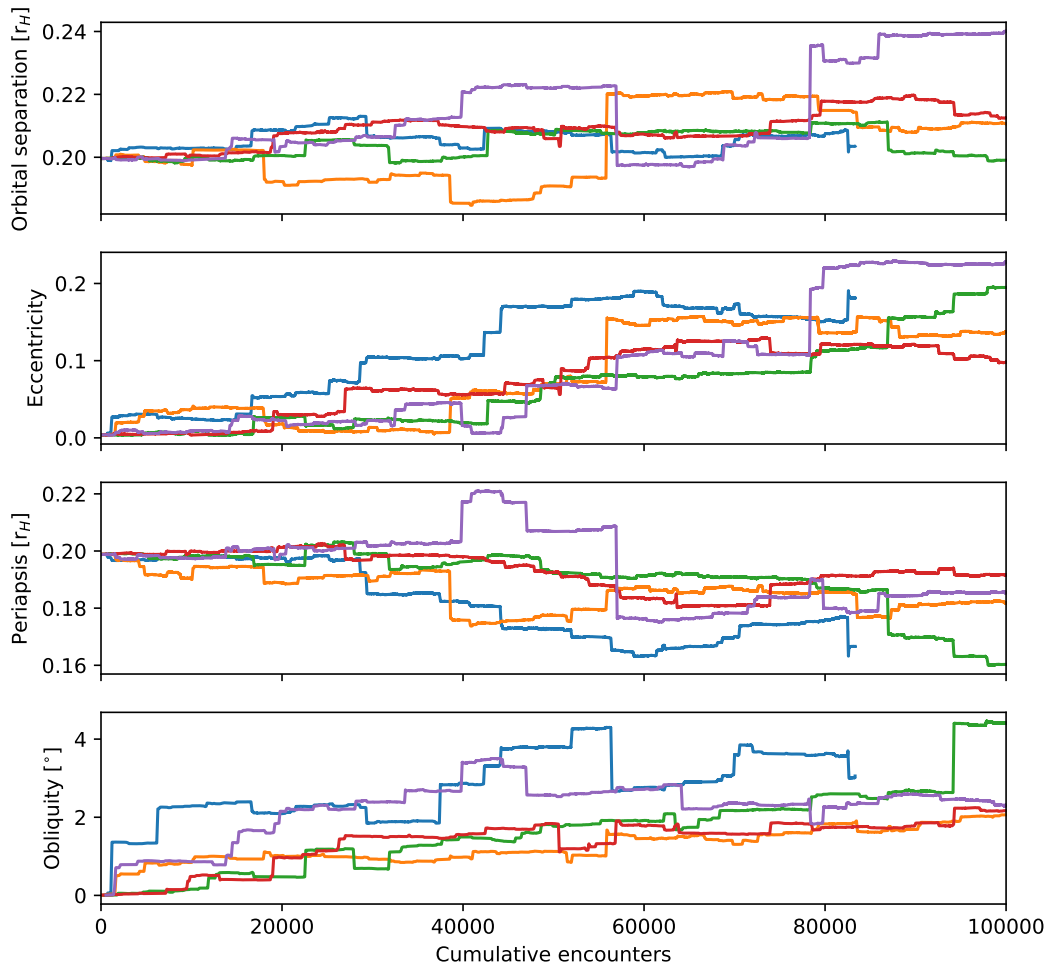


Figure 3.20: Evolution of orbital elements of 5 different binaries over the course of  $10^5$  random encounters. Each coloured line represents a different binary. The original binaries all begin with the same eccentricity and semi-major axis, in this case  $a_{\text{bin}} = 0.2 r_{\text{H}}$  and  $e_{\text{bin}} = 0$ .

Figure 3.20 shows the results of a set of these experiments on a binary with  $a_{\text{bin}} = 0.2 r_{\text{H}}$

and  $e_{\text{bin}} = 0$ . The colours in each panel of the plot represent the same binary. As is the previous case the binary evolves slowly, with most encounter having very little effect on the binary, and interactions with favourable combinations of factors, such as a large impactor and slow encounter speed, causing sudden changes in the orbital elements. The mutual orbital separation of the binaries seem to change randomly, spreading out but without a preference for increasing or decreasing. The eccentricity again tends to increase, and after  $10^5$  encounters usually has increased by at least 10%. The binary mutual inclination or obliquity also tends to increase, but by a very small amount.

Figure 3.21 shows binary evolution with a similar binary but with a non-zero eccentricity. In this case the eccentricity does not tend upwards as in the previous plots but spreads out randomly. We can see sudden major changes in the orbital elements. The larger jumps, which are a result of interactions with larger impactors, tend to increase the mutual orbital separation of the binary and pump up the eccentricity. Again the changes in the obliquity are small.

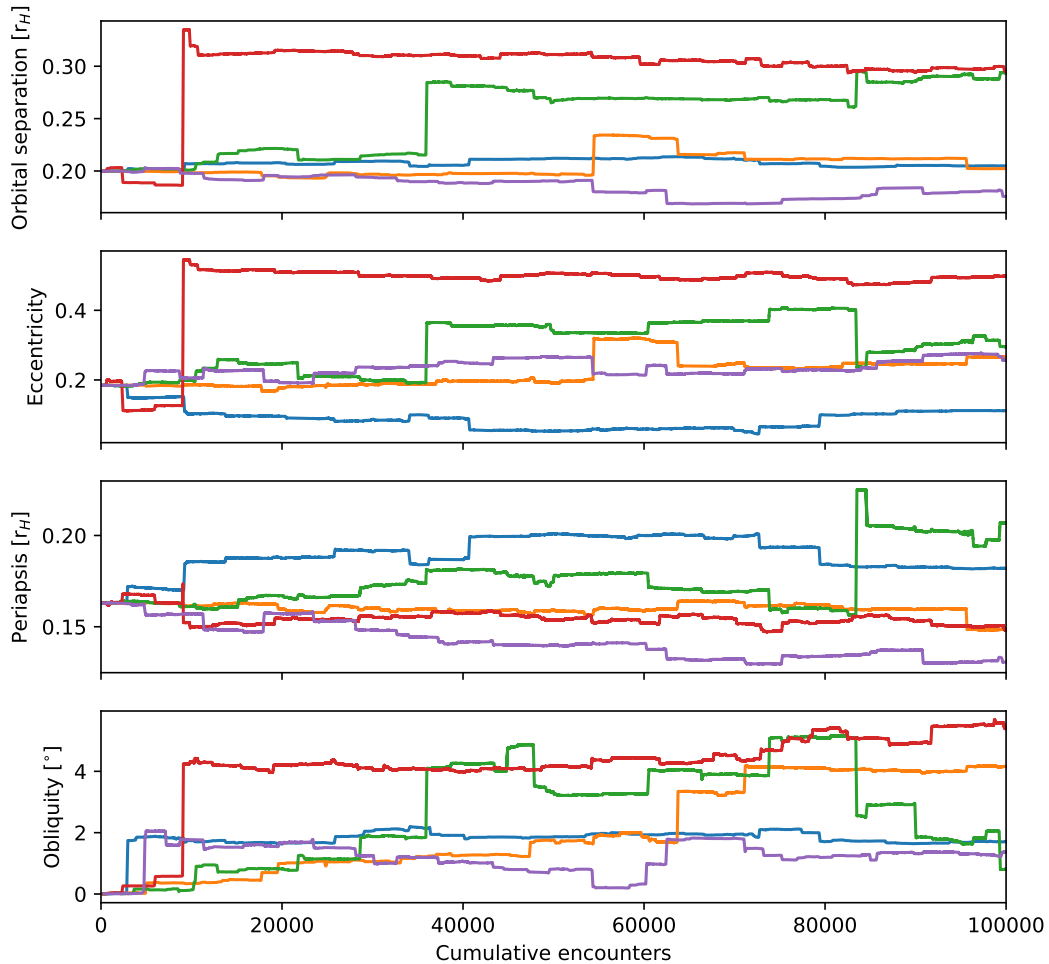


Figure 3.21: Evolution of orbital elements of 5 different binaries over the course of  $10^5$  random encounters. Each coloured line represents a different binary. The original binaries all begin with the same eccentricity and semi-major axis, in this case  $a_{\text{bin}} = 0.2 r_H$  and  $e_{\text{bin}} = 0.2$ .

Most encounters that any particular binary experiences will have a negligible effect. This is a result of the mass distribution heavily favouring low mass objects. As the gravitational force is dependant on mass, the force these less massive impactors have on the binary is very small.

In figures 3.19 and 3.20 the evolution of  $e_{\text{bin}}$  and  $a_{\text{bin}}$  is characterised by periods of little to no change interrupted by drastic changes which are a product of a particular combination of impactor mass and impact parameter  $b$ . The binaries beginning with  $e_{\text{bin}} = 0$  show a tendency for  $e_{\text{bin}}$  to increase. In figure 3.22 with binaries beginning with  $e_{\text{bin}} = 0.2$ , the eccentricity also tends to increase but the trend is not as pronounced. This is probably just a result of the eccentricity having nowhere to go but up when it starts at zero. The lines end when a binary is destroyed, either by total disruption or catastrophic collision.

Figure 3.22 displays the effects of many encounters on binaries with high initial obliquity. The obliquity again changes by small amounts. The eccentricity starts low for all of these binaries, but tends to be pumped up as a result of the encounters.

It is important to remember that these experiments only simulate a particular number of encounters one after the other, and not an amount of time that would result in these many encounters. Without the binary evolving on its own between encounters we lose the influence of the Kozai-Lidov effect on the eccentricity and obliquity of the binary.

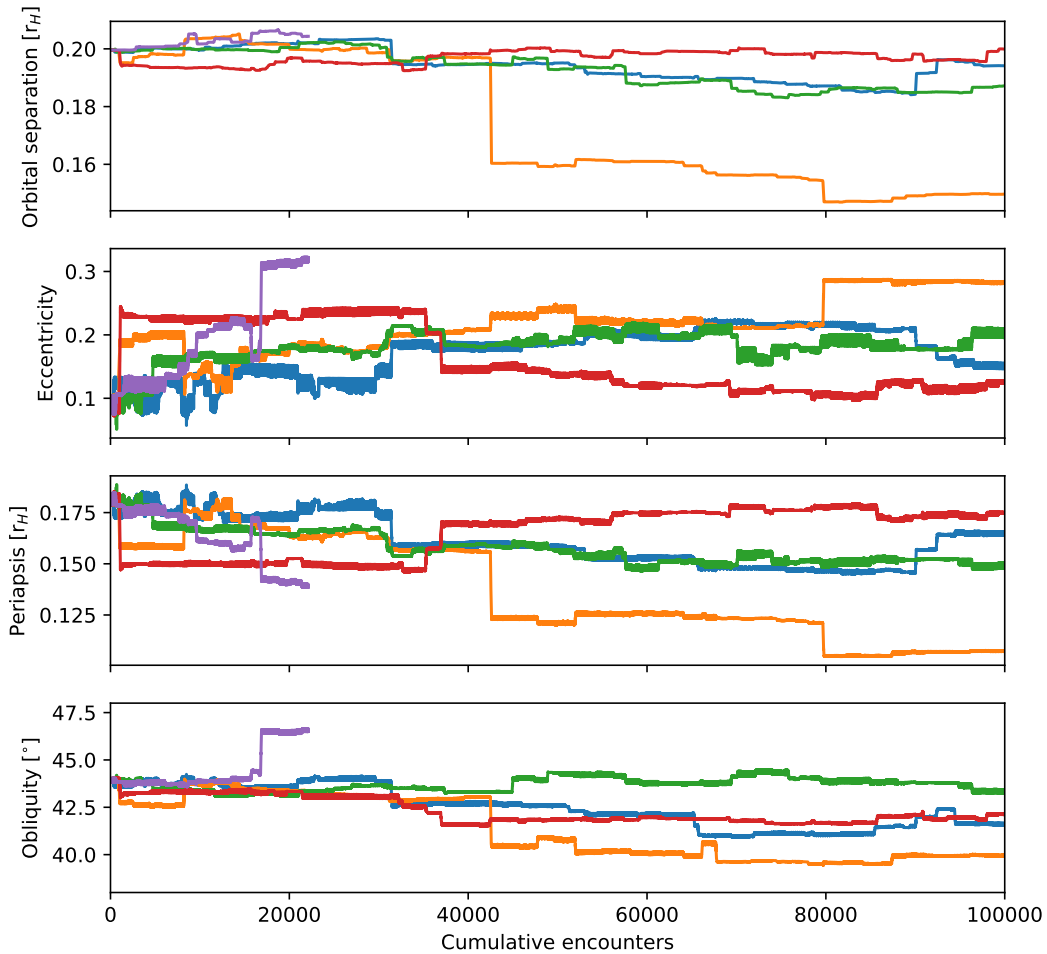


Figure 3.22: Evolution of orbital elements of 5 different binaries over the course of  $10^5$  random encounters. Each coloured line represents a different binary. The original binaries all begin with the same eccentricity, semi-major axis, and obliquity, in this case  $a_{\text{bin}} = 0.2 r_{\text{H}}$ ,  $e_{\text{bin}} = 0.1$  and  $i = 45^\circ$ .

### 3.5 Collision analysis

We have already seen how collisions can occur between each pair of components. Here we investigate the frequency of collisions and typical collision velocities and energies. Figure 3.23 shows the distribution of collision velocities as a result of encounters between an equal mass wide binary with mutual orbital separation of  $a_{\text{bin}} = 0.2 r_{\text{H}}$  and an impactor of the same mass and radius. Collisions are relatively common with this combination of initial conditions. The

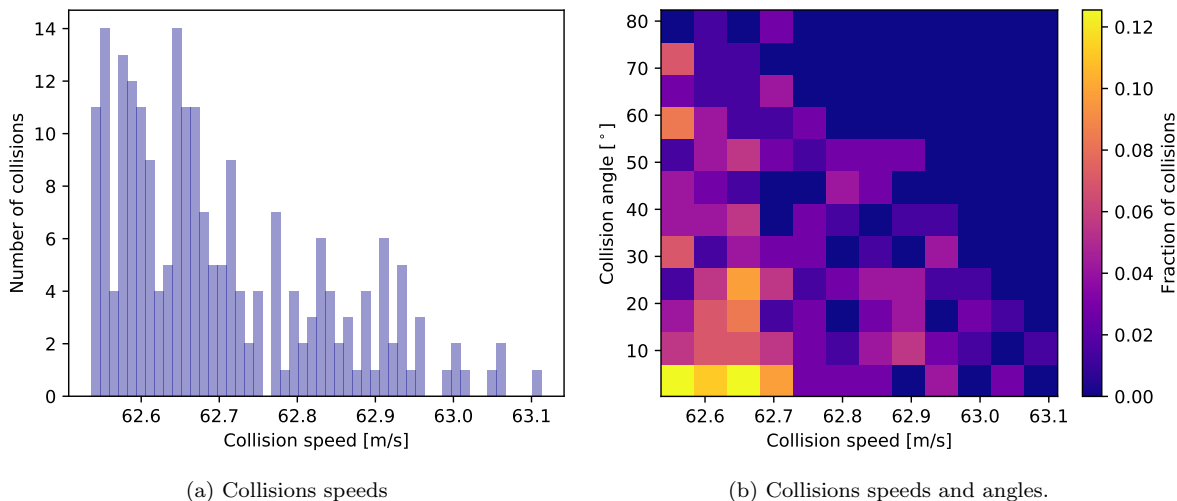


Figure 3.23: Distribution of collision speeds as a result of impacts occurring during encounters between an equal mass binary and impactor, as well distribution of speeds relative to impact angles.

only variable that differs between all of these encounters is the initial true anomaly of the binary, which was chosen randomly from a uniform distribution. The distribution peaks at just over  $62 \text{ m s}^{-1}$ , which corresponds to the escape velocity of a  $100 \text{ km}$  body with density  $700 \text{ kg m}^{-3}$ ,

$$v_e = \sqrt{\frac{2GM}{r}} = 62 \text{ m s}^{-1}. \quad (3.12)$$

Using the criteria for destructive impacts as those with collision speeds greater than the escape speed of the body, all of our impacts are right on this boundary. We can also compare the collisional energy to the gravitational binding energy. Using the peak of the collision speed distribution we get a collision energy of

$$Q_r = \frac{0.5\mu(dv)^2}{m_{\text{tot}}} = 2.9 \times 10^{21} \text{ J}, \quad (3.13)$$

and the binding energy of one of the bodies is

$$U = \frac{3Gm^2}{5r} = 3.4 \times 10^{21} \text{ J}. \quad (3.14)$$

These collisions are not very energetic in comparison to the binding energy of the bodies involved. For collisions to occur in our simulations we require long encounter timescales and slow relative velocities between binary and impactor. This is seen when we set up the impactor with zero eccentricity and inclination. As we just saw in the previous section, these particular types of encounters are rare. So while in the figure there are many collisions that could potentially lead

to contact binary formation, it is difficult to see this as an efficient formation pathway for contact binaries, given that this type of encounter is likely to be rare.

The collision speed is not the only factor in determining the outcome of any particular collision. The impact parameter will also be important. Figure 3.23b shows the distribution of collision angles calculated from the impact parameter in the same encounters as figure 3.23a. There are more collisions at smaller angles than at larger angles, indicating that impacts tend to be more head-on than oblique. This will lead to most of the kinetic energy of the two bodies being transferred to the collision. Figure 3.23b shows that there is a tendency for more head-on collisions to occur than oblique collisions. As the collision speeds increase there are fewer oblique collisions. These faster collisions tend to be more direct and therefore more destructive.

Figure 3.24 shows the collision speed distribution for collisions between a binary with a 10:1 mass ratio and an impactor equal in size to the primary, as well as the components of the collision along the position vector. In this case, collision speeds are grouped into two different

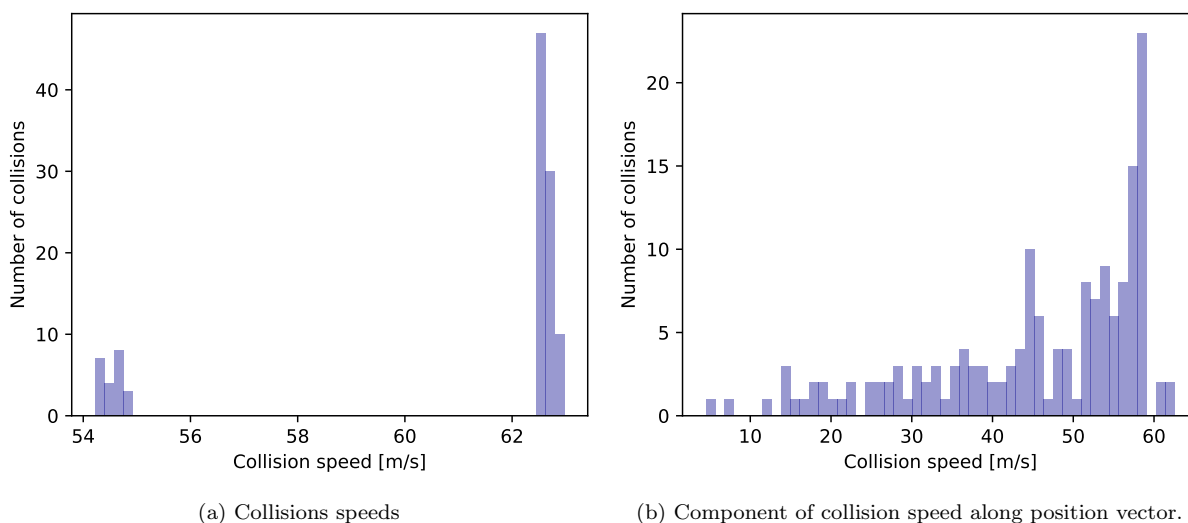


Figure 3.24: Distribution of collision speeds as a result of impacts occurring during encounters between 10:1 mass ratio binary and impactor.

categories. One of the groups corresponds to the peak of the distribution in figure 3.23 where all bodies had the same mass, indicating that these are all collisions between the primary and impactor, with the other group indicating collisions between the secondary and one of the other two components, and this latter group occur less frequently. Again all of these encounters are relatively low energy compared to the binding energy of the objects involved, particularly when accounting for the oblique angle at which encounters can occur. We also see again how the collision speed does not vary greatly, and is highly determined just by the mass of the objects. As our relative encounter velocities are smaller than the escape velocity of these bodies, the collision speed will not be significantly greater than this value.

# Chapter 4

## Discussion

### 4.1 Binary survival

The range of mutual orbital separations in the cold classical belt is quite wide. There is evidence for binaries of width up to  $0.23 r_H$  and as low as just  $0.005 r_H$  (Noll et al. 2020). Nesvorný et al. (2018) showed that the ability of binaries to survive push-out by Neptune is highly dependent on their width. We showed that the ability of a binary to survive encounters with an impactor is heavily dependant on the mutual orbital separation.

We investigated binaries with widths of  $0.05 r_H$ ,  $0.1 r_H$ ,  $0.2 r_H$ , and  $0.4 r_H$ . The ultra-wide binaries with  $a = 0.4 r_H$  were much more easily disrupted than the tighter binaries. So far there is no evidence for binaries this wide in the Kuiper belt. It is possible that the formation mechanisms that lead to binary creation are unable to produce ultra-wide binaries, or alternatively, they may have been created, and then disrupted. Most of the binaries yet discovered are very tight, with  $a < 0.05 r_H$ . We saw in figure 3.15 that binaries with this tight orbital separation survive close encounters with their initial components intact more often than the wider binaries.

We showed that the initial eccentricity of the binary has an effect on its ability to stay bound in figure 3.13. Circular binaries are more resilient to disruption than binaries with  $e = 0.5$ . The observed binaries in the Kuiper belt today display a range of eccentricities. There are extremely circular binaries, like the 90482 Orcus-Vanth system, which has a mutual eccentricity of  $e = 0.0009$  (Brown et al. 2010), while there are several with  $e \approx 0.5$ , with the largest known being that of 2006 CH69, which has  $e = 0.89$  (Parker et al. 2011). The more circular binaries are better able to survive encounters with similarly sized bodies.

In figure 3.15 we showed that during encounters that resulted in the primary and secondary being stripped away from each other, the most common result was the capture of one of the original components by the impactor and the creation of a new binary. This occurred in all cases except the widest binaries with a 10:1 mass ratio. While this result was common, the new binary tended to have orbital characteristics quite different from the original binary. The new binaries had very large eccentricity, as seen in figures 3.16 and 3.17. While binaries with very high eccentricity are seen in the Kuiper belt today, they are not common in the small number that have been discovered so far, as we showed in figure 1.7. This indicates that if contact binaries are formed during encounters such as those examined here, they are probably destroyed as a result of further encounters. The encounters with binaries with high initial eccentricity had the potential to create new binaries, but these also had very large eccentricities.

For a given impact parameter, a larger impactor tends to result in total disruption more often than the recapture and formation of a new binary. The energy added to the system by a

more massive impactor disrupting the binary leads to the newly free components having a larger kinetic energy than if the impactor was smaller. This greater kinetic energy means the impactor is often unable to capture one of the components into a new binary. We assume that encounters with very large impactors are rare, because there are far fewer of these larger bodies in the Kuiper belt. Encounters with bodies with similar mass to the two components of the binary are more likely to result in the creation of a new binary. The new mutual orbital separation of the new binary tended to be larger for the larger impactors as they have a larger Hill radius.

## 4.2 Binary mass ratios

We investigated both equal mass binaries, and binaries with a large mass ratio of 10:1. A commonly used criteria for classifying a binary as equal mass is a mass ratio of around a maximum of 2:1 (Nesvorný et al. 2018). It is equal mass binaries that are thought to be formed during the gravitational collapse that formed the two components (Nesvorný et al. 2010). The binary is created when the gas and dust that it collapses out of is rotating fast enough, and with enough angular momentum, that the cloud splits into two. In the cold classical region especially, probably all objects were born in binaries (Fraser et al. 2017) and have subsequently been disrupted. Binaries formed in this way are unlikely to have components of vastly different sizes.

Binaries with large mass ratios may have been formed after the formation of the individual components as a result of dynamical capture (Lee et al. 2007, Kominami et al. 2011), or for the larger bodies, from giant impacts (Canup 2005). These high mass ratio binaries are analogous to a Kuiper belt object having its own moon.

We showed that so-called equal mass binaries are more resilient to disruption than binaries with a mass ratio of 10:1, as can be seen in figure 3.15. Across a range of initial conditions and binary setups, the equal mass binaries survived encounters more easily than the larger mass ratio binaries. The much smaller mass of the secondary component is more easily stripped away by the approaching impactor. This effect is magnified if the impactor is more massive.

When a new binary was formed after one of these encounters, the impactor was more likely to capture the smaller secondary than the more massive primary. As with the equal mass binaries, this new binary was much more likely to have a very large eccentricity, and is therefore susceptible to disruption by subsequent encounters.

## 4.3 Formation of contact binaries

From simulations of the creation of contact binaries by collisions, such as those done in relation to Arrokoth (McKinnon et al. 2020) and 67P/Churyomov-Gerisemenko (Jutzi & Benz 2016), it was determined that contact binary forming collisions must be in the order of the escape speed of the smallest body. Collisions more energetic than this would seem to result in distortions to the shape of the two initial components which we do not see in the contact binaries for which there are good quality images.

While there are already several proposed mechanisms for contact binary formation, some of which were mentioned in section 1.5 (Rickman et al. 2015, Jutzi & Benz 2016, Nesvorný et al. 2018, Schwartz et al. 2018, Lyra et al. 2021), we were interested in whether encounters in the cold classical belt could cause the two components of the binary to collide frequently enough to provide another possible formation mechanism.

We find that collisions are common in our simulations. The vast majority of these collisions occur close to the escape speed of the largest body. These are also generally collisions between

either the impactor and the primary, or between the impactor and the secondary. The components of the contact binaries that have been studied so far seem to have similar properties (Grundy et al. 2020), indicating that they may have been formed close to each other, and making it unlikely they collided in the kinds of collisions we observed in our experiments, as collisions between the two components of the original binary were very rare. Figure 3.23 showed that the chaotic interactions between the three components during a close encounter can cause collisions with a speed similar to the escape speed. The probable prevalence of contact binaries in the Kuiper belt (Sheppard & Jewitt 2004, Thirouin & Sheppard 2017, Thirouin et al. 2017) would suggest that a more efficient and reliable formation path is present.

The appearance of Arrokoth suggests an oblique angle of impact because of the relatively undisturbed shapes of its two lobes (McKinnon et al. 2020). The angle of the collisions recorded in these simulations covered the entire range of 0 to 90° at most collision speeds. In general, most of the collisions recorded were more direct than oblique, particularly at the higher collision speeds, although there were far fewer collisions at these speeds anyway. As many of the low velocity collisions happened at highly oblique angles, they have the potential to cause non-destructive coalescence.

We showed that encounters such as those studied here do have the potential to alter the eccentricity and semi-major axis of the binary while allowing the binary to survive. Repeated encounters that remove angular momentum and energy and slowly reduce the mutual orbital separation of the binary could result in the slow collision of the two components and the formation of a contact binary, but that is not clear from our results. These effects are small, and required the impactor to closely approach the binary, remaining only just outside the area where chaotic effects take over and render the outcome unpredictable. A great number of encounters with just these characteristics would be needed to reliably create contact binaries. According to our work here, most encounters occur at a distance too great for the impactor to have a significant effect on the mutual orbit of the binary, or so close that the result becomes chaotic. Encounters close enough to consistently reduce the mutual orbital separation without disrupting the binary were rare in our simulations. This is noticeable in figures 3.16 and 3.17, as outside both sides of the chaotic regions the orbital separation was only affected in rare cases.

We conclude that the creation of contact binaries by the formation pathway investigated here, while possible, must only account for a very small minority of contact binaries in the current Kuiper belt. Following from this conclusion, it must be the case that another more efficient formation pathway must exist. As mentioned in section 1.5, there are already several proposed possible formation pathways. Mechanisms such as the destruction of a larger parent body and subsequent joining of two fragments (Rickman et al. 2015, Schwartz et al. 2018), are not related to binary evolution, but may be a source of contact binaries. Nesvorný et al. (2018) showed that contact binary formation is possible through the impact of the two components of an initially separated binary as a result of encounters with the giant planets as they migrate, but an important initial condition is that the original binary is tight. However, they concluded that this process is not efficient enough to produce enough contact binaries. In the case of 67P Churyumov/Gerasimenko, Lyra et al. (2021) found that formation and collision before the dissipation of the gas disc is possible with a combination of gas drag and Kozai-Lidov oscillations. The oscillations can increase the eccentricity, and lower the periapsis until collision occurs, with the removal of energy by gas drag aiding the process. They find that this process could lead to a contact binary fraction of 10% in the cold classical belt, agreeing with observations (Sheppard & Jewitt 2004). This combination of gas drag and Kozai-Lidov oscillations seems to be the most likely source for the majority of currently observed contact binaries, with possible small contributions from the effect investigated in this work.

## 4.4 Binary lifetime

We used a rough estimation to calculate that a binary could expect to be subjected to in the order of  $10^5$  encounters with other Kuiper belt objects with a minimum radius of around 10 km over the course of the lifetime of the solar system. We simulated individual binaries and followed their evolution over the course of  $10^5$  encounters with objects between 10 km and 300 km. This is a large number of encounters, but in keeping with the mass distribution of objects in this region, most of the encounters will be with objects that are too small to have any great effect on the binary. The evolution of the orbital elements of each binary was characterised by periods of slow changes punctuated by sudden jumps in their values. Most encounters were with bodies of low mass, and with inclination and eccentricity, that while low, were large enough to result in a low encounter timescale. Encounters require impactors with very low inclination and eccentricity to result in an encounter timescale large enough to allow the impactor to have a significant effect on the mutual orbit of the binary. This needs to be combined with an impactor that is massive enough and an impact parameter low enough to alter the binary.

Most binaries survived  $10^5$  such encounters, but not all of them did. In the current day Kuiper belt there are a lot of binaries, and the total binary fraction is high, probably at around 30% in the cold classical region (Noll et al. 2020). But according to Fraser et al. (2017), all objects here may have formed as binaries. This means that the majority were disrupted over the past 4 Gy. Encounters with similarly sized impactors may be the cause of these disruptions.

We showed that disruptive encounters are possible with the right size impactor and impact parameter, as well as a large enough encounter timescale, but we also saw that within a chaotic encounter there is a good chance that a new binary is formed to replace the one that was just destroyed. This replacement of the binary does not explain why most binaries have probably been destroyed. We can maybe explain this by observing that in almost all cases the new binary that is formed, while having a range of possible new mutual orbital separations, generally has an extremely high eccentricity, due to the chaotic circumstances of the capture of the two components into the new binary. Binaries with extreme eccentricities are more susceptible to disruption from close encounters than those on more circular orbits.

We followed a single binary that began with  $a = 0.4 r_H$ , and  $e = 0$ . These extremely wide binaries had much larger eccentricity after  $10^5$  encounters, if they survived at all. They also showed a trend of  $a$  decreasing, which in combination with the larger eccentricity meant that the periapsis decreased a lot over time. The obliquity of the binary increased by small amounts in all cases. In the case of the binaries with  $a = 0.2 r_H$ ,  $e = 0$ , the increase in eccentricity was also evident, but it progressed more slowly, and more of the binaries survived to the end of the simulations. This agrees with our results suggesting that the extreme wide binaries are more easily disrupted.

Across the different sets of binaries, around 80% survived all  $10^5$  encounters. There is a large discrepancy between this survival rate of 80% and the 30% binary fraction in the cold classical belt today. This is probably a result of a simplified encounter rate calculation used here, as well as the fact that we ignored other binary disruption mechanisms in this work. In particular, the push-out of the primordial disc of planetesimals during the outward migration of Neptune may have stripped the majority of binaries apart (Fraser et al. 2017). The effect investigated in this work may be responsible for the disruption of around 20% of binaries, but a more thorough calculation of the encounter rate will be required to more precisely determine if this is correct. An important part of this calculation is the determination of the number and size of the bodies in the cold classical belt. Future improvements in observations of the region will be helpful here. If we take the assumption that planetesimal formation can directly lead

to binary formation (Nesvorný et al. 2010), a more accurate understanding of the magnitude of the effect of encounters on binary disruption, in combination with more accurate measurements of the binary fraction in the cold classical belt, will put tighter boundaries of the effectiveness of push-out at disrupting binaries. This in turn may give a better understanding of the process of push-out by Neptune, such as the size of the initial disc, and the rate at which Neptune migrated outwards.

## 4.5 Encounter timescale

In this work we have tried to understand what happens when Kuiper belt binary planetesimals encounter similarly sized third bodies. We engineered a wide range of different kinds of encounters, including those with impactors that orbit the Sun with non-zero eccentricity and inclination. We discovered that the encounter time is critical in affecting the configuration of the binary. When the binary is on a circular orbit, and the impactor is orbiting in the same plane, and also on a circular orbit, the encounter time is simple to calculate using the Keplerian shear  $\Omega_K$ . All that determines the encounter time in these cases is the impact parameter. This is a situation that is not representative of the distribution of bodies even in the cold classical region of the Kuiper belt. Even these dynamically cold objects can have inclinations up to  $5^\circ$ , and eccentricities up to around 0.25, but with most having eccentricities of below around 0.1. To affect the binary in any meaningful way, the encounter timescale needs to be low. The encounter speed for an eccentric and inclined orbit can be estimated as (Lissauer & Stewart 1993)

$$v = (e^2 + i^2)^{1/2} v_K. \quad (4.1)$$

To achieve longer encounter timescales and more interesting interactions requires the impactor to have a low eccentricity and low inclination. Encounters like this would appear to be unlikely compared to the range of possible encounters, when we take into account the range of eccentricities and inclinations in the cold classical region. Added to this are the hot classicals, which will by definition have higher inclinations than  $5^\circ$ . So most of the third bodies that a binary on a circular orbit will have an encounter with will be much too fast to affect the binary itself.

So even with a high number of expected encounters, using a calculation of the number density of the classical Kuiper belt, and an estimate of the initial mass function, the high typical encounter speed may result in a binary surviving to the present day.

## 4.6 Limitations of this approach

The greatest challenge when performing numerical simulations is computation time. The greatest factor influencing the elapsed time taken to simulate a binary encounter was the mutual orbital separation of the binary. This restricted our ability to approach the problem in every way possible. Binaries tighter than about 5% of the Hill radius of the primary took an excessive amount of time to simulate. Small examples led us to believe that they were the least likely to be in any significant way altered by the passing of other bodies. These tight binaries are therefore likely to survive intact without much alteration. As seen in figure L.7, these tighter binaries are seen more often in the Kuiper belt today. We focused instead on the wider binaries, in large part because they are more likely to give interesting insights to the dynamics of the Kuiper belt. Further work in this area could benefit from more computing power to focus on tighter binaries.

We placed artificial restrictions on our simulations with the intention of engineering encounters. The binary centre of mass orbit around the Sun always began with  $e = 0$ . This allowed for more controlled encounter environments. We only created encounters with other cold classical objects, with low eccentricity and inclination, but we showed that encounter timescales become very small with even these small non-zero eccentricities and inclinations. The parameter space experiments were restricted to the 2D plane. This is not a true reflection of the conditions that a binary in the Kuiper belt will experience, but was meant to give a high-level view of the types of outcomes that are possible and the relative probability of each kind. We used a constant density for all bodies in our simulations. This helped simplify calculations and simulation setups. As we showed in figure 1.8, Kuiper belt bodies have a range of densities. Additional calculations of the density for each sized component would not have significantly improved the simulations, and would not have been more realistic, as the density of smaller bodies is not precisely known.

In the experiments following a single binary we restricted the population of impactors to those with orbital characteristics found in the cold classical belt. As mentioned previously, eventful encounters require a long encounter timescale, and encounters between cold classical binaries and members of the hot populations of the Kuiper belt will have much greater relative encounter velocities, and are unlikely to add much to the single binary simulations. Also in this experiment we made several assumptions when calculating the encounter rate that a binary is likely to experience, including about the mass distribution, the typical encounter speed, and the uneven distribution of objects in the volume

We used a simplified model to track and calculate the physics involved in the collisions that we observed, where mass and momentum were conserved. This was both a restriction imposed by the particular technologies we used, and also a choice to not focus on collisions. We could have calculated potential fragment sizes after destructive collisions, and tracked the orbits of the largest fragments, but this would not have added much to the main focus of the project.

We ignored any additional physics in our simulations, such as the effects of gas drag in the early solar system soon after the binaries would have formed. The period over which Kuiper belt objects will have been susceptible to gas drag is a small fraction of their entire lifetime (Williams & Cieza 2011), and therefore this effect will not apply to the vast majority of encounters.

## Chapter 5

# Conclusion

In this work we investigated the dynamics of encounters between binaries and other similarly sized bodies in the cold classical Kuiper belt. We used numerical  $N$ -body integrators to simulate these encounters with a range of initial conditions. We carried out three main experiments: the effect of the particular initial orientation of the binary, and starting position of its components, on the results of close encounters that involved the overlap of the Hill spheres of the binary and impactor; an examination of a binaries ability to withstand encounters with a parameter space of impactors; and the evolution of a single binary over its lifetime as a result of many encounters. The main conclusions are summarized as follows:

- Repeated encounters with similarly massed third bodies are unlikely to result in the efficient removal of angular momentum from a binary in a way that would reduce the mutual orbital separation enough to cause the two components to collide and create a contact binary. Collisions occurred during our encounters that may produce contact binaries, but they require very low encounter velocities and were usually not between the two original components. They are unlikely to be a main pathway to contact binary formation.
- Binary survival in the cold classical region of the Kuiper belt is dependant on the initial orbital elements of the binary. Wide binaries are particularly susceptible to disruption from passing impactors. Large mass ratio binaries and binaries with high eccentricity are also more vulnerable to disruption. Around 80% of binaries survive  $10^5$  encounters. Assuming an initial binary fraction of 100% and current binary fraction of 30%, this means other processes are required to disrupt the remainder, such as push-out by Neptune.
- An encounter with an impactor that involves the touching or overlapping of the Hill spheres of the impactor and the binary, becomes chaotic and unpredictable. However once disruption occurs, certain outcomes are more likely than others. The disruption of the tighter binaries preferentially results in the creation of a new binary composed of the impactor and one of the components of the original binary. When the mass ratio of the binary is large, then the secondary is more likely to be captured by the impactor and form the new binary.
- Over the course of its lifetime a binary in the cold classical region will experience many encounters. Due to the distribution of eccentricity and inclination in this region the average encounter time will be too low to greatly affect the binary, but eventually the cumulative effect of many encounters will pump up the eccentricity, and can either increase or decrease the mutual orbital separation. Currently, binaries in the cold classical belt have a wide

range of eccentricities. Assuming they form on near circular orbits, perhaps the large eccentricities are a result of repeated encounters.

- A possible direction for future work in this area to take would be the investigation of tighter binaries. While we showed that wider binaries are more easily affected by encounters, tighter binaries are much more common in the Kuiper belt, and observing how their orbits change as a result of encounters will be interesting. Greater computational power could be utilized to overcome the difficulty in simulating tight binaries. Also, more detailed estimations of the number of encounters that a binary will experience could better constrain their evolution.

## **Acknowledgement**

I would like to express my gratitude to Sebastian Lorek for his supervision of this project, and for his many valuable comments and suggestions.

# Bibliography

- Armitage, P. J. (2010), *Astrophysics of Planet Formation*.
- Batygin, K., Brown, M. E. & Fraser, W. C. (2011), ‘Retention of a Primordial Cold Classical Kuiper Belt in an Instability-Driven Model of Solar System Formation’, **738**(1), 13.
- Benecchi, S. D., Noll, K. S., Grundy, W. M., Buie, M. W., Stephens, D. C. & Levison, H. F. (2009), ‘The correlated colors of transneptunian binaries’, **200**(1), 292–303.
- Benz, W. & Asphaug, E. (1999), ‘Catastrophic Disruptions Revisited’, **142**(1), 5–20.
- Bernstein, G. M., Trilling, D. E., Allen, R. L., Brown, M. E., Holman, M. & Malhotra, R. (2004), ‘The Size Distribution of Trans-Neptunian Bodies’, **128**(3), 1364–1390.
- Bierson, C. J. & Nimmo, F. (2019), ‘Using the density of Kuiper Belt Objects to constrain their composition and formation history’, **326**, 10–17.
- Binzel, R. P., Rivkin, A. S., Stuart, J. S., Harris, A. W., Bus, S. J. & Burbine, T. H. (2004), ‘Observed spectral properties of near-Earth objects: results for population distribution, source regions, and space weathering processes’, **170**(2), 259–294.
- Brown, M. E. (2001), ‘The Inclination Distribution of the Kuiper Belt’, **121**(5), 2804–2814.
- Brown, M. E., Ragozzine, D., Stansberry, J. & Fraser, W. C. (2010), ‘The Size, Density, and Formation of the Orcus-Vanth System in the Kuiper Belt’, **139**(6), 2700–2705.
- Brucker, M. J., Grundy, W. M., Stansberry, J. A., Spencer, J. R., Sheppard, S. S., Chiang, E. I. & Buie, M. W. (2009), ‘High albedos of low inclination Classical Kuiper belt objects’, **201**(1), 284–294.
- Canup, R. M. (2005), ‘A Giant Impact Origin of Pluto-Charon’, *Science* **307**(5709), 546–550.
- Chiang, E. & Youdin, A. N. (2010), ‘Forming Planetesimals in Solar and Extrasolar Nebulae’, *Annual Review of Earth and Planetary Sciences* **38**, 493–522.
- Doressoundiram, A., Barucci, M. A., Romon, J. & Veillet, C. (2001), ‘Multicolor Photometry of Trans-neptunian Objects’, **154**(2), 277–286.
- Elliot, J. L., Kern, S. D., Clancy, K. B., Gulbis, A. A. S., Millis, R. L., Buie, M. W., Wasserman, L. H., Chiang, E. I., Jordan, A. B., Trilling, D. E. & Meech, K. J. (2005), ‘The Deep Ecliptic Survey: A Search for Kuiper Belt Objects and Centaurs. II. Dynamical Classification, the Kuiper Belt Plane, and the Core Population’, **129**(2), 1117–1162.
- Emel’yanenko, V. V., Asher, D. J. & Bailey, M. E. (2003), ‘A new class of trans-Neptunian objects in high-eccentricity orbits’, **338**(2), 443–451.

- Fraser, W. C., Bannister, M. T., Pike, R. E., Marsset, M., Schwamb, M. E., Kavelaars, J. J., Lacerda, P., Nesvorný, D., Volk, K., Delsanti, A., Benecchi, S., Lehner, M. J., Noll, K., Gladman, B., Petit, J.-M., Gwyn, S., Chen, Y.-T., Wang, S.-Y., Alexandersen, M., Burdullis, T., Sheppard, S. & Trujillo, C. (2017), ‘All planetesimals born near the Kuiper belt formed as binaries’, *Nature Astronomy* **1**, 0088.
- Fraser, W. C., Brown, M. E., Morbidelli, A., Parker, A. & Batygin, K. (2014), ‘The Absolute Magnitude Distribution of Kuiper Belt Objects’, **782**(2), 100.
- Gladman, B., Holman, M., Grav, T., Kavelaars, J., Nicholson, P., Aksnes, K. & Petit, J. M. (2002), ‘Evidence for an Extended Scattered Disk’, **157**(2), 269–279.
- Gladman, B., Marsden, B. G. & Vanlaerhoven, C. (2008), *Nomenclature in the Outer Solar System*, p. 43.
- Goldreich, P., Lithwick, Y. & Sari, R. (2002), ‘Formation of Kuiper-belt binaries by dynamical friction and three-body encounters’, **420**(6916), 643–646.
- Gomes, R., Levison, H. F., Tsiganis, K. & Morbidelli, A. (2005), ‘Origin of the cataclysmic Late Heavy Bombardment period of the terrestrial planets’, **435**(7041), 466–469.
- Gomes, R. S. (2003), ‘The origin of the Kuiper Belt high-inclination population’, **161**(2), 404–418.
- Grundy, W. M., Bird, M. K., Britt, D. T., Cook, J. C., Cruikshank, D. P., Howett, C. J. A., Krijt, S., Linscott, I. R., Olkin, C. B., Parker, A. H., Protopapa, S., Ruaud, M., Umurhan, O. M., Young, L. A., Dalle Ore, C. M., Kavelaars, J. J., Keane, J. T., Pendleton, Y. J., Porter, S. B., Scipioni, F., Spencer, J. R., Stern, S. A., Verbiscer, A. J., Weaver, H. A., Binzel, R. P., Buie, M. W., Buratti, B. J., Cheng, A., Earle, A. M., Elliott, H. A., Gabasova, L., Gladstone, G. R., Hill, M. E., Horanyi, M., Jennings, D. E., Lunsford, A. W., McComas, D. J., McKinnon, W. B., McNutt, R. L., Moore, J. M., Parker, J. W., Quirico, E., Reuter, D. C., Schenk, P. M., Schmitt, B., Showalter, M. R., Singer, K. N., Weigle, G. E. & Zangari, A. M. (2020), ‘Color, composition, and thermal environment of Kuiper Belt object (486958) Arrokoth’, *Science* **367**(6481), aay3705.
- Grundy, W. M., Noll, K. S., Nimmo, F., Roe, H. G., Buie, M. W., Porter, S. B., Benecchi, S. D., Stephens, D. C., Levison, H. F. & Stansberry, J. A. (2011), ‘Five new and three improved mutual orbits of transneptunian binaries’, **213**(2), 678–692.
- Grundy, W. M., Noll, K. S., Roe, H. G., Buie, M. W., Porter, S. B., Parker, A. H., Nesvorný, D., Levison, H. F., Benecchi, S. D., Stephens, D. C. & Trujillo, C. A. (2019), ‘Mutual orbit orientations of transneptunian binaries’, **334**, 62–78.
- Gulbis, A. A. S., Elliot, J. L., Adams, E. R., Benecchi, S. D., Buie, M. W., Trilling, D. E. & Wasserman, L. H. (2010), ‘Unbiased Inclination Distributions for Objects in the Kuiper Belt’, **140**(2), 350–369.
- Hahn, J. M. & Malhotra, R. (2005), ‘Neptune’s Migration into a Stirred-Up Kuiper Belt: A Detailed Comparison of Simulations to Observations’, **130**(5), 2392–2414.
- Heggie, D. C. (1975), ‘Binary evolution in stellar dynamics.’, **173**, 729–787.

- Hill, G. W. (1878), ‘Researches in the lunar theory’, *American Journal of Mathematics* **1**(1), 5–26.  
**URL:** <http://www.jstor.org/stable/2369430>
- Jewitt, D. C. & Luu, J. X. (2000), Physical Nature of the Kuiper Belt, *in* V. Mannings, A. P. Boss & S. S. Russell, eds, ‘Protostars and Planets IV’, p. 1201.
- Jewitt, D. C., Trujillo, C. A. & Luu, J. X. (2000), ‘Population and Size Distribution of Small Jovian Trojan Asteroids’, **120**(2), 1140–1147.
- Jewitt, D. & Luu, J. (1993), ‘Discovery of the candidate Kuiper belt object 1992 QB<sub>1</sub>’, **362**(6422), 730–732.
- Johansen, A., Oishi, J. S., Mac Low, M.-M., Klahr, H., Henning, T. & Youdin, A. (2007), ‘Rapid planetesimal formation in turbulent circumstellar disks’, **448**(7157), 1022–1025.
- Jorda, L., Gaskell, R., Capanna, C., Hviid, S., Lamy, P., Ādurech, J., Faury, G., Groussin, O., Gutiérrez, P., Jackman, C., Keihm, S. J., Keller, H. U., Knollenberg, J., Kührt, E., Marchi, S., Mottola, S., Palmer, E., Schloerb, F. P., Sierks, H., Vincent, J. B., A’Hearn, M. F., Barbieri, C., Rodrigo, R., Koschny, D., Rickman, H., Barucci, M. A., Bertaux, J. L., Bertini, I., Cremonese, G., Da Deppo, V., Davidsson, B., Debei, S., De Cecco, M., Fornasier, S., Fulle, M., Güttler, C., Ip, W. H., Kramm, J. R., Küppers, M., Lara, L. M., Lazzarin, M., Lopez Moreno, J. J., Marzari, F., Naletto, G., Oklay, N., Thomas, N., Tubiana, C. & Wenzel, K. P. (2016), ‘The global shape, density and rotation of Comet 67P/Churyumov-Gerasimenko from preperihelion Rosetta/OSIRIS observations’, **277**, 257–278.
- Jutzi, M. & Benz, W. (2016), Formation of bi-lobed 67P/C-G-like shapes by sub-catastrophic collisions, *in* ‘AAS/Division for Planetary Sciences Meeting Abstracts #48’, Vol. 48 of *AAS/Division for Planetary Sciences Meeting Abstracts*, p. 211.11.
- Kominami, J. D., Makino, J. & Daisaka, H. (2011), ‘Binary Formation in Planetesimal Disks. I. Equal Mass Planetesimals’, **63**, 1331–1344.
- Kozai, Y. (1962), ‘Secular perturbations of asteroids with high inclination and eccentricity’, **67**, 591–598.
- Lacerda, P. (2011), ‘A Change in the Light Curve of Kuiper Belt Contact Binary (139775) 2001 QG<sub>298</sub>’, **142**(3), 90.
- Lee, E. A., Astakhov, S. A. & Farrelly, D. (2007), ‘Production of trans-Neptunian binaries through chaos-assisted capture’, **379**(1), 229–246.
- Leinhardt, Z. M. & Stewart, S. T. (2012), ‘Collisions between Gravity-dominated Bodies. I. Outcome Regimes and Scaling Laws’, **745**(1), 79.
- Levison, H. F. & Morbidelli, A. (2003), ‘The formation of the Kuiper belt by the outward transport of bodies during Neptune’s migration’, **426**(6965), 419–421.
- Lidov, M. L. (1962), ‘The evolution of orbits of artificial satellites of planets under the action of gravitational perturbations of external bodies’, **9**(10), 719–759.
- Lissauer, J. J. & Stewart, G. R. (1993), Growth of Planets from Planetesimals, *in* E. H. Levy & J. I. Lunine, eds, ‘Protostars and Planets III’, p. 1061.

- Lyra, W., Youdin, A. N. & Johansen, A. (2021), ‘Evolution of MU69 from a binary planetesimal into contact by Kozai-Lidov oscillations and nebular drag’, **356**, 113831.
- Malhotra, R. (1993), ‘The origin of Pluto’s peculiar orbit’, **365**(6449), 819–821.
- Malhotra, R. (1995), ‘The Origin of Pluto’s Orbit: Implications for the Solar System Beyond Neptune’, **110**, 420.
- Malhotra, R., Duncan, M. J. & Levison, H. F. (2000), Dynamics of the Kuiper Belt, *in* V. Mannings, A. P. Boss & S. S. Russell, eds, ‘Protostars and Planets IV’, p. 1231.
- McKinnon, W. B., Richardson, D. C., Marohnic, J. C., Keane, J. T., Grundy, W. M., Hamilton, D. P., Nesvorný, D., Umurhan, O. M., Lauer, T. R., Singer, K. N., Stern, S. A., Weaver, H. A., Spencer, J. R., Buie, M. W., Moore, J. M., Kavelaars, J. J., Lisse, C. M., Mao, X., Parker, A. H., Porter, S. B., Showalter, M. R., Olkin, C. B., Cruikshank, D. P., Elliott, H. A., Gladstone, G. R., Parker, J. W., Verbiscer, A. J., Young, L. A. & New Horizons Science Team (2020), ‘The solar nebula origin of (486958) Arrokoth, a primordial contact binary in the Kuiper Belt’, *Science* **367**(6481), aay6620.
- Millis, R. L., Buie, M. W., Wasserman, L. H., Elliot, J. L., Kern, S. D. & Wagner, R. M. (2002), ‘The Deep Ecliptic Survey: A Search for Kuiper Belt Objects and Centaurs. I. Description of Methods and Initial Results’, **123**(4), 2083–2109.
- Morbidelli, A., Brown, M. E. & Levison, H. F. (2003), ‘The Kuiper Belt and its Primordial Sculpting’, *Earth Moon and Planets* **92**(1), 1–27.
- Morbidelli, A., Levison, H. F., Tsiganis, K. & Gomes, R. (2005), ‘Chaotic capture of Jupiter’s Trojan asteroids in the early Solar System’, **435**(7041), 462–465.
- Murray, C. D. & Dermott, S. F. (2008), *Solar System Dynamics*, 2008 edn.
- Nesvorný, D., Parker, J. & Vokrouhlický, D. (2018), ‘Bi-lobed Shape of Comet 67P from a Collapsed Binary’, **155**(6), 246.
- Nesvorný, D. & Vokrouhlický, D. (2019), ‘Binary survival in the outer solar system’, **331**, 49–61.
- Nesvorný, D., Vokrouhlický, D., Bottke, W. F. & Noll, K. (2011), Binary Constraints on Kuiper Belt Collisions, *in* ‘EPSC-DPS Joint Meeting 2011’, Vol. 2011, p. 1376.
- Nesvorný, D., Youdin, A. N. & Richardson, D. C. (2010), ‘Formation of Kuiper Belt Binaries by Gravitational Collapse’, **140**(3), 785–793.
- Noll, K., Grundy, W. M., Nesvorný, D. & Thirouin, A. (2020), *Trans-Neptunian binaries (2018)*, pp. 201–224.
- Noll, K. S., Grundy, W. M., Chiang, E. I., Margot, J. L. & Kern, S. D. (2008), *Binaries in the Kuiper Belt*, p. 345.
- Noll, K. S., Grundy, W. M., Stephens, D. C., Levison, H. F. & Kern, S. D. (2008), ‘Evidence for two populations of classical transneptunian objects: The strong inclination dependence of classical binaries’, **194**(2), 758–768.
- Parker, A. H. & Kavelaars, J. J. (2010), ‘Destruction of Binary Minor Planets During Neptune Scattering’, **722**(2), L204–L208.

- Parker, A. H., Kavelaars, J. J., Petit, J.-M., Jones, L., Gladman, B. & Parker, J. (2011), ‘Characterization of Seven Ultra-wide Trans-Neptunian Binaries’, **743**(1), 1.
- Petit, J. M. & Henon, M. (1986), ‘Satellite encounters’, **66**(3), 536–555.
- Pitjeva, E. V. & Pitjev, N. P. (2018), ‘Mass of the Kuiper belt’, *Celestial Mechanics and Dynamical Astronomy* **130**(9), 57.
- Rein, H. & Liu, S.-F. (2011), ‘REBOUND: Multi-purpose N-body code for collisional dynamics’.
- Rein, H. & Spiegel, D. S. (2015), ‘IAS15: a fast, adaptive, high-order integrator for gravitational dynamics, accurate to machine precision over a billion orbits’, **446**(2), 1424–1437.
- Rickman, H., Marchi, S., A’Hearn, M. F., Barbieri, C., El-Maarry, M. R., Güttler, C., Ip, W. H., Keller, H. U., Lamy, P., Marzari, F., Massironi, M., Naletto, G., Pajola, M., Sierks, H., Koschny, D., Rodrigo, R., Barucci, M. A., Bertaux, J. L., Bertini, I., Cremonese, G., De Deppo, V., Debei, S., De Cecco, M., Fornasier, S., Fulle, M., Groussin, O., Gutiérrez, P. J., Hviid, S. F., Jorda, L., Knollenberg, J., Kramm, J. R., Kührt, E., Küppers, M., Lara, L. M., Lazzarin, M., Lopez Moreno, J. J., Michalik, H., Sabau, L., Thomas, N., Vincent, J. B. & Wenzel, K. P. (2015), ‘Comet 67P/Churyumov-Gerasimenko: Constraints on its origin from OSIRIS observations’, **583**, A44.
- Schäfer, U., Yang, C.-C. & Johansen, A. (2017), ‘Initial mass function of planetesimals formed by the streaming instability’, **597**, A69.
- Schwartz, S. R., Michel, P., Jutzi, M., Marchi, S., Zhang, Y. & Richardson, D. C. (2018), ‘Catastrophic disruptions as the origin of bilobate comets’, *Nature Astronomy* **2**, 379–382.
- Sheppard, S. S. & Jewitt, D. (2004), ‘Extreme Kuiper Belt Object 2001 QG<sub>298</sub> and the Fraction of Contact Binaries’, **127**(5), 3023–3033.
- Simon, J. B., Armitage, P. J., Youdin, A. N. & Li, R. (2017), ‘Evidence for Universality in the Initial Planetesimal Mass Function’, **847**(2), L12.
- Stansberry, J. A., Grundy, W. M., Mueller, M., Benecchi, S. D., Rieke, G. H., Noll, K. S., Buie, M. W., Levison, H. F., Porter, S. B. & Roe, H. G. (2012), ‘Physical properties of trans-neptunian binaries (120347) Salacia-Actaea and (42355) Typhon-Echidna’, **219**(2), 676–688.
- Stansberry, J., Grundy, W., Brown, M., Cruikshank, D., Spencer, J., Trilling, D. & Margot, J. L. (2008), *Physical Properties of Kuiper Belt and Centaur Objects: Constraints from the Spitzer Space Telescope*, p. 161.
- Stern, S. A., Weaver, H. A., Spencer, J. R., Olkin, C. B., Gladstone, G. R., Grundy, W. M., Moore, J. M., Cruikshank, D. P. & Elliott, . (2019), ‘Initial results from the New Horizons exploration of 2014 MU<sub>69</sub>, a small Kuiper Belt object’, *Science* **364**(6441), aaw9771.
- Stewart, S. T. & Leinhardt, Z. M. (2009), ‘Velocity-Dependent Catastrophic Disruption Criteria for Planetesimals’, **691**(2), L133–L137.
- Tegler, S. C. & Romanishin, W. (2000), ‘Extremely red Kuiper-belt objects in near-circular orbits beyond 40 AU’, **407**(6807), 979–981.
- Thirouin, A. & Sheppard, S. S. (2017), ‘A Possible Dynamically Cold Classical Contact Binary: (126719) 2002 CC<sub>249</sub>’, **154**(6), 241.

- Thirouin, A., Sheppard, S. S. & Noll, K. S. (2017), ‘2004 TT<sub>357</sub>: A Potential Contact Binary in the Trans-Neptunian Belt’, **844**(2), 135.
- Tsiganis, K., Gomes, R., Morbidelli, A. & Levison, H. F. (2005), ‘Origin of the orbital architecture of the giant planets of the Solar System’, **435**(7041), 459–461.
- Veillet, C., Parker, J. W., Griffin, I., Marsden, B., Doressoundiram, A., Buie, M., Tholen, D. J., Connelley, M. & Holman, M. J. (2002), ‘The binary Kuiper-belt object 1998 WW31’, **416**(6882), 711–713.
- Vilenius, E., Kiss, C., Müller, T., Mommert, M., Santos-Sanz, P., Pál, A., Stansberry, J., Mueller, M., Peixinho, N., Lellouch, E., Fornasier, S., Delsanti, A., Thirouin, A., Ortiz, J. L., Duffard, R., Perna, D. & Henry, F. (2014), ‘“TNOs are Cool”: A survey of the trans-Neptunian region. X. Analysis of classical Kuiper belt objects from Herschel and Spitzer observations’, **564**, A35.
- Volk, K. & Malhotra, R. (2011), ‘Inclination Mixing in the Classical Kuiper Belt’, **736**(1), 11.
- Weinberg, M. D., Shapiro, S. L. & Wasserman, I. (1987), ‘The Dynamical Fate of Wide Binaries in the Solar Neighborhood’, **312**, 367.
- Williams, J. P. & Cieza, L. A. (2011), ‘Protoplanetary Disks and Their Evolution’, **49**(1), 67–117.
- Youdin, A. N. & Goodman, J. (2005), ‘Streaming Instabilities in Protoplanetary Disks’, **620**(1), 459–469.